

**THERMAL CROWN DEVELOPMENT IN HOT STRIP MILL WORK ROLLS
AND THE ROLE OF SPRAY COOLING**

By
XING YE

B.Sc., North-east Heavy Machinery Institute, China
M.Eng., North-east Heavy Machinery Institute, China

A THESIS SUBMITTED IN PARTIAL FULFILLMENT OF
THE REQUIREMENTS FOR THE DEGREE OF
MASTER OF APPLIED SCIENCE

in
THE FACULTY OF GRADUATE STUDIES
DEPARTMENT OF METALS AND MATERIALS ENGINEERING

We accept this thesis as conforming
to the required standard

THE UNIVERSITY OF BRITISH COLUMBIA
November, 1990

© XING YE, 1990

In presenting this thesis in partial fulfilment of the requirements for an advanced degree at the University of British Columbia, I agree that the Library shall make it freely available for reference and study. I further agree that permission for extensive copying of this thesis for scholarly purposes may be granted by the head of my department or by his or her representatives. It is understood that copying or publication of this thesis for financial gain shall not be allowed without my written permission.

Department of Metals and Materials Engineering

The University of British Columbia
Vancouver, Canada

Date December 18, 1990

ABSTRACT

The objective of this investigation was to determine the influence of work roll cooling on roll thermal behavior. The investigation has been conducted utilizing a previously developed computer model [1]. Three industrial operations were evaluated and features of an optimum configuration have been identified. The magnitude of the thermal zone near the roll surface within which the cyclic temperature variation is confined has been evaluated for different roll cooling conditions.

A two dimensional thermal model of a work roll has been developed to predict the thermal field inside the roll, based on which the thermal crown of the roll was calculated under an assumption of axi-symmetric deformation. The heat transfer equation was solved by the numerical finite difference method, the Alternating Direction Implicit (ADI) method. This method makes it possible to solve the problem on a personal computer making it suitable for industrial application due to the minimum requirements of computer storage and time. Also because the thermal model simulates operating conditions including the cooling configuration it is of value in studying a variety of industrial rolling conditions. The influence of roll spray arrangement, roll gap heat transfer and mill pacing on roll thermal crown has been investigated.

Table of Contents

Abstract	ii
Table of Contents	iii
Table of Figures	vi
Table of Tables	xi
Acknowledgement	xii
1. INTRODUCTION	1
2. LITERATURE REVIEW	3
2.1 MECHANISM OF WORK ROLL WEAR	3
2.1.1 Mechanism of the Thermal Fatigue	3
2.1.2 Abrasion Wear	5
2.1.3 Thermal Fatigue and Abrasion Wear in Mill Train	5
2.2 FAILURE OF WORK ROLL	6
2.2.1 Firecracking	6
2.2.2 Peeling	7
2.3 HEAT TRANSFER IN WORK ROLL	8
2.3.1 Analytical Solutions for Roll Heat Transfer	13
2.3.2 Numerical Solutions for Roll Heat Transfer	14
2.3.3 Effect of Operating Conditions on Roll Thermal Behavior	15
2.4 WORK ROLL COOLING	16
2.4.1 Justification for Work Roll Cooling	16
2.4.2 Factors Affecting Heat Removal by a Spray	17

2.4.3 Optimum Placement of Sprays	19
2.5 THERMAL CROWN CALCULATION	21
2.5.1 Roll Cooling Effect on Thermal Crown	24
3 SCOPE AND OBJECTIVES	37
4 INVESTIGATION OF WORK ROLL COOLING	39
4.1 MODEL DESCRIPTION	39
4.2 THE CYCLIC TEMPERATURE OF WORK ROLL	54
4.2.1 The Surface Temperature Gradient during Roll Bite	54
4.2.2 The Minimum Surface Temperature	55
4.3 EFFECT OF SPRAY NOZZLE POSITION ON ROLL THERMAL BEHAVIOR	55
4.3.1 Effect of Entry and Exit Spray Wipers	55
4.3.2 Effect of Upper Nozzle Positions	57
4.3.3 Effect of Water Stream Contact Area	58
4.4 EFFICIENT COOLING ARRANGEMENT	63
4.5 COMPARISON OF THREE INDUSTRIAL OPERATIONS OF WORK ROLL COOLING	66
4.6 EFFECT OF LUBRICANT IN ROLL BITE	73
4.7 EFFECT OF ROLL DIAMETER ON ROLL TEMPERATURE	78
4.8 ROLL SURFACE THERMAL LAYER THICKNESS δ	81
4.9 THE WORK ROLL TEMPERATURE FROM A SEVEN STAND FINISH MILL	87

5 THERMAL CROWN CALCULATION OF WORK ROLLS	93
5.1 MATHEMATICAL DESCRIPTION	94
5.2 NUMERICAL SOLUTION	104
5.3 VALIDATION OF THE MODEL	109
5.4 RESULTS AND DISCUSSION	111
5.4.1 Effect of Roll-Strip Heat Transfer on Roll Thermal Crown	121
5.4.2 Effect of Spray Cooling Arrangement on Roll Thermal Crown	124
5.4.3 Effect of Mill Pacing on Roll Thermal Crown	129
6 CONCLUDING REMARKS AND FURTHER WORK	132
7 REFERENCES	134
8 APPENDICES	132
8.1 APPENDIX A	138
8.2 APPENDIX B	141

Table of Figures

Figure 2.1 Development of stress-strain hysteresis loop for roll surface.	26
Figure 2.2 Variation of hardness with temperature for finishing stand roll materials.	27
Figure 2.3 Roll peeling on a stand F1 bottom work roll	27
Figure 2.4 An example of fleck scale and roll peer imprint in hot band	28
Figure 2.5 General relation between T and heat removal rate for various heat transfer modes	28
Figure 2.6 Variation of the heat transfer coefficient in the roll gap	29
Figure 2.7 Schematic of the work roll showing the different cooling zones	30
Figure 2.8 Thermal response of first stand work roll for first 10 revolutions	31
Figure 2.9 Effect of roll cooling efficiency on build up of surface temperature of a finishing stand work roll	32
Figure 2.10 The influence of cooling surface temperature on the heat transfer coefficient	32
Figure 2.11 The typical recommended location of spray headers	33
Figure 2.12 Effect of roll cooling on the backup/work roll temperature	34
Figure 2.13 Measured and calculated work roll camber vs. time	35

Figure 2.14 a) Comparison of calculated and measured values of roll thermal crown	35
Figure 2.14 b) The predicted thermal crown by preheating work roll with hot water	35
Figure 2.15 Relationship between thermal camber and the width of the strip	36
Figure 2.16 Theoretical variation of camber with time	36
Figure 4.1 Sketch showing the heat flow into a work roll.	46
Figure 4.2 Sketch showing the heat losses from a work roll.	46
Figure 4.3 Sketch showing the rate of heat flow in three dimensions.	47
Figure 4.4 The basic positions of the spray headers relative to the work roll	48
Figure 4.5 Spray-cooling arrangement without the entry-wiper	49
Figure 4.6 Spray-cooling arrangement with the entry-wiper	49
Figure 4.7 The upper spray-nozzles are positioned away from work backup roll contact and close to the lower one	50
Figure 4.8 The arrangement without upper nozzles	50
Figure 4.9 The arrangement with the upper spray-nozzles and entry nozzle close to the work/backup roll contact	51
Figure 4.10 The arrangement with larger surface area of spray impingement from the exit-side spray	51

Figure 4.11 The discretization of work roll into nodes for finite difference analysis	52
Figure 4.12 Effect of lubrication on the heat transfer coefficient in the roll gap	53
Figure 4.13 The effect of introducing the entry and exit wipers on work roll temperature	59
Figure 4.14 The effect of the upper nozzle positions on work roll temperature	61
Figure 4.15 The effect of increasing the spray-impingement area over the roll surface on the roll temperature	62
Figure 4.16 The variation of the peak surface temperature with the spray cooling arrangement	65
Figure 4.17 The variation of the roll center temperature with the spray cooling arrangement	65
Figure 4.18 a) Schematic showing spray configuration from company B.	70
Figure 4.18 b) Schematic showing spray configuration from company C.	71
Figure 4.18 c) The surface temperature profiles from three different industrial operations	72
Figure 4.18 d) The center temperature profiles from three different industrial opera- tions	72

Figure 4.19 a) The influence of lubrication on the computed thermal cycle at the surface of the roll.	76
Figure 4.19 b) The influence of lubrication on the computed thermal cycle within the core of the roll.	76
Figure 4.20 The influence of the roll gap heat transfer on the computed surface temperature of strip on a seven stand mill	77
Figure 4.21 The influence of the roll gap heat transfer on the computed centerline temperature of strip on a seven stand mill	77
Figure 4.22 The effect of changing the roll diameter on the peak surface and center temperatures of the roll	80
Figure 4.23 The normalized temperature difference vs. thickness proportional constant, C_1	85
Figure 4.24 The temperature variation along the roll interior boundary at different surface layer depths	86
Figure 4.25 The roll surface temperature at different surface layer depth	86
Figure 4.26 Computed variation of the HGP with time in the roll bite for two successive passes on a pilot mill.	90
Figure 4.27 The work roll temperatures from a seven stand finish mill	91
Figure 5.1 Schematic diagram showing different modes of heat transfer to work roll.	102

Figure 5.2 The computing domain and boundary conditions.	103
Figure 5.3 The flow chart of the roll thermal crown calculation	108
Figure 5.4 The temperature profiles at the angular position just before roll gap entry	110
Figure 5.5 Temperature contour of the work roll at steady state	115
Figure 5.6 Temperature contour of the work roll after 5 min. rolling	116
Figure 5.7 Temperature contour of the roll after 30 min. rolling	117
Figure 5.8 The temperature contour of the roll at steady state at $HGP=30kW/m^2^{\circ}C$	118
Figure 5.9 The thermal crowns from the temperature distributions shown in Fig.5.5- 5.7.	119
Figure 5.10 The temperature profiles for various angular positions of the roll at steady state.	120
Figure 5.11 The effect of HGP on the thermal crown.	122
Figure 5.12 The development of the thermal expansion before steady state at different roll gap heat transfer.....	123
Figure 5.13 The effect of spray configurations on the thermal crown	127
Figure 5.14 The development of thermal expansion before steady state at different spray configurations	128
Figure 5.15 The development of thermal expansion at different mill pacing	131

Table of Tables

Table IV-I Roll cooling condition	45
Table IV-I-I Temperature Values for the Six Different Arrangements	64
Table IV-II Roll cooling and rolling condition for company B.....	68
Table IV-III Roll cooling condition for company C	69
Table IV-IV The regression parameters of the curve of heat transfer coefficient with lubrication	75
Table IV-V The variation of h and Bi during roll-cooling	83
Table IV-VI The normalized temperature at different depths	84
Table IV-VII Rolling parameters for a seven stand operation	89
Table V-I Roll spray-cooling arrangements	126
Table V-II summary of results	130

ACKNOWLEDGEMENT

I would like to express my immense gratitude to my research supervisor Professor I.V.Samarasekera for her invaluable guidance and encouragement throughout the course of research work and in the preparation of this thesis. Financial support from NSERC in the form of a research and teaching assistantship is gratefully acknowledged.

I wish to thank my husband and my parents for their support and encouragement throughout my graduate studies.

1. INTRODUCTION

In the hot-rolling process, metal is subjected to compressive plastic deformation by the rotating work rolls. The process involves extremely high pressures and high temperatures which may produce large enough stresses in the work rolls to cause roll wear. Roll wear gradually changes the surface finish and profile of the roll leading to dimensional changes in the work rolls. The small variations along the roll axis may cause variable reduction in thickness across the strip, leading to poor strip shape. As a consequence, the work roll performance is deleteriously affected by the roll wear.

Furthermore the high temperatures will cause roll thermal expansion which may lead to a large thermal crown affecting the roll profile or strip shape. On the other hand, an optimum roll thermal crown will compensate for the bending crown induced by the high pressure. In order to reduce the roll wear to improve roll life and to develop a suitable roll thermal crown, a knowledge of the roll temperature variation with operating conditions is necessary.

Roll cooling has been found to greatly affect roll wear. Improper or insufficient cooling causes large thermal gradients near the roll surface, inducing thermal stresses which accelerate roll wear. In addition relatively high temperatures reduce the strength and wear resistance of the rolls and create difficulties in obtaining proper roll profile. As a consequence, the effect of roll cooling on thermal behavior of the work rolls in a hot-rolling mill has always been of great concern to the mill designer and operator, especially in designing an effective cooling system to keep the temperature within an allowable range.

1 . INTRODUCTION

Work roll spray cooling can help decrease the work roll temperature through forced convection. However there is a wide variety of spray nozzle types and spray header configurations currently in use in industry, indicating that optimum design criteria have not been established for roll cooling. Therefore it is important to investigate the influence of different cooling arrangements on the roll thermal behavior in an attempt to arrive at a proper arrangement to improve the work roll life.

Considerable work has been done in studying the thermal behavior of the rolls in the hot-rolling process. However only limited attention has been focused on the roll cooling evaluation [1]. Even fewer studies have been conducted to determine thermal crown of the work rolls, and coarse approximations were made which have not included the effect of cooling configuration. This limits their application in industrial rolling. Therefore from the stand point of industrial rolling it is essential that the effect of roll cooling on roll thermal crown is properly simulated.

2. LITERATURE REVIEW

2.1 MECHANISM OF WORK ROLL WEAR

Work roll wear occurs due to the mechanical and thermal fatigue induced in the surface layer and the loss in roll hardness at high temperature. The mechanical fatigue results from the cyclic mechanical stresses induced by the deforming strip and backup/work roll contact, whilst the thermal fatigue is due to the temperature cycles undergone by the roll surface layer resulting in thermal stress buildup. The loss in hardness of roll surface is due to the overall temperature increase which induces abrasion wear in the contact area with the strip and the backup roll. This study is concerned with thermally induced work roll damage or failure.

2.1.1 Mechanism of the Thermal Fatigue

The mechanism of thermal fatigue in the roll surface layer has been discussed by Stevens *et al.* [2]. The thermal fatigue of the roll surface layer is due to the build-up of plastic strain resulting from the compressive and tensile stress-strain hysteresis during each revolution. As the roll surface temperature increases within the roll bite, the elemental roll material attempts to expand due to the increase in temperature. However this expansion is resisted by the main body of the roll that remains cold. This results in a compressive stress in the roll surface in the circumferential direction. Depending on the temperature difference between the roll surface and roll main body, this stress can be severe enough to cause yielding of the roll surface material.

2.1 MECHANISM OF WORK ROLL WEAR

The circumferential compressive stress increases as the surface temperature increases. As the roll surface ceases to have contact with the strip and begins to cool down, a tensile yield stress can be reached if the surface temperature is low enough. Thus a compressive and tensile stress hysteresis is formed on each revolution, as seen in Fig. 2.1.

The number of cycles to failure increases with a decrease in the plastic strain per cycle. The plastic strain can be greatly influenced by two temperatures [2]-[3]: the maximum and the minimum surface temperature. The maximum surface temperature occurs within the roll bite and is largely determined by the roll bite condition. The minimum surface temperature can occur in a roll cooling zone and is determined by the roll cooling conditions.

Spray cooling has been widely employed in hot strip mills. Depending on the intensity of the cooling and location of the spray headers the minimum surface temperature can be depressed below the roll body temperature [2]. The depression of the roll surface temperature due to cooling could produce an additional plastic tensile strain in the surface. Stevens *et al.* [2] suggested a new cooler at exit to minimize the depression of surface temperature. The spray header reduced the difference between the body temperature and surface temperature from 40°C to 15°C. The plastic strain / cycle for the new cooler is 1.2×10^{-3} compared to 2.0×10^{-3} for the sprays which is a 60% decrease. This reduction in cyclic plasticity produces a significant increase in roll surface life with respect to thermal fatigue failure.

2.1.2 Abrasion Wear

Abrasion wear occurs by the loss in hardness of the roll surface. Because the roll hardness decreases with increasing temperature as shown in Fig. 2.2, the abrasion wear is more severe at high temperatures.

Abrasion has been considered to be the basic mechanism of wear in the later finishing stands [2]. The roll/slab contact time decreases in later stands due to the increase in roll speed. The maximum roll surface temperature obtained in the final finishing stands may be not high enough to cause thermal fatigue and consequently abrasion in the roll bite is the dominant factor in roll wear for these stands.

2.1.3 Thermal Fatigue and Abrasion Wear in Mill Train

Both the thermal fatigue and abrasion wear are strongly affected by the roll surface temperature. With higher surface temperature, both the mechanisms of thermal fatigue and abrasion wear operate to shorten the roll life [2]. Sekimoto *et al.* [3] computed roll temperature variations in the mill train and concluded that the roll surface temperature became higher at the intermediate stands in a finishing train, but the depth of the heated surface layer was greater in the roughing stands. Harper [4] illustrated that the thermal fatigue and wear resistance requirement increase in opposite directions and in the later stands of a finishing mill wear resistance is more critical. For the roughing mill where roll/slab contact times are long, higher temperatures exist and higher thermal fatigue resistance is required.

2.2 FAILURE OF WORK ROLL

Work rolls are subjected to mechanical rolling forces induced by the deforming strip and undergo thermal cycling due to periodic contact with the strip at high temperature. According to the investigation done by Stelco's Lake Erie Works [5], separating forces can exceed 1.6 metric tons per millimeter of width with reductions as high as 60% and 45%. These severe rolling conditions result in work roll degradation in the form of firecracking, peeling, and abrasion wear.

2.2.1 Firecracking

Roll surface firecracks are the fine network of cracks observed in the roll surface layer. The firecracks form due to the thermal fatigue of the roll material on each revolution. An explanation of the mechanism of firecracks is that a compressive stress caused by the thermal expansion of surface layer due to rapid heating in the roll bite exceeds the yield strength of the roll material and induces the plastic strain in the roll surface layer. This plastic strain changes into elastically retained tensile strain which exceeds the tensile yield strength, thus causing the firecracks.

Williams [6] has shown that these cracks formed predominantly in directions normal and parallel to the roll surface. Under severe conditions as a result of interconnected networks of cracks, particles of metal break away from the roll surface. Thus the disintegration of the roll surface by thermal fatigue is produced by continuous development and growth of these cracks

2.2 FAILURE OF WORK ROLL

which result in removal of the roll barrel face.

The depth of firecracks is related to the roll surface temperature and the depth of the zone subjected to cyclic temperature variations, since thermal stresses are a function of the temperature difference.

2.2.2 Peeling

Peeling, as indicated by Averink [5], is caused by thermal and mechanical fatigue, acting to propagate the fine network of firecracks originally found on the surface of hot mill work rolls, which allow small surface particles to break away. Once the mechanism is initiated, adjacent particles are removed by the rolling shear forces. This results in the creation of a rough band around the rolls, as shown in Fig. 2.3. With time the entire working surface can be removed.

The roll surface peeling can cause a severe deterioration of strip surface quality. Averink [5] has reported through the examination of roll surface peeling and the strip surface at Stelco's Lake Erie Works that the roughened roll surface in peeled regions became encrusted with scale particles that were transferred and pressed back into the strip, as shown in Fig. 2.4. This causes patches or bands of fine "fleck scale" to coincide with peeled roll surfaces. The "fleck scale" particles are difficult to remove via pickling, and remain as a surface defect through cold rolling. As roll peeling progresses during rundown, the roughened roll surfaces increase friction in the roll bite, increasing the roll separating force and resulting in catastrophic deterioration of the roll surface.

2.3 HEAT TRANSFER IN WORK ROLL

Stelco's Lake Erie Works has run a program of hot rolling lubrication with the objective of reducing roll peeling [5]. Lubricating oil was injected into cooling headers of the work roll and back-up roll cooling systems. As a result the roll wear was greatly reduced and a decrease in fleck scale on the strip was found. It was found [5] that the flow control and the timing of the oil application were critical to the success of a lubrication system.

2.3 HEAT TRANSFER IN WORK ROLL

The Governing Equation

During hot rolling the work rolls receive heat from the hot strip in the arc of contact. At the same time the rolls lose heat through the roll surface due to subsequent cooling. The basic law that controls the roll thermal conduction is Fourier's Law. In three dimensions in cylindrical coordinates without a heat source, the governing equation [7-8] is

$$\frac{\partial^2 T}{\partial r^2} + \frac{1}{r} \frac{\partial T}{\partial r} + \frac{1}{r^2} \frac{\partial^2 T}{\partial \theta^2} + \frac{\partial^2 T}{\partial z^2} = \frac{1}{\alpha} \left(\frac{\partial T}{\partial t} + \omega \frac{\partial T}{\partial \theta} \right) \quad (2.1)$$

where $\alpha = \frac{k}{\rho c_p}$ is the thermal diffusivity, T is the roll temperature, t is the time and r, θ, z represent the radial, the circumferential and the axial coordinates respectively.

Under the assumptions mentioned later Devadas [9] has simplified the equation to the one-dimensional equation expressed by

2.3 HEAT TRANSFER IN WORK ROLL

$$k \frac{\partial^2 T}{\partial r^2} + \frac{k}{r} \frac{\partial T}{\partial r} = \rho c_{ps} \frac{\partial T}{\partial t} \quad (2.2)$$

Tseng [11-12] incorporate a two dimensional governing equation ignoring the axial heat transfer

$$\frac{\partial^2 T}{\partial r^2} + \frac{1}{r} \frac{\partial T}{\partial r} + \frac{1}{r^2} \frac{\partial^2 T}{\partial \theta^2} = \frac{\omega}{\alpha} \frac{\partial T}{\partial \theta} \quad (2.3)$$

where ω is the roll angular speed. Employing the transformation

$$\theta = \omega t$$

then

$$\frac{\partial^2 T}{\partial r^2} + \frac{1}{r} \frac{\partial T}{\partial r} + \frac{1}{r^2} \frac{\partial^2 T}{\partial \theta^2} = \frac{1}{\alpha} \frac{\partial T}{\partial t} \quad (2.4)$$

Equation (2.4) must be solved subject to work roll boundary conditions which are related to the roll gap heat transfer and roll cooling conditions.

The Roll Boundary Conditions

Roll boundary conditions include the roll gap heat transfer and roll cooling conditions. An accurate estimate of roll boundary conditions is essential for determining the roll temperature history.

1). Roll Gap Heat Transfer

The heat gain of work rolls within the roll gap during each revolution comes from three sources: the heat due to the significant difference in temperature between the hot strip and work

2.3 HEAT TRANSFER IN WORK ROLL

rolls, the friction heat generated due to the roll/strip relative movement during contact, and the strip deformation heat. Devadas [9] has determined the roll gap heat transfer coefficient through measurements of the thermal response of an instrumented sample during rolling. It turns out that the heat transfer coefficient rises rapidly in the initial stage of entry into the roll gap and reaches a fairly constant value for the rest of the roll gap region, as shown in Fig. 2.6. The increase in the heat transfer coefficient was considered to be due to the increase in rolling pressure yielding better contact between the rolls and strip. Devadas [9] also analyzed the effect of rolling parameters such as reduction, roll lubrication and rolling speed, on the heat transfer coefficient. It has been indicated that with greater reduction the heat transfer coefficient is higher again due to increased pressure; the application of roll gap lubrication can cause a dramatic decrease in the roll gap heat transfer coefficient due to the insulating effect of the lubricant; a higher rate of increase in the heat transfer coefficient is observed with higher rolling speed due to the higher rate of increase in the specific pressure in the initial portion of the roll gap with the faster deformation conditions.

2). Roll Cooling

The heat loss from work rolls is accomplished through the roll surface cooling conditions.

At the roll surface:

$$t > 0, \quad k \frac{\partial T}{\partial r} = h(t^*) (T - T_{a(t^*)}) \quad (2.5)$$

where $h(t^*)$ is the heat transfer coefficient for each cooling zone dependent on the roll temperature; $T_{a(t^*)}$ is the ambient temperature of the medium around a roll.

2.3 HEAT TRANSFER IN WORK ROLL

In the case of water-spray cooling, the general relation between heat removal rate and the surface temperature of a hot sample surface is shown in Fig. 2.5 from Hill and Gray [10]. The region AB represents cooling by convection with evaporation occurring at the water surface. The region BC represents the nucleate boiling region. The region CD represents the transition region or partial film boiling, and the region DE is the stable film boiling. Hill and Gray [10] indicated that within the range of roll surface temperatures expected in the hot rolling process, the region AD represents the principal modes of heat transfer during water spray cooling: a convective mode, a nucleate boiling mode and a partial film boiling mode. Devadas in his thesis [9] has determined the roll heat removal by the three modes on roll surface temperature. In addition radiation could play a role in regions where roll surface temperature is high.

Fig. 2.7 shows a schematic diagram of a work roll and its different cooling zones labelled from 1 to 12, suggested by Devadas [9]. Regions 1,6 and 11 are the zones in which heat losses are by radiant cooling and natural convection or natural convection only. In the regions 2,4,8 and 10 the roll surface is covered with a film of water streaming down from the spray zones of 3,5,7 and 9.

The Cyclic Steady State of Roll Temperature Distribution

Depending on the work roll cooling configuration, the roll temperature distribution may reach a cyclic steady state. Devadas [9] has calculated the thermal response of the work roll of the first stand of a finishing mill for the first 10 revolutions, at the roll surface and at depths of 1, 5, and 10 mm below the surface as shown in Fig 2.8 a). It is seen that the temperature gradients are very steep at the surface, especially at entry where the thermal shock exists. The core

2.3 HEAT TRANSFER IN WORK ROLL

temperature rises gradually over the 10 revolution and remains steady thereafter. The temperature gradient in the radius direction is also very steep because a dramatic decrease in temperature is observed at a small distance from the surface; for example, at the depth of 1 mm the peak temperature is about 120°C compared to 400°C at the surface. It turns out that the cyclic temperature variations occur within a thin surface layer. Several authors [11-13] have analyzed that since the roll rotates at a very high speed, and the convective heat flow is confined within a thin thermal layer near the roll surface, the thickness of which (δ) is illustrated in Fig.2.8 b). Tseng [12] indicated that the resulting situation is numerically favorable for the upwinding scheme. Tseng defined the skin layer thickness δ as the depth beneath the roll surface where the cyclic temperature differences during rolling are less than 1%

$$\delta = A r_0 Pe^{-\frac{1}{2}} \quad (2.6)$$

and

$$Pe = r_0^2 \omega \alpha^{-1} \quad (2.7)$$

where r_0 is the roll radius, ω is the roll angular speed, α is the roll thermal diffusivity and Pe is the Peclet Number. A is the skin thickness-proportional coefficient, equal to 7 at $Pe = 10^5$ and $Bi = 10^2$. It can be seen that the surface skin layer thickness is inversely proportional to the roll speed. From Tseng's study [12] the skin layer thickness has also been related to Biot number and Peclet number through the influence on A . Devadas [9] has chosen the value of 7 for A in determining the surface skin layer thickness.

2.3.1 Analytical Solutions for Roll Heat Transfer

Some analytical models [14-17] have been formulated to solve equation (2.1). Patula [14] developed an analytical model to determine a two dimensional (radial and circumferential) cyclic steady-state temperature distribution in a rotating roll subject to constant surface heat input over one portion of roll surface and convective cooling over another portion of the roll surface. The solution technique involved an expansion of the standard method of separation of variables and resulted in an infinite series solution which was in the form of a Fourier series with respect to an angular coordinate θ . Thus the accuracy of analytical solution depends on the number of terms retained in the infinite series. Haubitzer [15] calculated the two dimensional steady-state temperature distribution in a rotating roll that had a prescribed constant surface temperature. Troeder *et al.* [16] incorporated only the strength of a heat input to rolls but not the spray cooling condition, and derived an unsteady-state, three dimensional heat transfer solution by using Bessel functions and the δ -function, which is expressed by an infinite series.

In general although the governing equation and boundary conditions can be determined for the problem of roll heat transfer, no simple analytical solutions can be found. Also the analytical solutions mentioned above were obtained by simplifying the boundary conditions. None of them incorporate the complex spray cooling configurations which is necessary for improving the roll life in hot rolling operations. Tseng [11] has shown that to obtain an accurate analytical solution by using Patula's model, 401 simultaneous equations had to be solved and the computational time is very consuming. However an analytical model can serve as a convenient check for numerical solutions.

2.3.2 Numerical Solutions for Roll Heat Transfer

Numerical techniques have been employed for obtaining approximate solutions to the problem of roll heat transfer. This enables the calculation of the roll heat transfer with complex boundary conditions. Several numerical approaches [1, 11-13, 18-19] have been reported. Parke and Baker [13] developed a two dimensional finite-difference model to investigate transient roll behavior. Poplawski and Seccombe [18] extended the Parke and Baker model to include a third dimension. Their models are all based on a Lagrangian coordinate which is fixed in the roll and the boundary conditions rotate with respect to the system. Tseng [11-12] used an Eulerian coordinate system that allowed fixed boundary conditions, which was found to reduce computing time significantly. With a reasonably fine mesh and a first order upwinding scheme, very accurate results of heat transfer behavior of a two-dimensional rotating roll could be achieved by using the finite difference method. In Tseng's study, aspects of the numerical scheme were emphasized rather than physical phenomena. It was concluded that the numerical accuracy was greatly affected by changing mesh size in the radial direction.

None of the above numerical approaches have incorporated spray cooling configuration, and cooling due to boiling on the roll surface and natural convection. Devadas [9] has calculated the work roll thermal history for normal cooling conditions, which include the spray configuration, boiling and natural convection on the roll surface. The model has been validated by reproducing the conditions published by Stevens *et al.*[2] for a roughing mill operation. The predicted maximum surface temperature is 535°C compared reasonably well with the maximum measured temperature which is 515°C reported by Stevens *et al.*[2].

2.3.3 Effect of Operating Conditions on Roll Thermal Behavior

The Roll Speed

When the roll speed decreases, the roll surface temperature also decreases, but the roll internal temperature rises [3]. The decrease in roll surface temperature is due to the decrease in the frictional heat within the roll bite caused by the decrease in the relative speed of strip movement with respect to the roll. Sekimoto *et al.* [3] calculated the heat generated at the roll bite which has shown that the amount of heat generated by friction was far greater than that by plastic deformation of strip; about two orders of magnitude larger in calorie/cm² sec. The increase in roll bulk temperature with decreasing roll speed is considered to be due to a longer time per revolution at slower roll speed which allows more heat to flow into the roll [3-4].

Reduction

Work roll temperature increases with higher percentage reduction. This is due to the increase in both the plastic deformation and strain rate. The heat-transfer coefficient along the arc of contact is also higher as indicated by Devadas [9].

The Strip Thickness

2.4 WORK ROLL COOLING

The roll surface temperature is higher when thinner gauge strip is rolled, as pointed out by Sekimoto *et al* [3]. This is because high rolling force induced by rolling thinner gauge strip causes larger frictional heat.

The Lubrication in Roll Bite

Work roll temperature can be significantly decreased by employing lubrication in the roll bite, which has the added benefit of reducing roll forces. Devadas [9] reported that with lubrication for a reduction of 50%, a heat transfer coefficient in the roll bite was 40% of the value attained without lubrication.

2.4 WORK ROLL COOLING

2.4.1 Justification for Work Roll Cooling

The work roll surface temperature can be reduced by effective roll cooling. Sekimoto *et al.*[3] calculated the variation in roll temperature with cooling condition by changing the heat transfer coefficient between the cooling water and the roll surface. With reduced cooling, the roll body temperature rises and consequently the roll surface temperature rises, and a cyclic steady state may not be reached.

Stevens *et al.*[2] and Park and Baker's [13] findings are in accordance with Sekimoto's [3]. Stevens *et al.* discussed the effect of roll cooling on the build up of surface temperature of a finishing stand work roll, and demonstrated that the roll surface temperature required for thermal

2.4 WORK ROLL COOLING

fatigue to occur, was higher than that for the hardness loss *i.e.* abrasion wear. With good roll cooling, the maximum roll surface temperature reached could be well below the level for thermal fatigue to occur, as shown in Fig. 2.9, and roll deterioration would be minimal. Also the rate of wear due to abrasion is decreased since the loss of hardness is limited. The hot hardness tests given in Fig. 2.2 for finishing stand roll materials conducted by Stevens *et al.* [2] have shown that a relatively modest increase in temperature can cause a significant loss in hardness of a roll material. Above 200°C, the hardness of materials reduces rapidly and at 500°C their hardness is about 50% of the initial room temperature value.

2.4.2 Factors Affecting Heat Removal by a Spray

Work roll cooling occurs predominantly by convection. The quantity of heat transferred (Q) based on Newton's law is proportional to the surface convective heat transfer coefficient (h), the time during which cooling occurs, the area of cooling, and the temperature difference between the roll surface and the water. Therefore any factor that affects one of the above would influence the work roll cooling.

Water Flux

The water flux during roll spray cooling influences the roll cooling through its influence on the convective heat transfer coefficient. Mitsutsuka [20] found the relationship between the coefficient, h , and the water flow rate, \dot{W} , for values of \dot{W} greater than $5 \times 10^{-4} \text{ l/cm}^2/\text{min}$ to be of the form

$$h \propto \dot{W}^p \quad (2.8)$$

2.4 WORK ROLL COOLING

where p has values ranging from 0.65 to 0.75. Thus h is increased with increasing water flow rate, resulting in a larger amount of heat extraction from the roll. Sekimoto *et al.* [3] have employed Stender's heat transfer coefficient which is the value obtained for water flow in a tube by forced convection. The relationship is the form of

$$h = 725v^{0.85}(1 + 0.014T_w) \quad (2.9)$$

where v is the water flow velocity (m/sec), T_w is the water temperature. In Devadas's calculation of spray cooling of rolls the heat transfer coefficient is determined from Yamaguchi *et al.* [21] correlation based on experimental measurements of the thermal response of a heated plate to spray cooling. The correlation is

$$\dot{q}_{sp} = (1.11)(1.63)(10^5)\dot{W}^{0.521} \quad (2.10)$$

where \dot{W} is the water flow flux $lm^{-2}s^{-1}$.

Mitsutsuka [20] computed the heat-transfer coefficient as a function of cooling surface temperature. The data showing the influence of cooling surface temperature on the heat transfer coefficient for various flow rates from the spray is shown in Fig. 2.10. It can be seen that h is increased for temperatures between 100°C and 200°C, and is decreased between 200°C and 550°C. The heat transfer coefficient is also decreased with decreasing rate of water flow. This is in accordance with Sekimoto *et al.*[3].

Water Pressure

Water pressure is required to force the water on the roll surface. All water cooling applications should aim to employ a moderate rather than high pressure, which would result in rebounding. Harper [4] indicated that one of the operational difficulties for water spray cooling was the inefficient heat transfer rate from roll to water, and concluded that when an increase in water flow is desirable, it should be achieved without increasing the pressure. It has been found from today's rolling operation that reducing water pressure is giving the expected advantages [4]. Current cooling practices in strip rolling involve pressure up to about 200 psi. Flow rates are varied between stands.

2.4.3 Optimum Placement of Sprays

Current commercial hot rolling mills have employed a wide variety of spray nozzle types and cooling configurations. Hill *et al.* [10] has commented that the significant differences in both the water quantity and the cooling configuration from one operation to another indicates a lack of design criteria regarding the roll cooling or heat removal capability of spray nozzles. Roberts [22] mentioned that the three spray cooling parameters that affect roll temperature are: 1) the position of the sprays around the periphery of the work roll; 2) the water spray density (flow rate divided by the impingement area); 3) the length of spray contact with the roll in the peripheral direction. Therefore it becomes necessary to investigate their influence on the cooling efficiency.

Nozzle Position and Nozzle Angle

Carpenter *et al.* [23] have indicated that the effectiveness of spray cooling could be improved by changing spray nozzle positions and the angles of the spray headers. It can be recognized that because the quantity of heat transferred (Q) is proportional to the roll/water contact area (A) and the temperature difference (ΔT) between the roll surface and the water, a change in nozzle position around the roll surface would change the roll/water temperature difference if the water temperature remains unchanged, and a change in the contact angle can change the cooling arc length so as to change the roll/water contact area. Thus the quantity of heat transferred is influenced by the change in both nozzle position and contact angle. The recommended cooling nozzle location by Carpenter *et al.* [23] is shown in Fig. 2.11, but no quantified comparison of the roll temperature achieved relative to other configurations was given in this paper. Stevens *et al.* [2] indicated that a difference in relative position of spray nozzles might be the reason for the difference in state of deterioration of top and bottom work rolls on removal from stands. Patula [14] has indicated through experiments that the value of the centerline temperature changed very little whenever the spray location was changed.

The Exit Spray Nozzle

Some investigators [2,10,13,22,23] have indicated the important role of exit or delivery sprays in reducing roll temperature. Roberts [23] stated that computer simulation studies revealed that typically, delivery side spray cooling was about 40 per cent more effective than entry side cooling, but a direct comparison between the two methods of cooling has not been reported.

2.5 THERMAL CROWN CALCULATION

Parke and Baker [13] have launched a research program on roll cooling for finishing stands. It has been reported that the advantage of early and long exit cooling was that it reduced the bulk roll temperature. A further advantage is a more efficient use of the cooling water. This could be explained by a comparison of the heat transfer rate into the roll by conduction in the material with the achievable rates of heat transfer to the cooling water when the roll surface temperature is above 150° or 200°C. Stevens *et al.* [2] also reported a significant increase in the roll life of roughing stand rolls by initiating the cooling early and sustaining it for some time on the delivery side.

The Backup/Work Rolls Cooling

Parke and Baker [13] compared the model-predicted temperature history of uncooled finish rolls after two revolutions and cooled finish rolls after three revolutions with an entry and an exit spray near the contact of backup/work rolls. The sharp surface temperature quench by comparatively cool backup roll was observed in the case of uncooled roll, as shown in Fig. 2.12 at location 3. It was suggested that an important part of proper cooling should be to control the surface temperature difference between the work roll and the backup roll. Carpenter *et al.* [23] recommend locating two upper spray nozzles near the backup/work roll contact.

2.5 THERMAL CROWN CALCULATION

In the hot rolling operation, the thermal crown of the work roll is developed as a result of

2.5 THERMAL CROWN CALCULATION

radial work roll expansion due to the temperature distribution in the rolls. This could cause a change in the roll gap geometry leading to the strip dimensional precision problems, *i.e.* the variation in strip thickness and flatness. Therefore modification of work roll surface profile is important in today's technology. Techniques such as variable crown roll [24], continuous variable crown control [25], flexible flatness control [26] and universal crown control [27] systems, have been implemented to control the shape of the roll gap by compensating for roll bending and crown. To achieve precise thermal crown control on line, it is necessary to predict the roll surface profile or thermal crown.

Some researchers have investigated the evolution of roll thermal crown [28-35]. Wilmotte and Mignon [31] calculated the roll surface displacement by the equation

$$U_R = (2\alpha/R_w) \int_0^{R_w} T x dx \quad (2.11)$$

where α is the roll thermal expansion coefficient, R_w is radius of the work roll, x is the distance from the roll axis in the radial direction and T is the temperature at a radial distance x .

Roberts [30] introduced Ueda's calculation for the thermal crown given below

$$U_j = (2/r_0) (1 + \nu) \alpha \sum_{i=1}^{l_0} (T_{i,j} - T_0) \Delta r_i r_i \quad (2.12)$$

where i and j are the node positions along the radial and axial direction respectively.

It is observed from the above equations that the roll thermal crown is related to the bulk roll temperature. In calculating the roll thermal expansion or thermal crown, the three dimensional analysis for roll heat transfer may be simplified to a two dimensional analysis since the

2.5 THERMAL CROWN CALCULATION

temperature variation in the circumferential direction due to the rapid rotation of rolls will not significantly affect crown. Yuen [28] has developed a mathematical model to examine the thermal characteristics and shape correction capability of a cooling header. It turns out that the thin thermal boundary layer near roll surface is unimportant and can be disregarded in calculating the roll surface contraction. In calculating the temperature distribution of work roll associated with thermal crown calculation, Roberts [30] introduced Ueda's calculation in which an equivalent condition to simulate the real roll condition was employed. The equivalent heat transfer coefficient of roll-gap and beyond the roll-gap as well as the surrounding medium temperature were obtained through heat exchange theory. This may limit its application since a real roll state has to be converted to an equivalent state.

Few reports on the comparison of measured and calculated work roll thermal crown have been given in the literature. Jonsson and Mantylar [32] described briefly a thermal expansion model of a work roll as a part of off-line analysis of rolling process in a cooperative research project of Scandinavian Steel Works and the Foundation of Metallurgical Research. Fig.2.13 shows the results of measured and calculated work roll camber. A good agreement can be seen from the figure. It was made by adjusting thermal data for the mill, *e.g.* heat transfer coefficient, until measured and calculated work roll thermal profile and surface temperature agreed. Ohike *et al* [33] calculated the roll thermal camber described as the sum of the distribution functions of mass-averaged roll temperature along the roll axis. The comparison of measured and calculated values of roll thermal camber was presented in Fig.2.14 a). The maximum measured thermal crown can be seen to be about $260\ \mu\text{m}$, but no detail about the measurement was given in the paper. A report from Stelco [34] has presented a predicted thermal crown by preheating work

2.5 THERMAL CROWN CALCULATION

roll with hot water to avoid roll breakage due to thermal shock. Fig.2.4 b) shows the results of the roll crown investigation. No results for work roll thermal crown development during rolling were reported.

A number of operating factors influence the thermal crowns of work rolls. Roberts [30] has indicated that the most important factors are

- 1). the roll cooling condition.
- 2). the width of strip
- 3). the deformation of strip
- 4). the pacing of the mill.

With respect to roll cooling, Wilmotte and Mignon [31] has found that a 100% variation in water pressure caused a 13% variation in the asymptotic value of the thermal crown. From Fig. 2.15 the width of strip does not affect the shape of roll surface profile significantly. Concerning the deformation condition of strip, Sibakin *et al.*[35] indicated that the thermal crown at any instant depended on the contact period between strip and rolls during the preceding half hour. It has been seen from Fig. 2.16 that the thermal crowns developed in an approximately exponential manner with a time constant of about half an hour.

2.5.1 Roll Cooling Effect on Thermal Crown

The main reason for the thermal profile of work rolls is the intense heat supplied to the center of the roll barrel in the deformation zone. Thus a reduction in heat supplied to the center of the rolls would reduce the thermal profile of the work roll during rolling. Khloponin *et al.*

2.5 THERMAL CROWN CALCULATION

[29] have studied the effect of interim water cooling of strip surface directly before entry into the deformation zone. It was found that the interim cooling of the central area across the strip width reduced the magnitude of change in radius at the middle of roll barrel by 27-33% in a rolling cycle and reduced the roll surface temperature by an average 15-10°C. Also the rejection of strip because of " waviness " has been reduced by about a factor of 1.5.

Yuen [28] has examined roll shape correction capability of a segmented cooling header. It was concluded that the angular location of the segmented header played no role in the shape correction performance, and an increase in coolant flow rate and/or a reduction in coolant temperature would improve the shape correction capability of the header. Improper cooling causes large thermal gradients near the roll surface which, in turn, create thermal stresses large enough to accelerate roll thermal fatigue and wear, as already mentioned before.

2.5 THERMAL CROWN CALCULATION

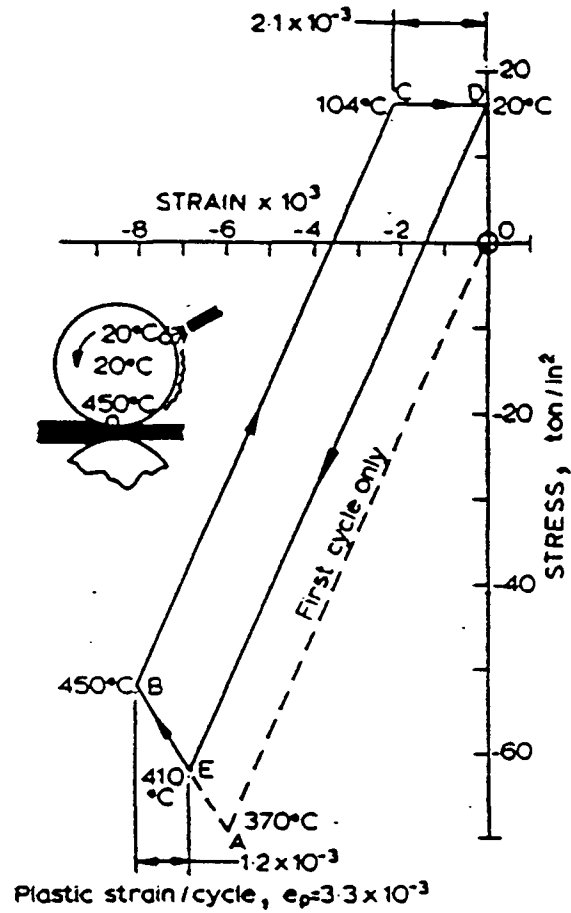


Fig.2.1 Development of stress-strain hysteresis loop for roll surface at beginning of rolling (Stevens *et al.* [2]).

2.5 THERMAL CROWN CALCULATION

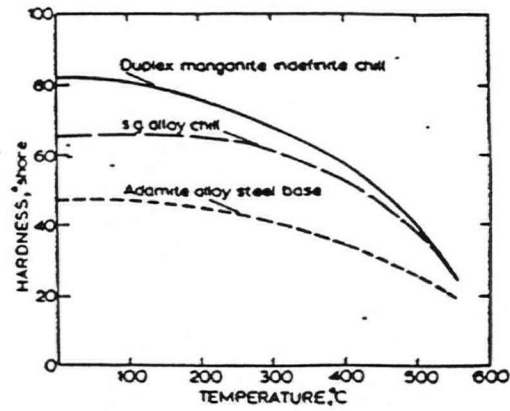


Fig.2.2 Variation of hardness with temperature for finishing stand roll materials (Stevens *et al.* [2])

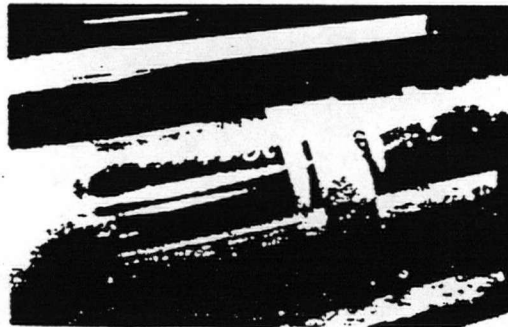


Fig.2.3 Roll peeling on a stand F1 bottom work roll after 10 wear-kilometers (H.J.Averink [5]).

2.5 THERMAL CROWN CALCULATION

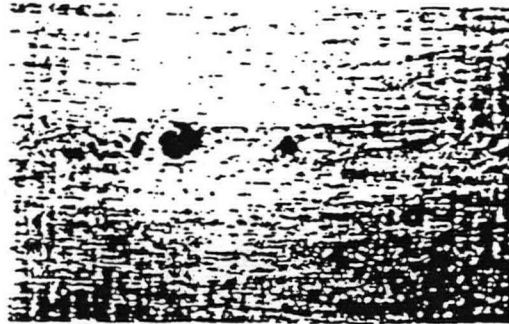


Fig.2.4 An example of fleck scale and roll peel imprint in hot band (4.5X)(H.J.Averink [5]).

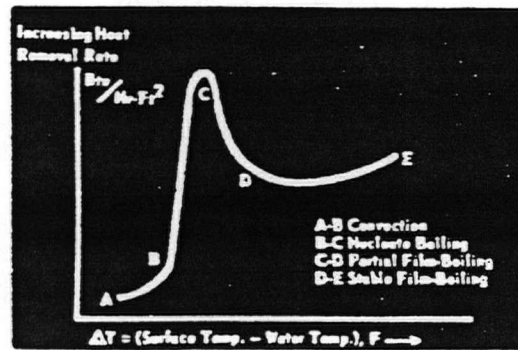


Fig.2.5 General relation between ΔT and heat removal rate for various heat transfer modes (Hill and Gray [10]).

2.5 THERMAL CROWN CALCULATION

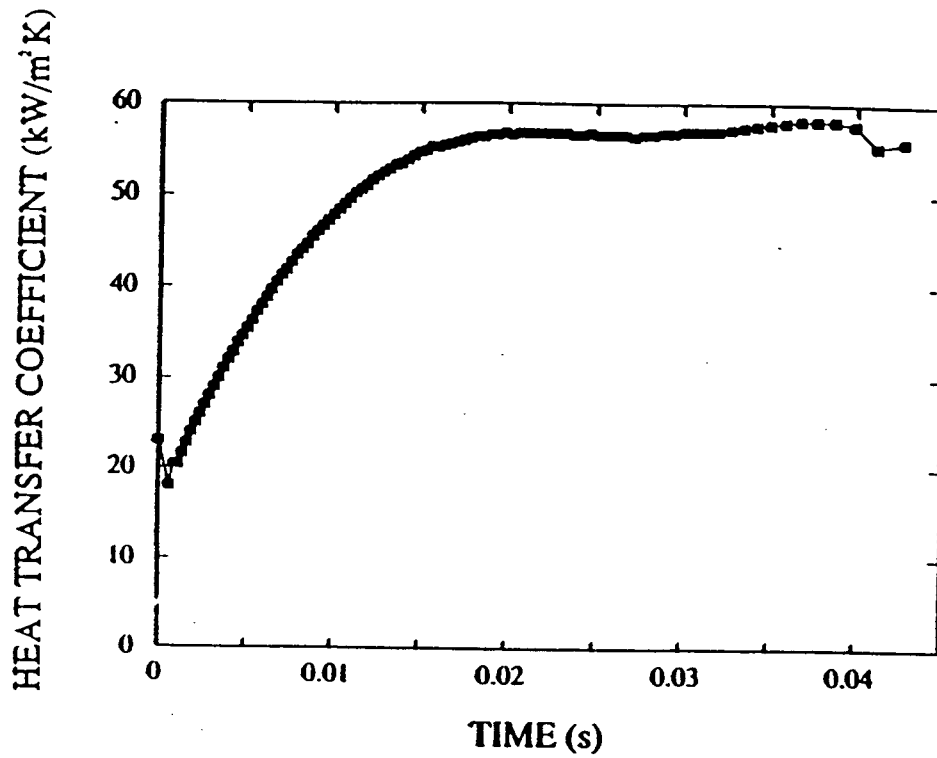
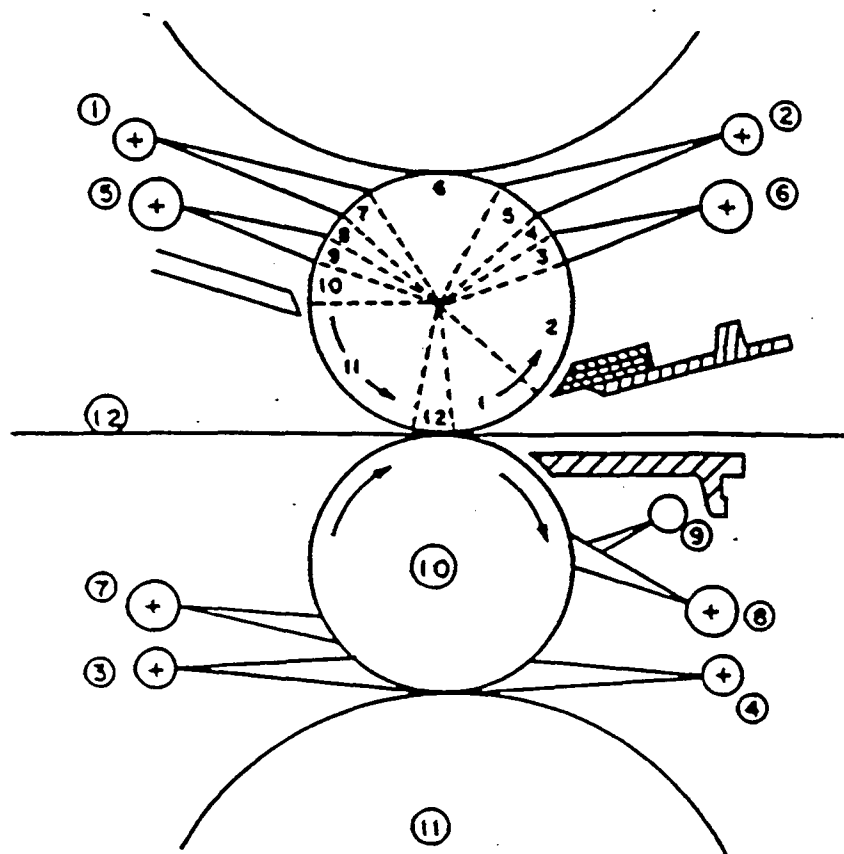


Fig.2.6 Variation of the heat transfer coefficient in the roll-gap for test-4 with no lubrication (Devadas [9]).

2.5 THERMAL CROWN CALCULATION



No.	ITEM	No.	ITEM
(1)	Top Mid Zone Entry Header	(7)	Bottom Main Entry Header
(2)	Top Mid Zone Exit Header	(8)	Bottom Main Exit Header
(3)	Bottom Mid Zone Entry Header	(9)	Auxiliary Header
(4)	Bottom Mid Zone Exit Header	(10)	Work Roll
(5)	Top Main Entry Header	(11)	Back Up Roll
(6)	Top Main Exit Header	(12)	Strip

Fig.2.7 Schematic of the work rolls showing the different cooling zones (Devadas [9]).

2.5 THERMAL CROWN CALCULATION

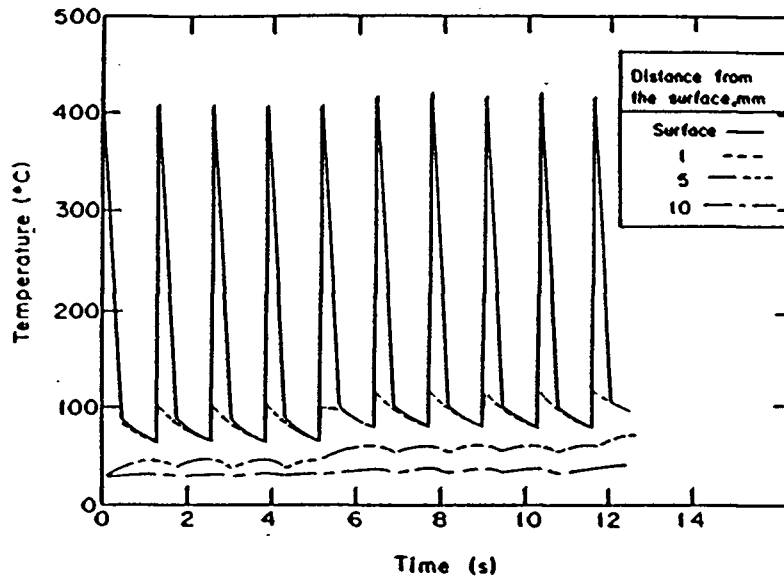


Fig.2.8 a) Thermal response of first stand work roll for first 10 revolutions (Devadas [9]).

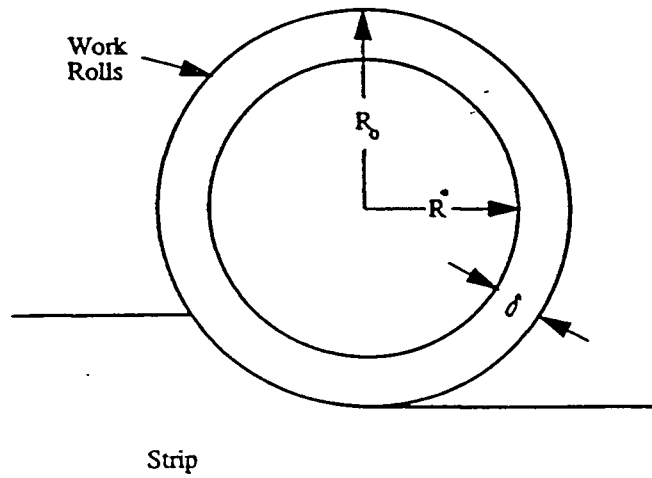


Fig.2.8 b) Schematic showing the thermal zone and its thickness δ .

2.5 THERMAL CROWN CALCULATION

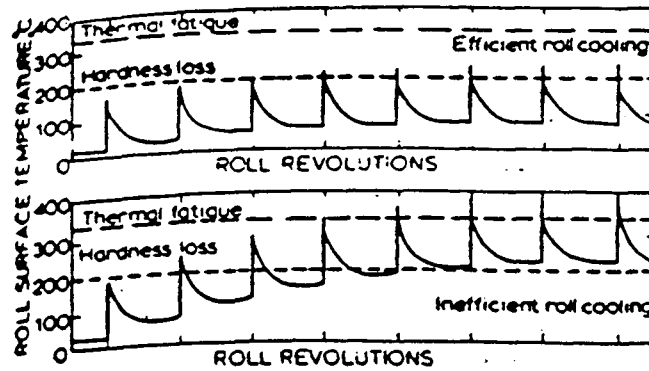


Fig.2.9 Effect of roll cooling efficiency on build up of surface temperature of a finishing stand work roll (Stevens *et al.* [2]).

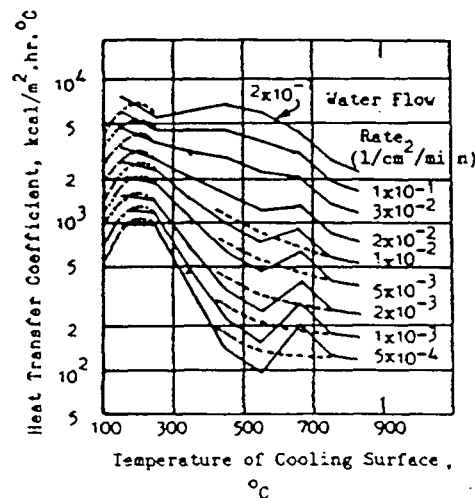


Fig.2.10 The influence of cooling surface temperature on the heat transfer coefficient (W.L.Roberts [23]).

2.5 THERMAL CROWN CALCULATION

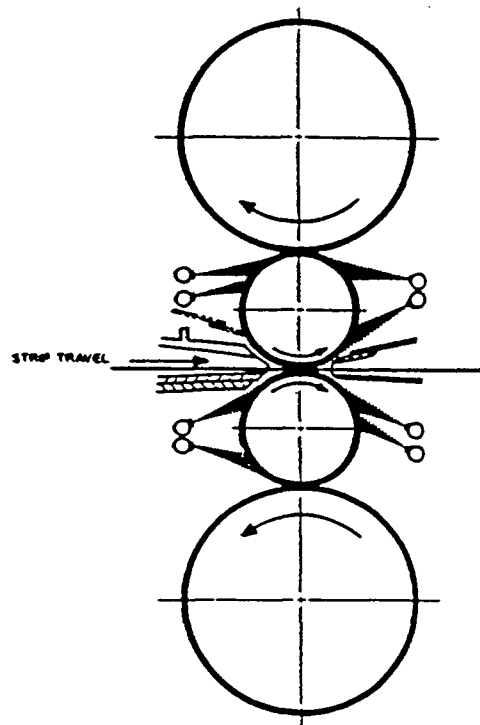
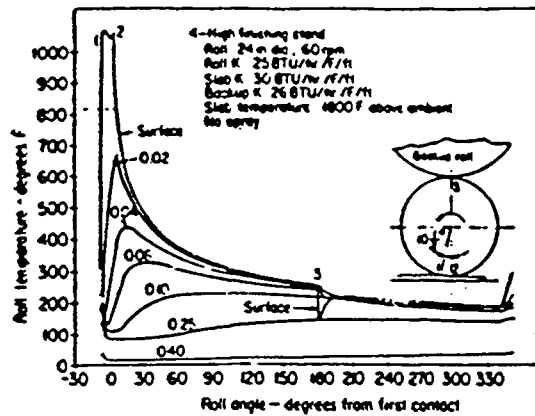
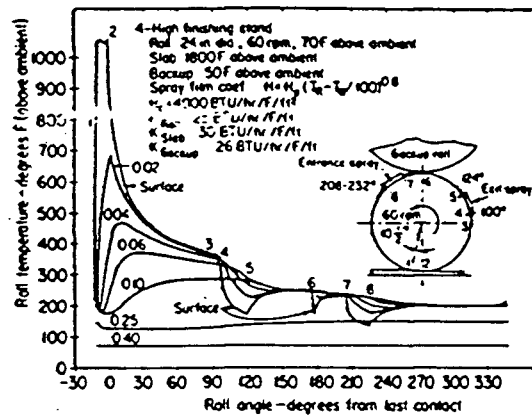


Fig.2.11 The typical recommended location of spray headers (Carpenter and Hannan [22]).

2.5 THERMAL CROWN CALCULATION



– Uncooled finishing roll after two revolutions.



– Cooled finishing roll after three revolutions.

Fig.2.12 Effect of roll cooling on the backup/work roll temperature (Parke and Baker [13]).

2.5 THERMAL CROWN CALCULATION

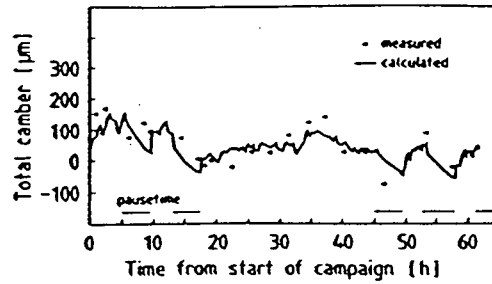


Fig.2.13 Measured and calculated work roll camber vs. time from start of campaign.[32]

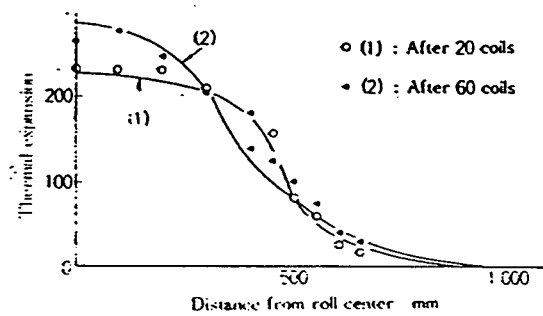


Fig.2.14 a) Comparison of calculated and measured values of roll thermal crown.[33]

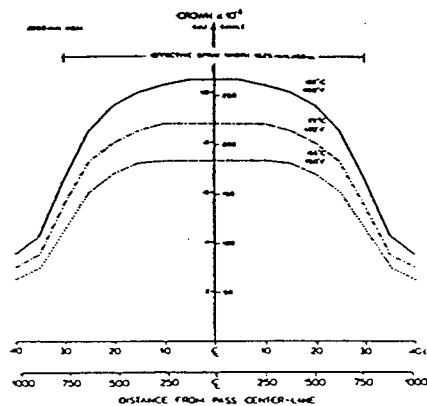


Fig.2.14 b) The predicted thermal crown by preheating work roll with hot water.

2.5 THERMAL CROWN CALCULATION

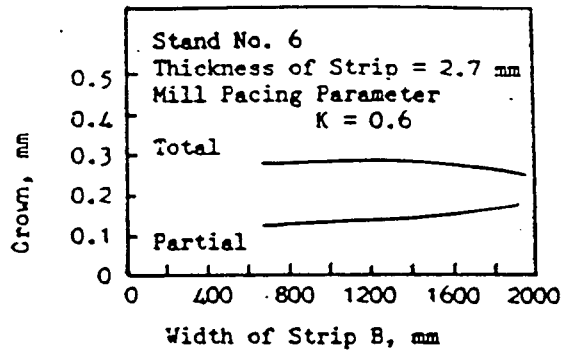


Fig.2.15 Relationship between thermal camber and the width of the strip (Wilmotte and Mignon [31]).

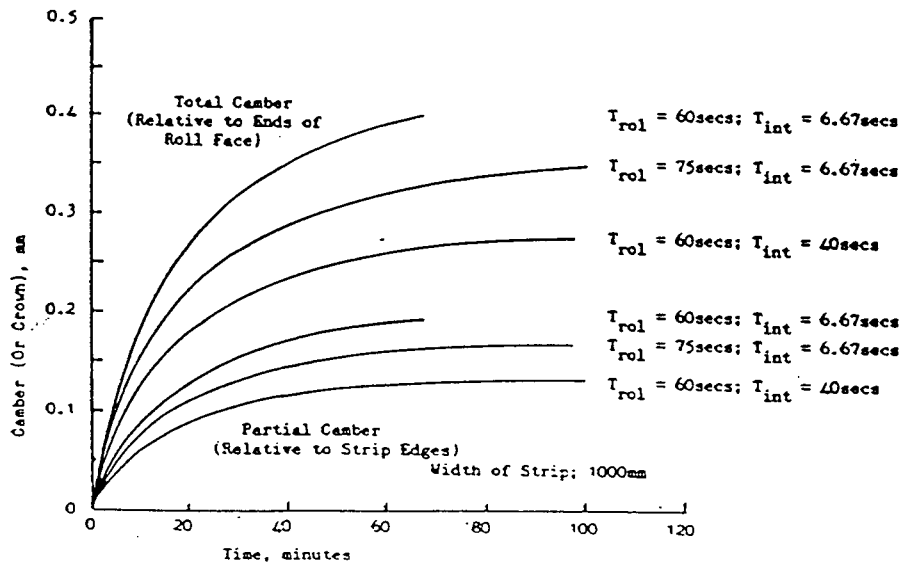


Fig.2.16 Theoretical variation of camber with time (Wilmotte and Mignon [31]).

3 SCOPE AND OBJECTIVES

The comprehensive literature review highlights the gap in knowledge of work roll thermal behavior in a hot mill. The present work was undertaken to increase the understanding of the application of the roll cooling to work roll thermal behavior and thermal crown development. The ultimate goal is to arrive at an optimum design of work roll cooling to improve work roll life and provide suitable compensation for the roll bending crown.

To achieve the above goal, the following objectives were pursued:

1. To investigate the influence of the spray-cooling configuration of a work roll on the roll thermal behavior.
2. To investigate the effects of the roll-gap heat transfer coefficient and roll diameter respectively on the roll temperature.
3. To reevaluate the factors influencing the thickness of the thermal layer near the roll surface.
4. To develop a two-dimensional model of heat transfer for calculating the thermal field inside the work roll.
5. To calculate roll thermal expansion and crown based on the thermal field predicted by the two dimensional thermal model.
6. To investigate the effects of spray-cooling configuration and roll-gap heat transfer respectively on the roll thermal crown. The effect of mill pacing which is a measure with respect to rolling and idle times is also examined.

3 SCOPE AND OBJECTIVES

This work was primarily focussed on examining the roll spray-cooling effect on the work roll thermal behavior in a hot-rolling mill.

The methodology adopted to achieve the above objectives are as follows:

1. The investigation of work roll cooling was based on a previously developed one dimensional model of heat transfer [9].
2. The roll-gap heat transfer coefficients with and without lubrication were obtained by interpolation of the data from Devadas' thesis (Fig.4.12). An average roll-gap heat transfer coefficient of $60\text{kw/m}^2\text{°C}$ was also considered in the calculation for comparison purposes.
3. The thermal layer thickness near the roll surface was recalculated by a comparison of temperatures along the roll interior boundary at a given thermal layer thickness of the surface until the normal temperature difference was less than 1% and the temperature gradient in the radial direction decreased to zero.
4. A two dimensional thermal model of the work roll was developed and solved by the numerical finite difference method: the Alternating Direction Implicit method (ADI).
5. The roll thermal expansion was calculated assuming axi-symmetric deformation of the roll.
6. The rolling force, strip reduction, and other rolling parameters from an industrial operation were estimated using rolling theory and were incorporated into the model calculation.

4 INVESTIGATION OF WORK ROLL COOLING

The investigation of work roll cooling has been carried out using Devadas' one-dimensional thermal model of work roll[9]. The validity of the model has been tested by simulating the conditions at Stelco's hot strip mill and comparing model prediction of strip surface temperature with measurements. In this model the work roll thermal history has been calculated for normal cooling conditions in a hot strip mill and spray configuration has been employed to calculate water flux and heat transfer coefficients. Therefore the model is a convenient tool to study the effect of work roll cooling on roll thermal history to gain insight into the process.

4.1 MODEL DESCRIPTION

In hot rolling the work rolls receive heat from the following sources given in Fig. 4.1. 1). by conduction from the hotter strip through a layer of oxide; 2). by radiation from the strip on the entry and delivery side of the roll bite; 3). by frictional effects along the arc of contact in the roll bite; 4). from other sources such as friction in the roll-neck bearings and rolling friction at the backup/work roll contact. The heat losses depends on the roll surface boundary conditions given in Fig. 4.2, i.e. through cooling sprays, conduction to the backup roll, boiling and natural convective loss to the coolant. The heat transfer in the rolls should be ideally determined by 3-dimensional analysis given in Fig. 4.3 along directions r , θ , z , as described in equation (2.1). Devadas [9] has employed the following assumptions to simplify the equation

- (1). Conduction along the axial direction z of roll is negligible;

4.1 MODEL DESCRIPTION

(2). Heat conduction in the circumferential direction is negligible compared to bulk flow by rotation of the rolls.

(3). The work rolls operate in a cyclic steady state.

Then the simplified equation is expressed by

$$\frac{\partial^2 T}{\partial r^2} + \frac{1}{r} \frac{\partial T}{\partial r} = \frac{1}{\alpha} \omega \frac{\partial T}{\partial \theta} \quad (4.1)$$

The heat transfer during rolling involves periodic variations of temperature and heat flow with the angle θ which can be related to time through the expression

$$\theta = \omega t$$

i.e.

then

$$\frac{\partial^2 T}{\partial r^2} + \frac{1}{r} \frac{\partial T}{\partial r} = \frac{1}{\alpha} \frac{\partial T}{\partial t} \quad (4.3)$$

To solve equation (4.3) for temperature distribution in the work roll, we need to specify boundary conditions, *i.e.* the heat transfer coefficient in the contact arc and cooling conditions. The cooling conditions can be divided into three types:

4.1 MODEL DESCRIPTION

1). Spray cooling in which we need to specify the rate of water flow. The heat transfer coefficient in Devadas's [9] calculation has been determined from Yamaguchi *et al.*'s [21] correlation

$$\dot{q}_{sp} = (1.11)(1.163)(10^5)\dot{W}^{0.521} \quad (4.4)$$

2). Boiling and natural convection depending on the surface temperature of the rolls

For $T < T_{sat}$, heat transfer is by natural convection

$$h = \left(\frac{k_w}{D} \right) \left\{ 0.11((0.5Re_w^2 + Gr_D)Pr)^{0.315} \right\} \quad (4.5)$$

For $T_{sat} < T < T_{max}$, Rohsenow's [36] correlation for nucleate boiling has been employed

$$\dot{q} = \mu_w h_{fg} \left\{ \left(g \frac{(\rho_w - \rho_s)}{\sigma_{st}} \right) \right\}^{\frac{1}{2}} \left(\frac{c_{pl}\Delta T_x}{c_{sf}h_{fg}Pr_l^n} \right)^3 \quad (4.6)$$

For $T > T_{max}$, the heat transfer coefficient of unstable film boiling is obtained by interpolating Nukiyama's [37] boiling heat transfer data.

3). Radiant cooling and natural convection: A pseudo heat transfer coefficient to account for radiation is employed

$$h_{rad} = S\epsilon(T) \frac{(T^4 - T_a^4)}{(T - T_a)} \quad (4.7)$$

4.1 MODEL DESCRIPTION

The rolling temperature dependent emissivity [38] is used

$$\varepsilon(T) = \frac{(T - 273)}{1000} \left\{ 0.125 \frac{(T - 273)}{1000} - 0.38 \right\} + 1.1 \quad (4.8)$$

For all of the three types we must describe the angles for each cooling zones along the circumference and the associated heat transfer coefficients. Devadas and Samarasekera [1] in their calculation have employed the relevant mathematical expressions in equations (4.4) to (4.8) to determine the heat transfer coefficients of the three different cooling types and combined with equation (4.3) to have solved for the temperature distribution by the finite difference method. It turns out that the cyclic temperature variations occurring during each revolution of the roll are confined to a surface layer. According to Tseng's [12] definition as indicated in section 2.3,

$$\delta = Ar_o Pe^{-\frac{1}{2}} \quad (4.9)$$

But the case Tseng [12] has considered is the one with uniform convection cooling over the circumference. While Devadas [9] has considered the three types of cooling conditions around the roll as mentioned above, which could influence the value of A because of its dependence on Biot number. This would cause a change in δ . Therefore A should be evaluated based on the three types of cooling. This will be checked in section 4.7.

because [39]

$$Pe_x = Re_x Pr$$

$$Re_x = \frac{\rho u_{\infty} x}{\mu}$$

4.1 MODEL DESCRIPTION

$$Pr = \frac{c_p \mu}{k}$$

then

$$Pe_x = u_\infty x \alpha^{-1}$$

where Re_x is the Reynolds number, Pr is the Prandtl number, x is the radial distance from the roll center.

Hence at the roll surface, $x = r_o$

$$Pe_x = r_o^2 \omega \alpha^{-1} \quad (4.10)$$

The approach employed in this investigation is to change the position of the spray headers with respect to the reference point in an attempt to investigate the influence on roll cooling. The basic mill cooling configuration from company A is shown in Fig. 4.4, which shows the relative positional relation between the four spray nozzles and wipers that prevent the spray water from pouring on to the strip. The roll cooling condition has been given in Table IV-I. Various cooling arrangements could be developed from the basic configuration by adjusting the relative positions of these spray nozzles with respect to the roll bite exit. In this study the following aspects have been investigated.

- 1). The effect of the entry and exit wipers on the work roll temperatures.
- 2). The effect of the position of upper spray nozzles on roll temperatures.

4.1 MODEL DESCRIPTION

- 3). The effect of increasing the water spray contact area on the roll surface.
- 4). The effect of employing a lubricant in the roll bite on the roll temperature.
- 5). The influence of the variation in the roll diameter on the roll temperatures and the surface layer thickness δ

The six typical cooling arrangements are considered as shown in Fig. 4.5--Fig. 4.10. The angles for each cooling zone have been changed in each configuration, but the water flow rates for the four cooling nozzles have been kept the same. The discretization of the work roll into nodes for finite difference analysis is shown in Fig. 4.11 with thirty nodes over the roll surface layer δ . The heat transfer coefficient with lubrication in the roll bite at a reduction of 50% is obtained by either the regression or interpolation from empirical data of heat transfer coefficient vs. rolling time as shown in Fig. 4.12. The temperature data is obtained for different specified cooling arrangements by employing the program developed by Devadas and Samarasakera [1]. A program to plot temperature vs. positions (or the angle θ) has been subsequently developed.

4.1 MODEL DESCRIPTION

Table IV-I Roll Cooling Condition for Company A

Number of Cooling Zones 12			
Angle Number	Degrees	Type	Water Flow l/min.
1	37.0	1	0.0
2	37.0	2	0.0
3	35.0	2	0.0
4	13.0	3	2660.8
5	12.0	2	0.0
6	20.0	3	1090.1
7	63.0	1	0.0
8	14.0	3	1090.1
9	13.0	2	0.0
10	10.0	3	2660.8
11	25.0	2	0.0
12	71.5	1	0.0
Type 1 : Radiation and Air CC Type 2 : Boiling and Water CC Type 3 : Spray Cooling			

4.1 MODEL DESCRIPTION

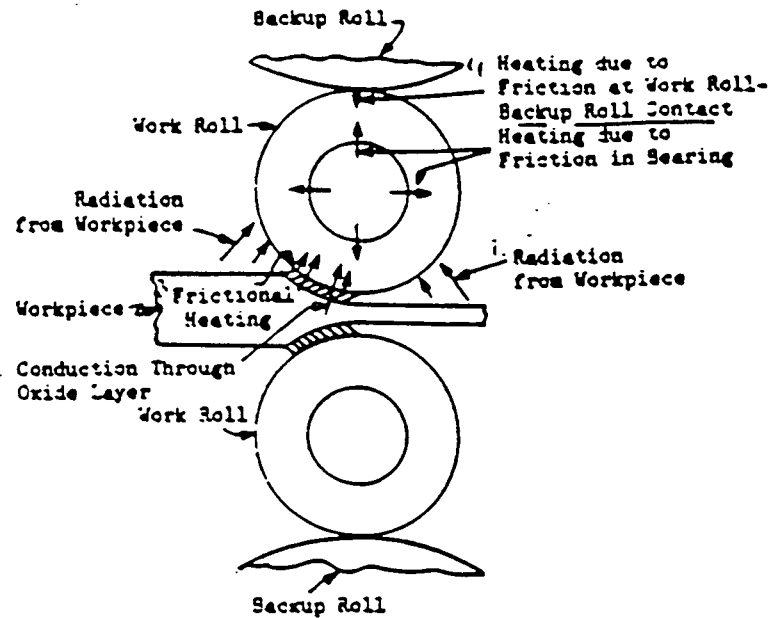


Fig.4.1 Sketch showing the heat flow into a work roll.

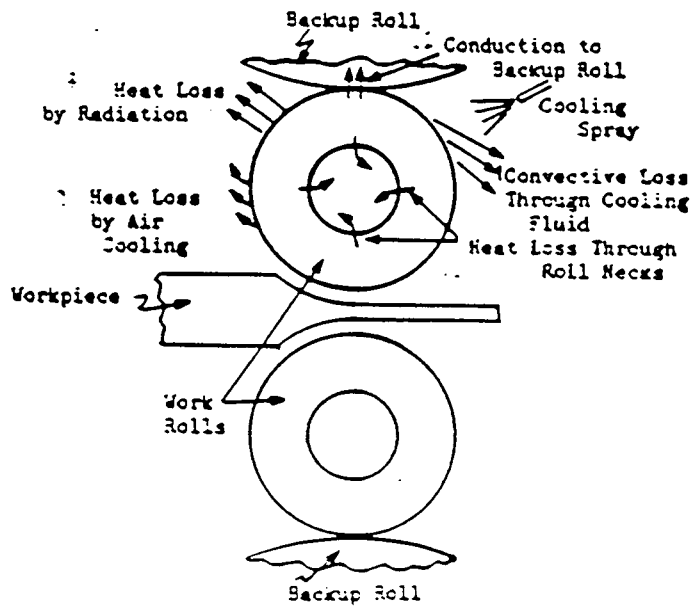


Fig.4.2 Sketch showing the heat losses from a work roll.

4.1 MODEL DESCRIPTION

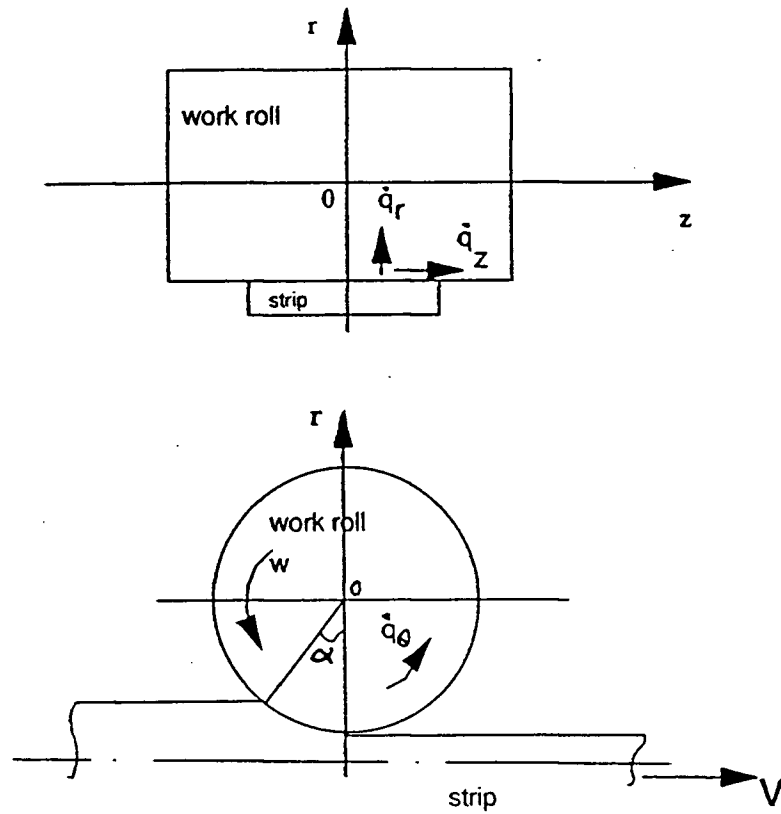


Fig.4.3 Sketch showing the rate of heat flow in three dimensions.

4.1 MODEL DESCRIPTION

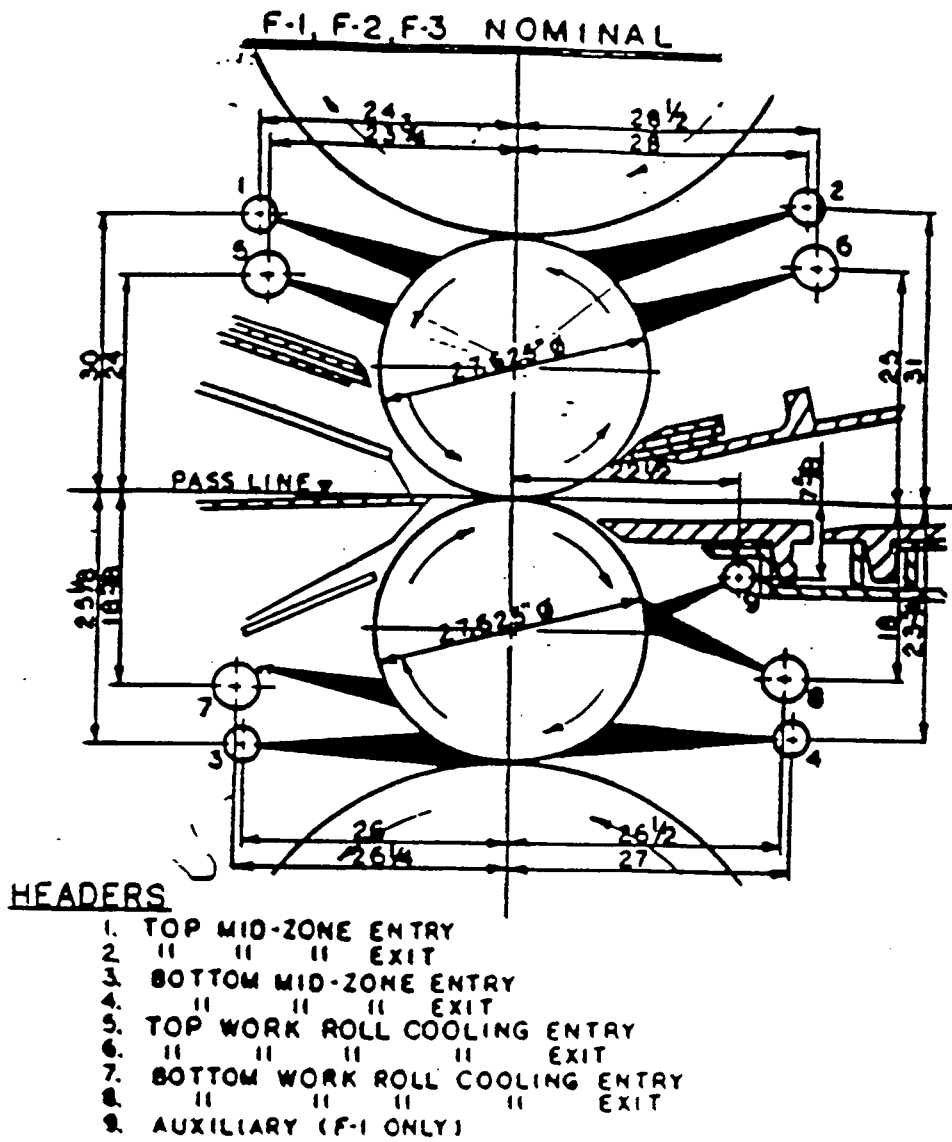


Fig.4.4 The basic positions of the spray headers relative to the work roll.

4.1 MODEL DESCRIPTION

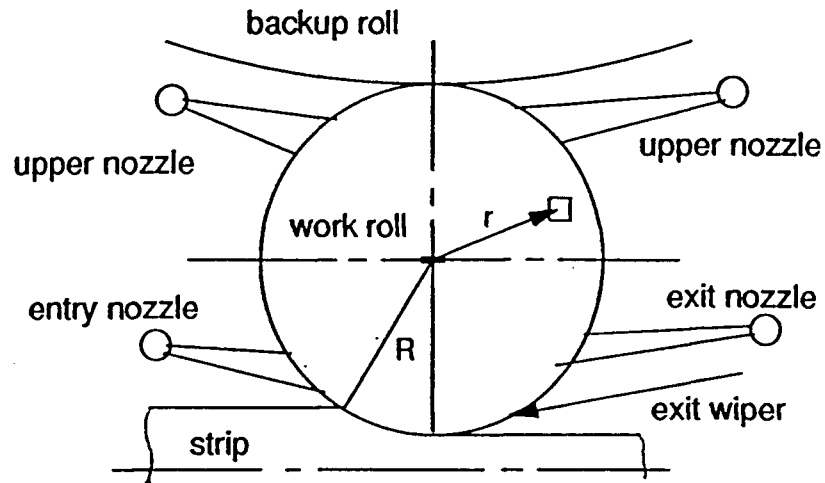


Fig.4.5 Spray-cooling arrangement without the entry-wiper.

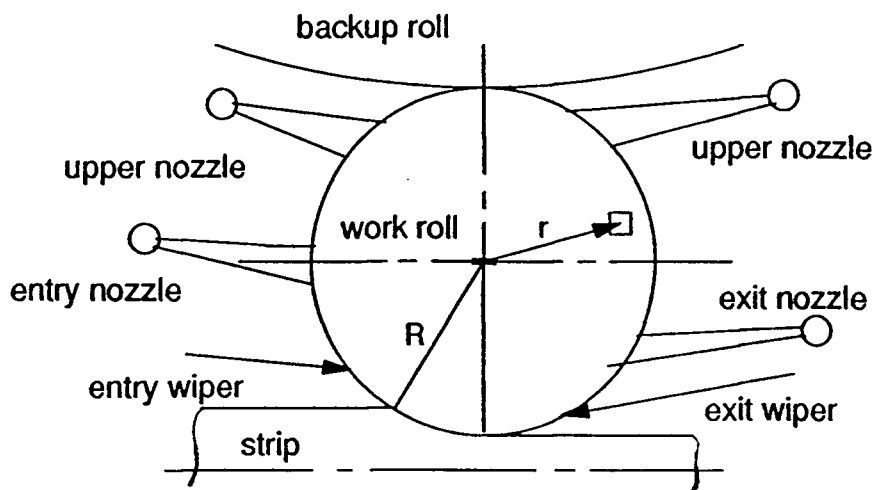


Fig.4.6 Spray-cooling arrangement with the entry-wiper.

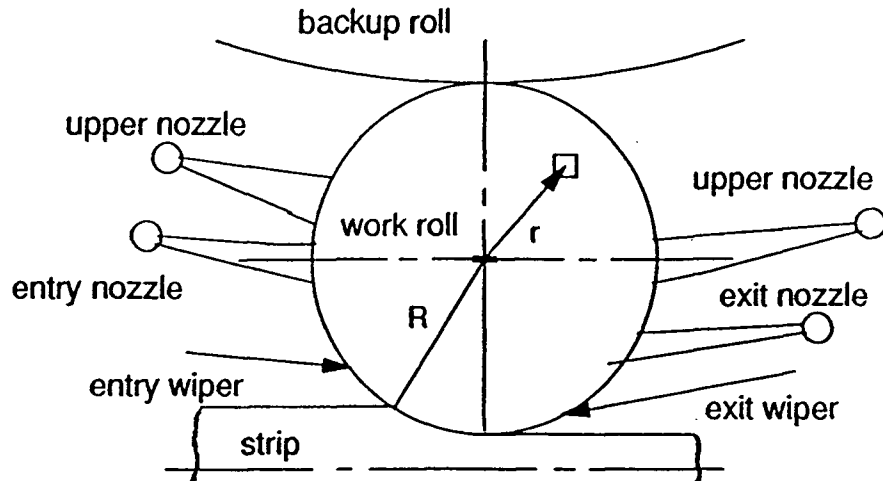


Fig.4.7 The upper spray-nozzles are positioned away from work/backup roll contact and close to the lower ones.

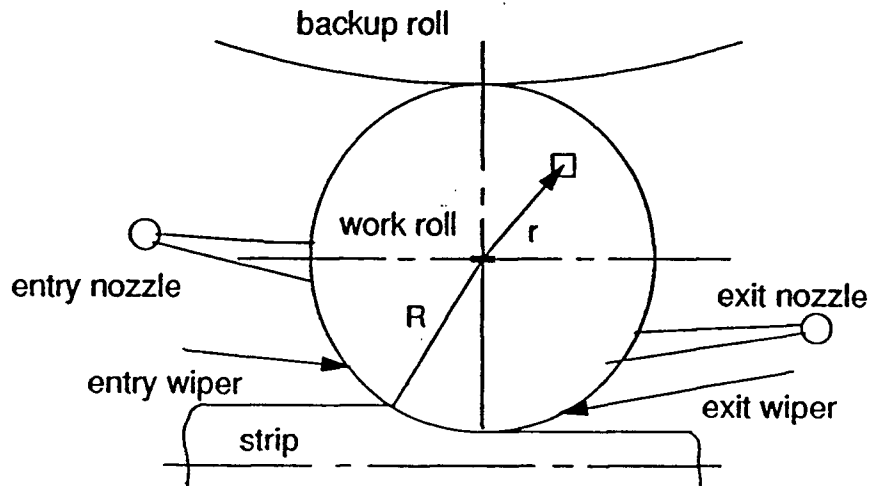


Fig.4.8 The arrangement without upper nozzles.

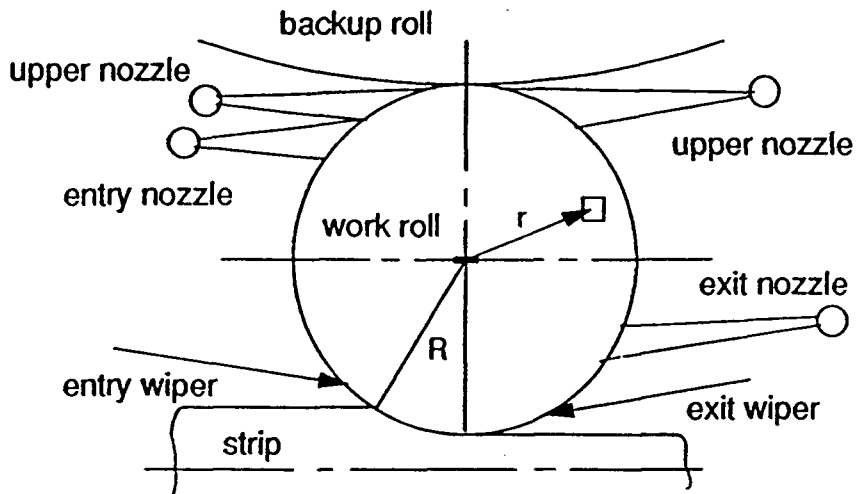


Fig.4.9 The arrangement with the upper spray-nozzles and the entry-side nozzle close to the work/backup roll contact as much as possible.

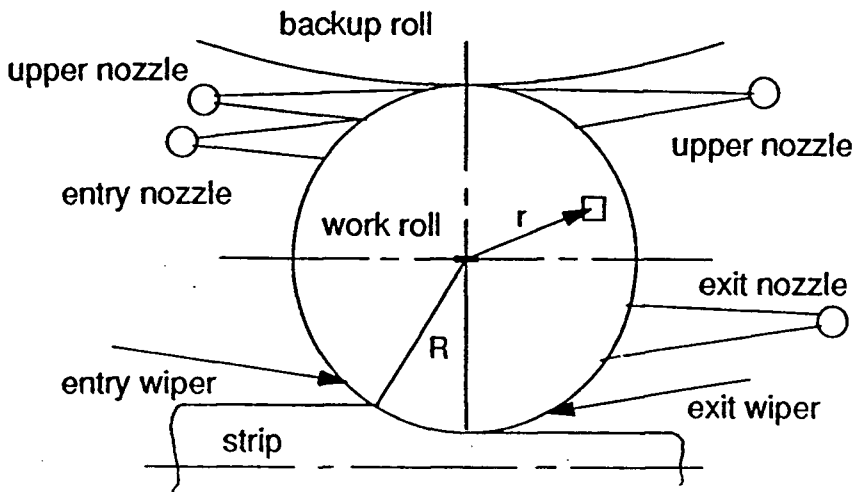


Fig.4.10 The arrangement with larger surface area of spray impingement from the exit-side spray.

4.1 MODEL DESCRIPTION

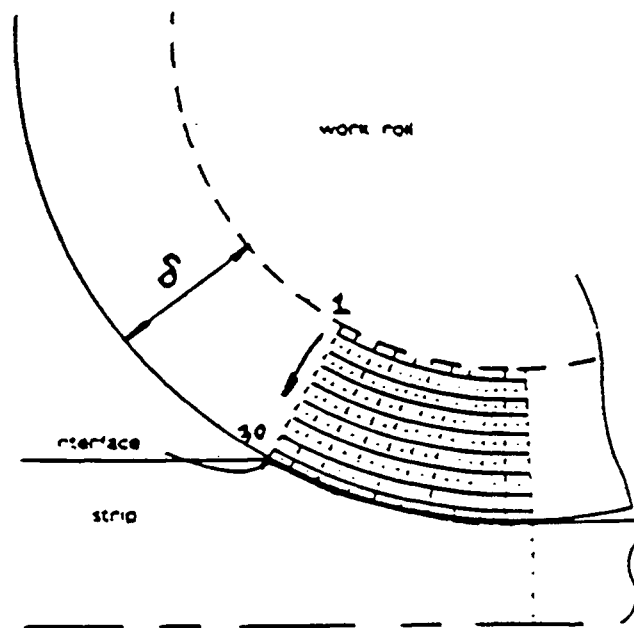


Fig.4.11 The discretization of work roll into nodes for finite difference analysis.

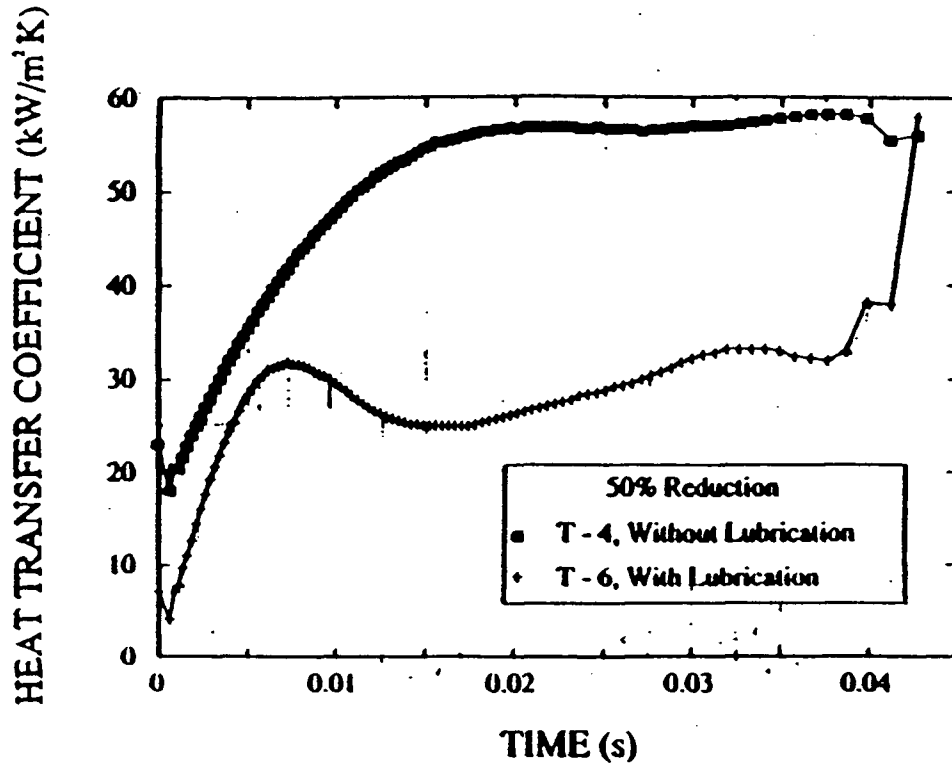


Fig.4.12 Effect of lubrication on the heat transfer coefficient in the roll-gap from Devadas's thesis.

4.2 THE CYCLIC TEMPERATURE OF WORK ROLL

It is evident from the model predictions of the work roll temperatures in Fig. 4.13--Fig. 4.15 that the roll surface temperature experiences the largest variation during each revolution. For example in Fig. 4.13a the cyclic temperature difference between the maximum temperature and the minimum temperature of the roll surface ($r/R=1$) is 303°C . This is because the maximum surface temperature is largely determined by conditions in the roll gap. When the rolls first come into contact with hot strip the rate of heat flow into the roll is highest since it is proportional to the temperature difference between hot strip and work roll surface. The work roll surface has a much lower temperature than the strip at entry on each revolution. Furthermore the heat transfer coefficient in the roll bite, as shown in Fig. 4.12, rises rapidly within the roll bite possibly due to the rapid rise in roll pressure over the backward slip region. Both parameters contribute to the rapid increase in temperature. At increasing depths beneath the roll surface ($r/R=0.99, 0.98$, and 0.97 respectively) the cyclic temperature difference is much smaller than that at the roll surface. For example in Fig. 4.13a the maximum cyclic temperature difference for $r/R=0.99$ inside the roll surface is only 16°C .

4.2.1 The Surface Temperature Gradient during Roll Bite

It can be seen from Fig. 4.13--Fig. 4.15 that the temperature gradient in the roll bite is very steep at the surface during each revolution due to the large heat input into the roll, and it declines later in the roll bite. The decrease could be due to two reasons: one is that the temperature

4.3 EFFECT OF SPRAY NOZZLE POSITION ON ROLL THERMAL BEHAVIOR

difference between the strip and work roll surface decreases with the rapid increase in the roll surface temperature; another is that the heat transfer coefficient remains almost constant towards the end of the roll bite.

4.2.2 The Minimum Surface Temperature

The minimum surface temperature is determined by the roll cooling conditions. As shown in Fig. 4.13a, the surface temperature ($r/R=1$) has been depressed to 26°C by the intensive local action of the spray headers resulting in the severe drop in roll surface temperature. The minimum surface temperature is depressed 40°C below the roll core temperature at the internal boundary ($R-\delta$ shown in Fig.2.8 b).). The surface temperature depression should be minimized as much as possible since it produces tensile strain in the surface leading to thermal fatigue. Thus it appears that the roll life could be improved by developing a new roll cooling arrangement with the aim of reducing the magnitude of the surface temperature depression. Stevens *et al.* [2] has recommended a new cooler for this purpose.

4.3 EFFECT OF SPRAY NOZZLE POSITION ON ROLL THERMAL BEHAVIOR

4.3.1 Effect of Entry and Exit Spray Wipers and Lower Spray-nozzle Position

4.3 EFFECT OF SPRAY NOZZLE POSITION ON ROLL THERMAL BEHAVIOR

In industrial practice the entry and exit wipers have been applied to prevent cooling water from pouring onto the strip and reducing the strip temperature which causes a change in strip properties. The use of the wipers requires that the entry and exit spray-nozzles are positioned away from the roll gap which influence the rate of heat flow out of the roll. Fig.4.13 shows the effect of the entry wiper and exit wiper on work roll temperature. Fig. 4.13a is the case without an entry wiper, with a cooling arrangement shown in Fig. 4.5. There are four spray cooling nozzles distributed around the work roll: an entry spray nozzle, two upper spray nozzles and an exit spray nozzle. The entry spray nozzle is positioned close to the strip entry point. It is seen from Fig. 4.13a that the surface temperature rises to 329°C in the roll gap and drops to 26°C during spray cooling. The cyclic temperature difference rapidly decreases with depth beneath the roll surface, and at a distance δ from the surface the roll body temperature is 63°C at strip entry with only a slight variation during roll rotation.

Fig. 4.13b is the case with an entry wiper and also an exit wiper. It is arranged by displacing the entry spray nozzle some distance from the entry wiper and putting the entry wiper close to the strip entry as shown in Fig. 4.6. It turns out that the surface temperature rises to 333°C, which is an increase of 5°C compared to the case in Fig. 4.13a, and drops to 26°C during spray cooling. The roll core temperature is 64.5°C at strip entry, an increase of 2°C.

Fig. 4.13c is the case without the entry and exit wipers. The exit and entry spray nozzles are positioned close to the strip exit and entry points respectively as shown in the sketch in Fig. 4.13c. The peak surface temperature is observed to be 323°C, a decrease of 6°C compared to the case in Fig. 4.13a. The roll core temperature drops to 46°C from 63°C at the strip entry

4.3 EFFECT OF SPRAY NOZZLE POSITION ON ROLL THERMAL BEHAVIOR

point which causes a 27 percent change in roll core temperature. Although this case gives the lowest core and surface temperature it is not a practical arrangement because there would be too much water on the strip. It demonstrates however that the roll core temperature is more sensitive to the position of exit spray nozzle than the entry one. The peak temperature at the roll surface can be decreased when either the entry spray nozzle or exit spray nozzle, or both of them, are positioned close to the roll bite.

4.3.2 Effect of Upper Nozzle Positions

Fig. 4.14a shows the roll temperature distribution for the cooling configuration shown in Fig. 4.7 where the upper spray nozzles are displaced near the lower exit and entry nozzles. The roll surface temperature goes up to 335°C at the end of roll bite and drops to 27°C during spray cooling. The roll core temperature is 67°C at the gap entry. Again only a slight change in temperature in the surface layer of work roll is observed. Fig. 4.14b shows the roll temperature distribution for the cooling configuration without the two upper spray nozzles present as shown in Fig. 4.8. The peak surface temperature turns out to be 342°C, an increase of 7°C compared to that in Fig. 4.14a.

In Fig. 4.9, the two upper nozzles are directed at the contact point between backup rolls and work rolls. This arrangement assures coverage of a larger portion of roll surface. The peak surface temperature is observed from Fig. 4.15a to be 333°C, and the minimum surface temperature is 26°C. The roll core temperature is 61°C, a decrease of 6°C compared to that in Fig. 4.14a. Thus the upper nozzles and their positions influence both the surface temperature

4.3 EFFECT OF SPRAY NOZZLE POSITION ON ROLL THERMAL BEHAVIOR

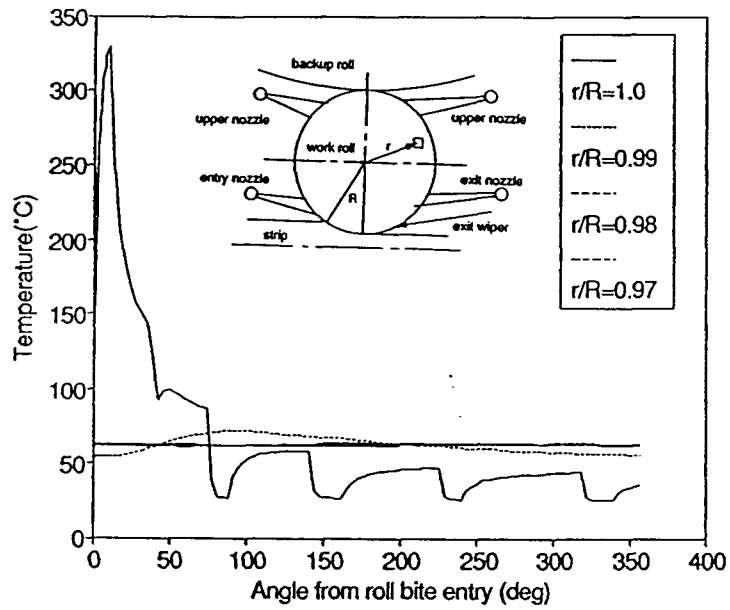
and the roll core temperature, with the influence on the core temperature being stronger.

It is seen from comparing Fig. 4.14a and Fig. 4.13a that the closer the upper nozzles are to the exit and entry nozzles, the greater is the increase in the roll core temperature. Also the temperature rises appreciably when removing the two upper nozzles as seen from Fig. 4.14b. Two possible reasons for the temperature increase are that first owing to the longer time between sprays as in the case of Fig. 4.14a more heat is allowed to transfer into the roll to cause the roll temperature to increase; secondly the water stream contact area is reduced when the spray nozzle is located closer to the entry nozzle as in the case of Fig. 4.14a, resulting in smaller amount of heat extracted from the work roll.

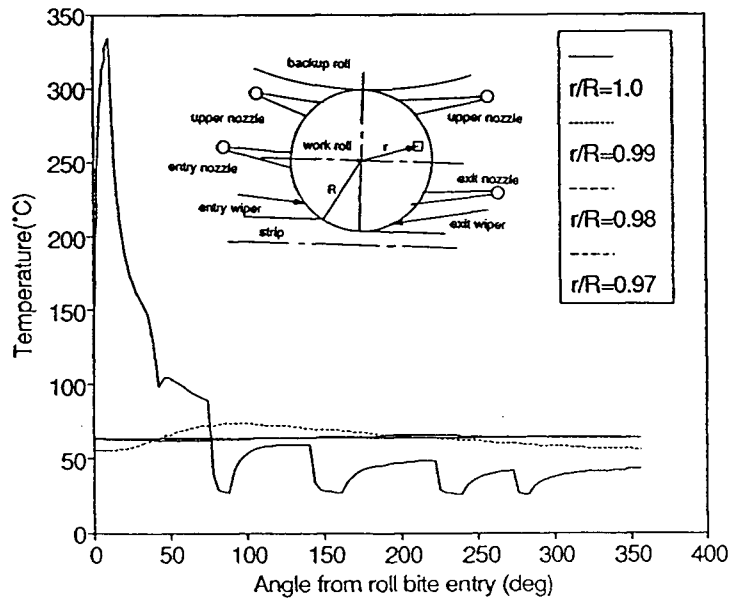
4.3.3 Effect of Water Stream Contact Area

Fig. 4.15b shows the results of the roll temperature for the cooling configuration in Fig. 4.10. By adjusting the spray header position the roll contact angle of the water stream from the exit spray nozzle can be increased as shown from 15°C in Fig. 4.9 to 30°C in Fig. 4.10. The position of the rest of the spray nozzles remain unchanged. It is observed in Fig. 4.15b that the peak surface temperature reaches 332°C, and the roll core temperature is 58°C, A decrease 3°C compared to Fig. 4.15a. Thus the core temperature can be reduced by increasing the contact angle, i.e. increasing the contact area. Because the quantity of heat transferred (Q) is proportional to the contact area, more heat flows out of the roll when a larger spray contact area is applied.

4.3 EFFECT OF SPRAY NOZZLE POSITION ON ROLL THERMAL BEHAVIOR



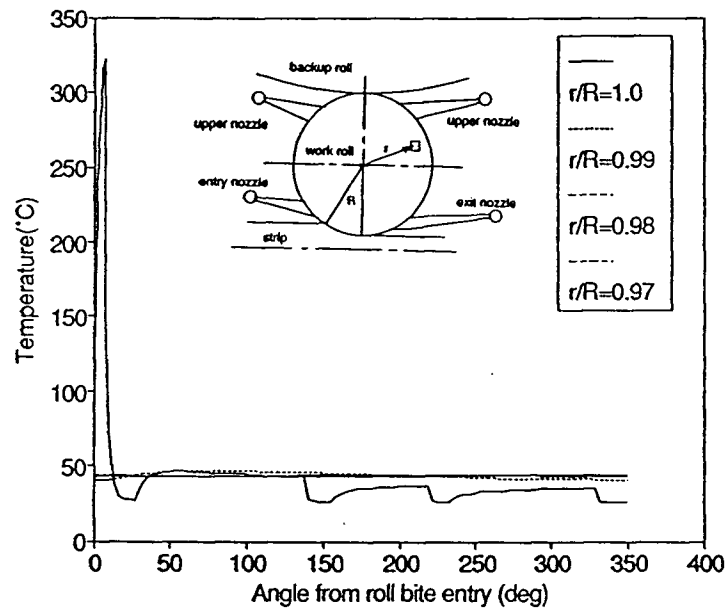
a).



b).

Fig.4.13 The effect of introducing the entry and exit wipers on work roll temperature.

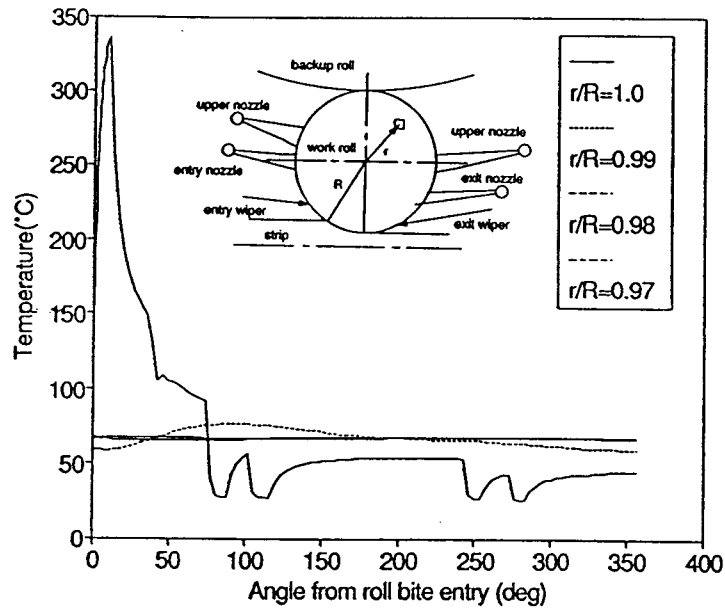
4.3 EFFECT OF SPRAY NOZZLE POSITION ON ROLL THERMAL BEHAVIOR



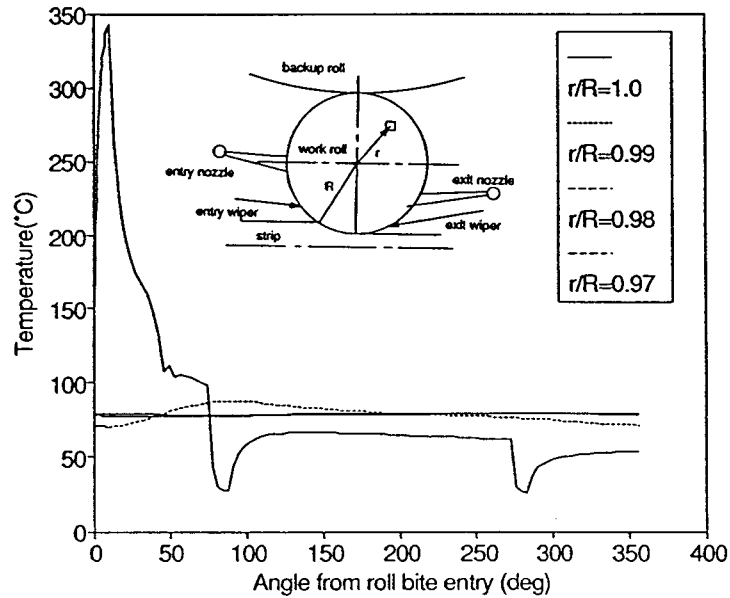
c).

Fig.4.13 The effect of introducing the entry and exit wipers on work roll temperature.

4.3 EFFECT OF SPRAY NOZZLE POSITION ON ROLL THERMAL BEHAVIOR



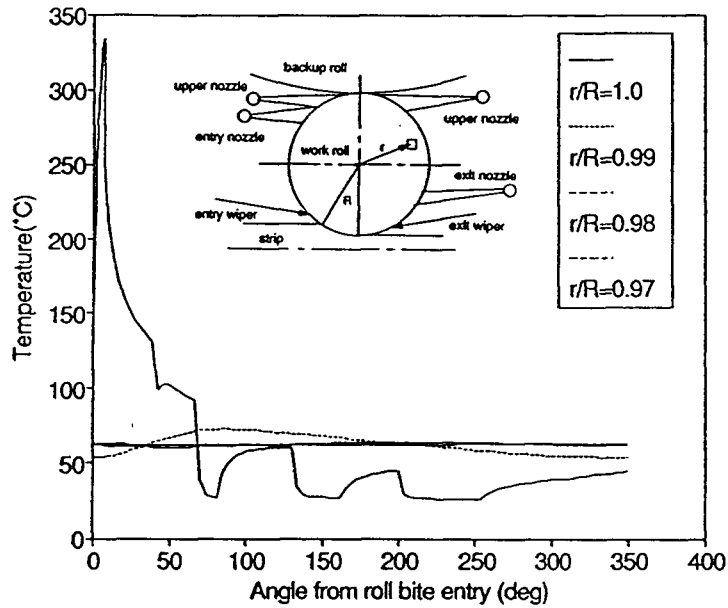
a).



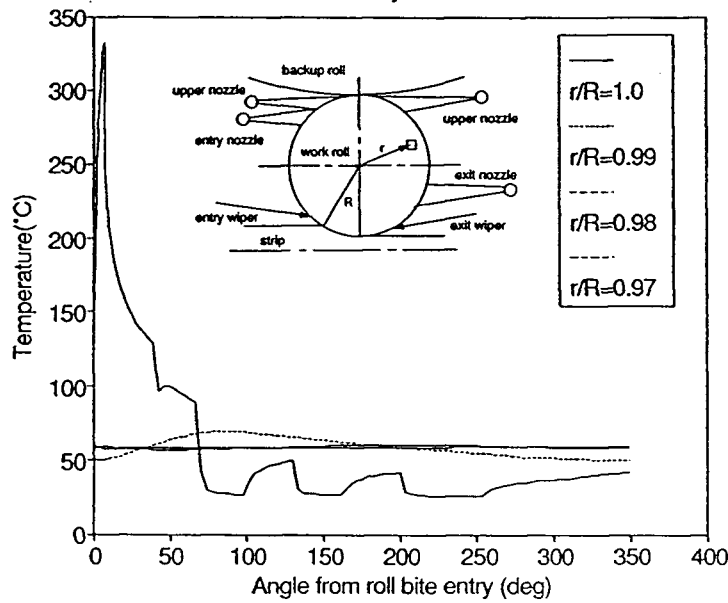
b).

Fig.4.14 The effect of the upper nozzle positions on work roll temperature.

4.3 EFFECT OF SPRAY NOZZLE POSITION ON ROLL THERMAL BEHAVIOR



a).



b).

Fig.4.15 The effect of increasing the spray-impingement area over the roll-surface on the roll temperature.

4.4 EFFICIENT COOLING ARRANGEMENT

The peak surface temperature vs. cooling arrangements is shown in Fig. 4.16 for the six cooling configurations of Fig. 4.5 -- Fig. 4.10. The purpose of reducing the cyclic temperature variation in the roll surface is to reduce thermal strain and improve the roll life; also for reducing abrasion wear, the low peak surface temperature and small cyclic temperature variation are required. Thus the cooling configuration No.6 shown in Fig. 4.10, which gives the lowest peak surface temperature and smallest cyclic temperature variation, is recommended. For the cooling arrangement (No.4) in which the two upper nozzles were removed, the highest temperature is observed indicating the important role of the upper nozzles in decreasing the roll surface temperature.

Fig. 4.17 shows the roll core temperature vs. cooling arrangements. The tendency is the same as that observed for the surface temperature and cooling arrangement No.6 gives rise to the lowest roll core temperature. From the stand point of work roll cooling to minimize the temperature variation within the body of the roll, to reduce the possibility of roll breakage and minimize the change in roll surface profile due to thermal camber, a small difference between the roll core and peak surface temperature is required. Cooling arrangement No.3 which gives smaller difference between the core and peak surface temperature may be desirable. It is observed that the roll core temperature is more sensitive to the change in spray nozzle arrangement, since larger relative changes in temperature are obtained. For example, comparing configuration No.4 with No.6 the change in the magnitude of the peak surface temperature is 3% as indicated in Fig. 4.16 for the case of no lubrication, while the corresponding change in magnitude of the roll

4.4 EFFICIENT COOLING ARRANGEMENT

core temperature is 34% as indicated in Fig. 4.17. It has been evident that the closer the lower sprays are to the exit and entry of the roll bite, the lower the roll core temperature will be, especially for the exit spray. An exit spray positioned as close as possible to the roll bite can gain the most efficient cooling since the rate of heat transfer is proportional to the temperature difference. However it can cause large difference in the roll core and surface temperature. The conclusion can be clear through a thermal stress analysis of the roll combined with mechanical stress by the influence of high pressure process. The influence of lubrication on roll temperatures will be examined in the following section. The following table shows the comparison of the temperature data from the six arrangements.

Table IV-I-I Temperature Values for the Six Different Arrangements

Temperatuer (°C)	Cooling arrangement					
	No.1	No.2	No.3	No.4	No.5	No.6
T_{max}	329	333	335	342	333	332
T_{min}	26	26	26	26	26	26
T_{core}	63	64.5	67	79	61	58
T_{cyc}	303	307	309	316	307	306
$T_{max-core}$	266	268.5	268	263	272	274

* Arrangement No.1 is not applicable in industry since a wiper must be considered at the roll gap entry and exit.

4.4 EFFICIENT COOLING ARRANGEMENT

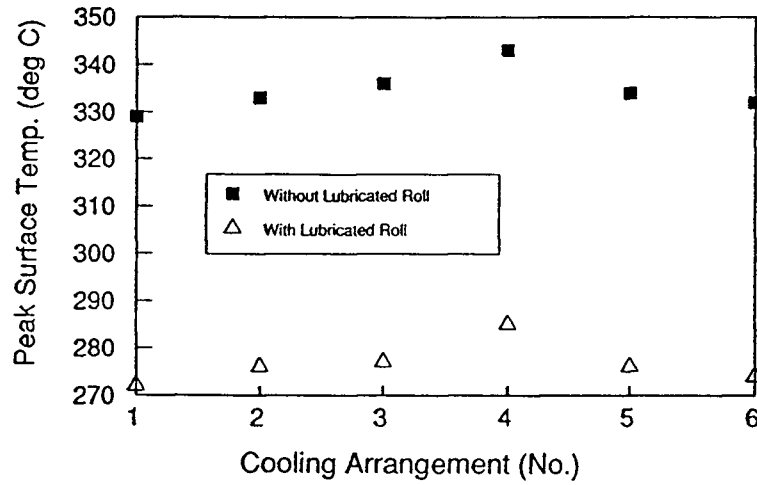


Fig.4.16 The variation of the peak surface temperature with the spray-cooling arrangement.

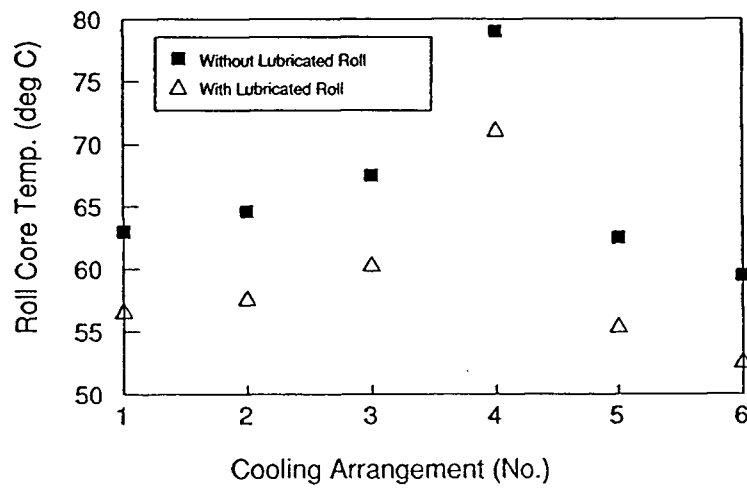


Fig.4.17 The variation of the roll core temperature with the spray-cooling arrangement.

4.5 Comparison of Three Industrial Operations of Work Roll Cooling

Spray cooling arrangements from three industrial operations have been utilized to compute the roll temperature and to compare their respective cooling systems. The three arrangements are the one previously shown in Fig.2.7 which referred to company A and two other configurations illustrated in Fig.4.18 a) and b) respectively. The three cooling conditions are listed in Table IV-I in section 4.1, Table IV-II and Table IV-III respectively. The calculated temperature profiles are shown in Fig.4.18 c) and d). Fig.4.18 c) shows the roll surface temperature profiles from the three cooling operations. The cooling arrangement from company B operation gives rise to the largest peak surface temperature leading to the largest cyclic temperature variation among the three operations since the minimum temperature is about the same for all of the operations. Large cyclic surface temperature variation will cause high thermal strain of the roll and could reduce roll life which is not desirable. Fig.4.18 d) shows the roll core temperature profiles from the three operations. The lowest roll core temperature was obtained with the operating conditions from company C since the areas of the roll in contact with water spray were largest. Large surface area coverage by the sprays results in high rate of heat transfer out of the roll due to forced convection leading to a decrease in the roll temperature. This is consistent with the previous conclusion obtained in section 4.3.3. Although the maximum surface cyclic temperature variations are about the same for the operations from company A and C as seen in Fig.4.18 c),

4.5 Comparison of Three Industrial Operations of Work Roll Cooling

the roll core temperature is about 20°C different between the two cases. Since there is a larger water stream contact area of the exit-sprays over the roll surface in the company C operation, the lower center temperature of 57°C is obtained in this case.

From a stand point of reducing thermal fatigue, a small difference between peak surface and roll core temperatures is desirable since thermal stress depends on this temperature differences. Therefore, as indicated by this prediction, the cooling operation from company A which gives rise to the smallest difference between roll surface and roll core temperatures as well as the lowest surface cyclic temperature variation may be the most efficient cooling operation among the three arrangements to reduce roll thermal stress and improve roll life.

4.5 Comparison of Three Industrial Operations of Work Roll Cooling

Table IV-II Roll Cooling and Rolling Condition for Company B

Number of Cooling Zones 12			
Angle Number	Degrees	Type	Water Flow l/min.
1	28.0	1	0.0
2	61.0	2	0.0
3	18.0	3	3884.8
4	13.0	2	0.0
5	20.0	2	0.0
6	20.0	1	0.0
7	20.0	1	0.0
8	59.0	3	1202.2
9	10.0	2	0.0
10	17.0	3	1202.2
11	38.0	2	0.0
12	45.3	1	0.0
Type 1 : Radiation and Air CC Type 2 : Boiling and Water CC Type 3 : Spray Cooling			
* Rolling condition: Roll reduction is 40% Roll speed is 30rpm Strip velocity is 0.8m/s Strip thickness is 0.032m HGP is given in Fig. 2.6			

4.5 Comparison of Three Industrial Operations of Work Roll Cooling

Table IV-III Roll Cooling Condition for Company C

Number of Cooling Zones 8			
Angle Number	Degrees	Type	Water Flow l/min.
1	42.0	1	0.0
2	27.0	3	2880.7
3	50.0	3	2820.7
4	19.0	3	2861.0
5	42.0	3	2740.8
6	103.0	2	0.0
7	22.0	3*	784.23*
8	44.25	1	0.0
Type 1 : Radiation and Air CC Type 2 : Boiling and Water CC Type 3 : Spray Cooling			

* Only for stand F1 to F3 where there is entry spray action.
 Rolling condition is given in Table IV-VII.
 HGP is given in Fig. 2.6.

4.5 Comparison of Three Industrial Operations of Work Roll Cooling

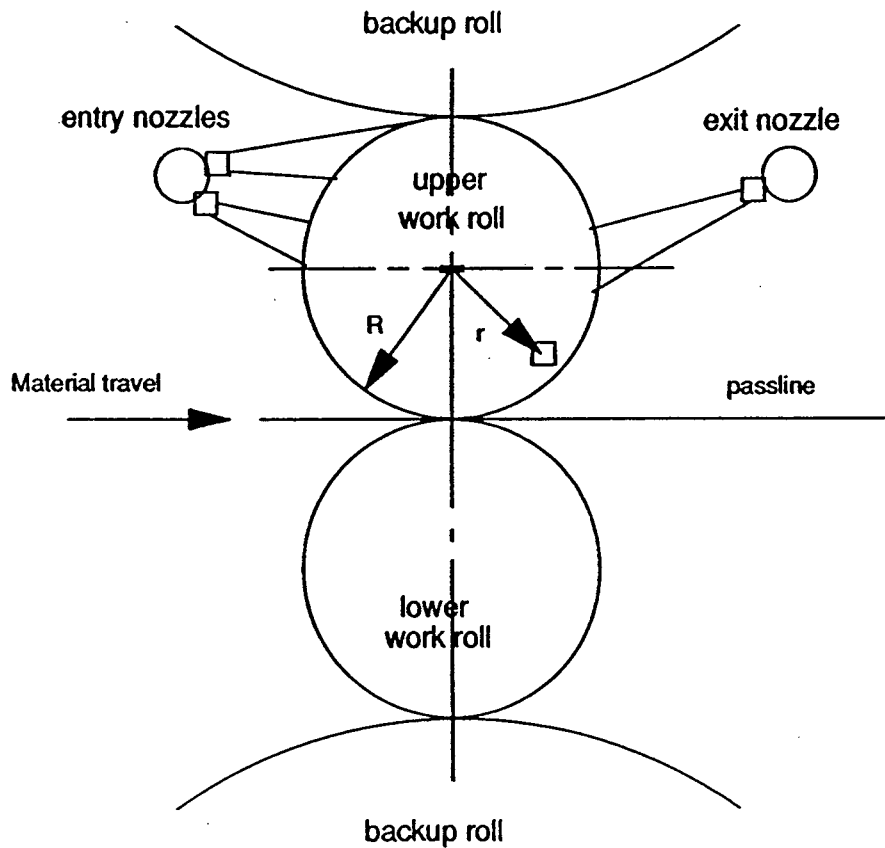


Fig.4.18 a) Schematic showing spray configuration from company B.

4.5 Comparison of Three Industrial Operations of Work Roll Cooling

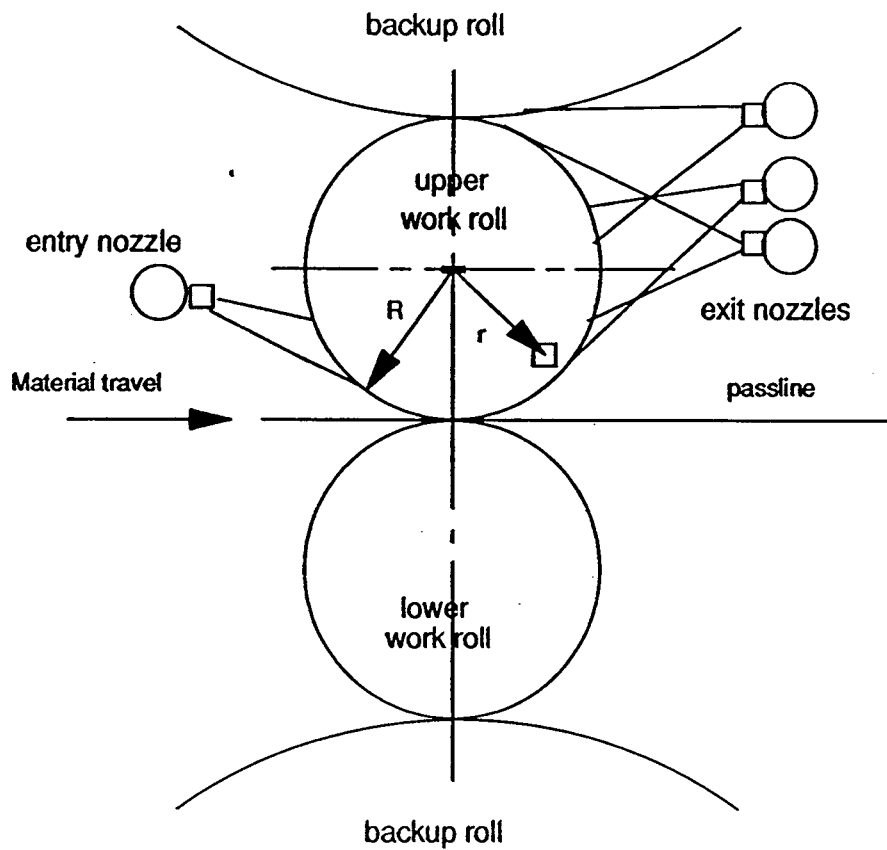


Fig.4.18 b) Schematic showing spray configuration from company C.

4.5 Comparison of Three Industrial Operations of Work Roll Cooling

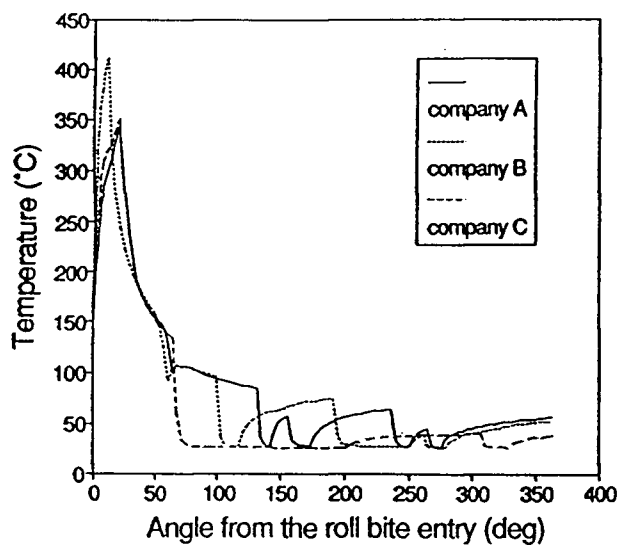


Fig.4.18 c) The surface temperature profiles from three different spray-cooling arrangements of industrial operations.

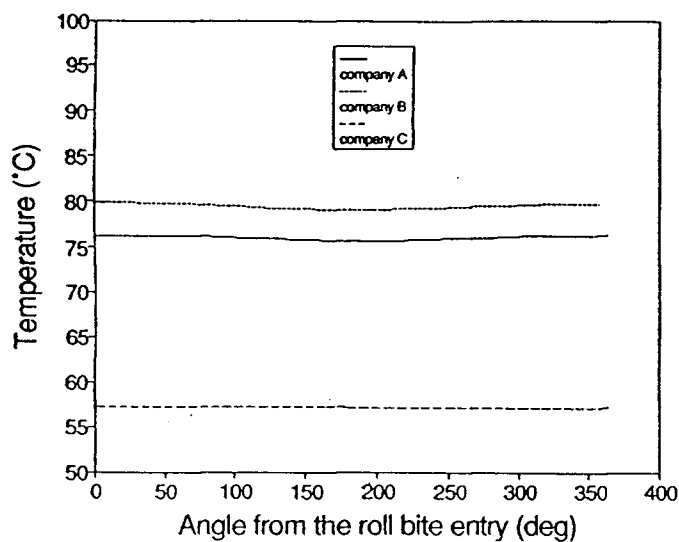


Fig.4.18 d) The roll core temperature profiles from three different spray-cooling arrangements of industrial operations.

4.6 EFFECT OF LUBRICANT IN ROLL BITE

The influence of the roll bite lubrication on roll temperature has been examined by employing the heat transfer coefficient from pilot mill experiments [9]. The curve of heat transfer coefficient vs. roll bite time has been given in Fig. 4.12 for a reduction of 50%. It can be seen that the heat transfer coefficient was much smaller with lubrication. For example, a decrease of 57% occurred at a roll bite time of 0.015 second. The data from the curve in Fig. 4.12 can be either regressed or interpolated for use in the model. The regression equation that was chosen is

$$H = a + bt + ct^2 + dt^3 \quad (4.11)$$

The values of a, b, c, d for segmental regression equation are listed in Table IV-IV. The r-squared for this correlation was 0.97.

The roll temperature distributions predicted by the model for the cooling arrangement in Fig. 4.6 are shown in Fig. 4.19. The effects of spray nozzles on work roll temperature are similar to those observed without roll lubrication. It is apparent that lubrication employed in the roll bite caused a decrease in both the roll-surface temperature and roll-core temperature, as expected. The two curves in Fig.4.19 a) showed the effect of lubrication on the roll-surface temperature. It can be seen that the peak surface temperature was reduced from approximately 340°C without lubrication to 275°C with lubrication, a decrease of 17%, while a 7°C reduction in the roll-core temperature was also obtained from this model prediction, as shown in Fig.4.19 b). This will undoubtedly reduce the propensity for the roll spalling by thermal fatigue. As recently indicated

4.6 EFFECT OF LUBRICANT IN ROLL BITE

by Averink [5], the adoption of lubrication in the first two stands of the Lake Erie Works hot-strip mill decreased the incidence of roll peeling. This demonstrates the efficiency of roll lubrication in reducing roll temperatures in addition to the documented benefits of lowering roll forces.

To assess the influence of roll-strip heat transfer on strip thermal history, Devadas' model [9] has been employed to compute the strip and roll temperatures for a seven stand operation. Mean roll-gap heat transfer coefficient of $60\text{kw/m}^2\text{C}$ and $30\text{kw/m}^2\text{C}$, which corresponds to steady-state values determined on the pilot mill with and without lubrication, have been chosen for comparative purposes. The computed surface and centerline temperature variation of the strip during rolling are compared in Fig.4.20 and 4.21 for the two heat transfer coefficients. From Fig.4.20 it is evident that roll contact causes considerable chilling at the surface as seen earlier, but more importantly gives rise to a 100°C difference in finish mill exit surface temperature which decreases to a difference of 30°C due to conduction from the interior. The steeper gradients established between the surface and the interior when $60\text{kw/m}^2\text{C}$ is employed as a roll-gap, heat-transfer coefficient is primarily responsible for the greater decline in centerline temperature in the interstand region in comparison to the other case. The resulting difference in centerline temperature at the exit of the seven stand operation is approximately 30°C . Although the rolls chill a narrow zone near the surface of the strip their influence extends to the centerline because of conduction and hence accurate characterization of the roll gap heat transfer coefficient is essential for a reliable prediction of the thermal field in the strip. The roll temperature from the seven stand mill will be presented later in section 4.9.

4.6 EFFECT OF LUBRICANT IN ROLL BITE

Table IV-IV The Regression Parameters of the Curve of heat transfer coefficient with lubrication

No.	Time (sec)	$h = a + bt + ct^2 + dt^3$				R squared
		a	b	c	d	
1	0.0 - 0.00716	5.766872	1241.496	1568368.	-1.7e+08	0.9758
2	0.00716 - 0.0175	23.122	3843.4	-466337	14496639	0.9951
3	0.0175-0.03875	40.83279	-2660.17	1332372	-1786701	0.9723
4	0.0375-0.5	3575.06	-179383	2271780	0	0.9300

4.6 EFFECT OF LUBRICANT IN ROLL BITE

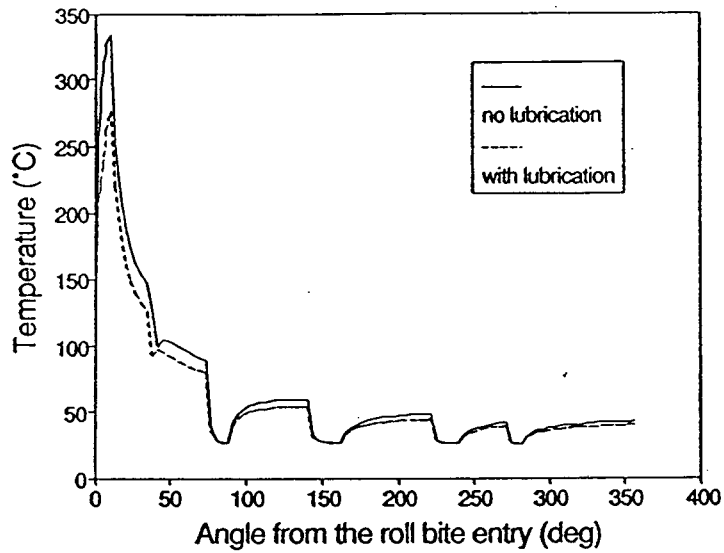


Fig.4.19 a) The influence of lubrication on the computed thermal cycle at the surface of the work roll.

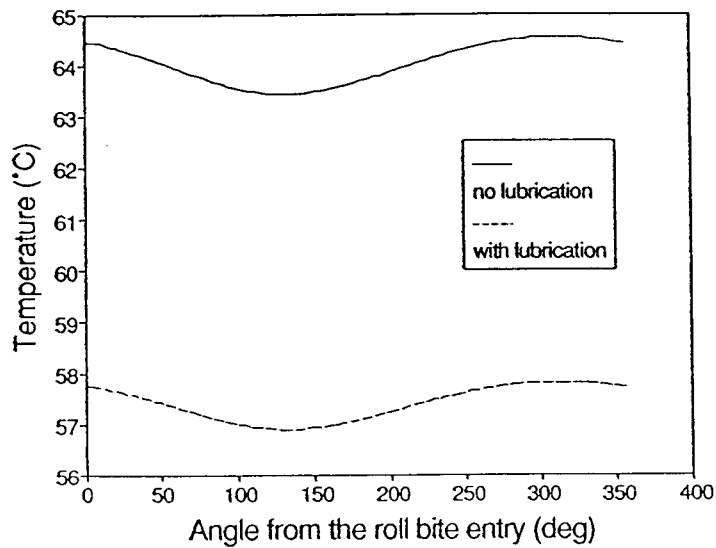


Fig.4.19 b) The influence of lubrication on the computed thermal cycle within the core of the work roll.

4.6 EFFECT OF LUBRICANT IN ROLL BITE

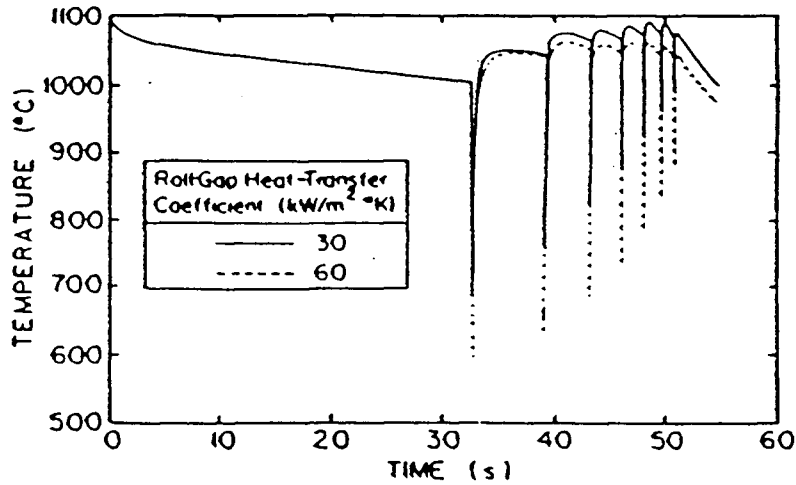


Fig.4.20 The influence of the roll-gap heat transfer coefficient on the computed surface temperature of strip during rolling on a seven stand finishing mill.

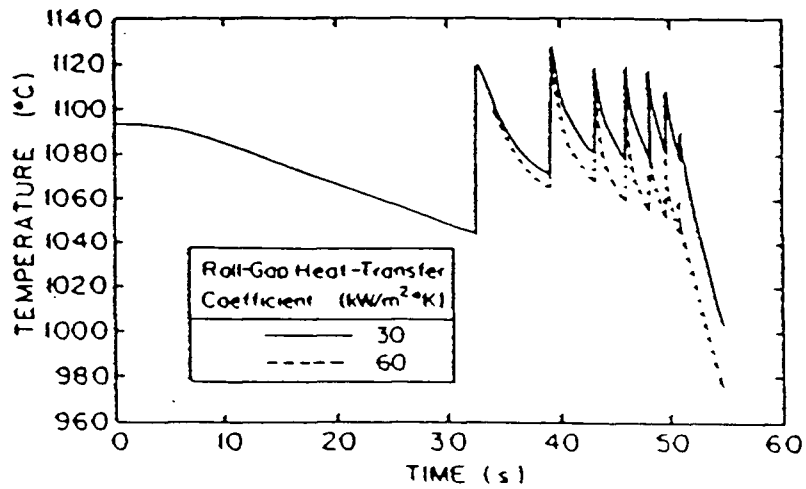


Fig.4.21 The influence of roll-gap heat transfer coefficient on the computed centerline temperature of strip during rolling on a seven stand finishing mill.

4.7 EFFECT OF ROLL DIAMETER ON ROLL TEMPERATURE

The effect of the variation in roll diameter on the roll temperature was also investigated. This was achieved by fixing all initial conditions and changing only the roll diameter. The example given here is for the cooling arrangement shown in Fig. 4.5 with lubrication in the roll bite. The curves showing the changes in roll peak surface temperature and roll body center temperature with roll diameter can be seen in Fig. 4.22. Both curves exhibit approximately a linear relationship.

It has been observed that the peak surface temperature is more sensitive to the change in roll diameter than the roll core temperature, since the steeper temperature gradient is observed in the peak surface temperature curve with changing roll diameter. This could be due to the change in roll bite angle with roll diameter. The roll bite angle is given by

$$\theta = \arccos \left(1 - \frac{h_1 - h_2}{2R} \right) \quad (4.12)$$

where R is the undeformed roll diameter, h_1 is the entry thickness of the strip; h_2 is the exit thickness of strip. It can be seen that when the roll diameter is decreased, the roll bite angle increases resulting in the longer roll-strip contact time if roll speed (41.38 rpm employed in the model prediction) remains unchanged during rolling. For example the roll bite angle for the roll diameter of 0.729 m was 9.9° which results in the roll-strip contact time of 0.04 second, while for the roll diameter of 0.4 m it was 13.3° resulting in the contact time of 0.05 second. The longer contact time for smaller roll diameter allowed more heat to flow into work rolls from

4.7 EFFECT OF ROLL DIAMETER ON ROLL TEMPERATURE

strip causing an increase in the surface temperature.

The core temperature on the other hand is related to the cooling configuration. When the cooling nozzle configuration is fixed, the angle of spray cooling increases with reduction in the roll diameter, *i.e.* the relative contact area of spray on the roll surface is increased. As a result more heat is extracted from the roll surface by the spray water resulting in a lower roll center temperature. Due to the compensating effects of roll cooling, the effect of roll bite angle on roll core temperature is attenuated with the result that the core temperature does not increase appreciably with decreasing roll diameter as observed in Fig. 4.22.

4.7 EFFECT OF ROLL DIAMETER ON ROLL TEMPERATURE

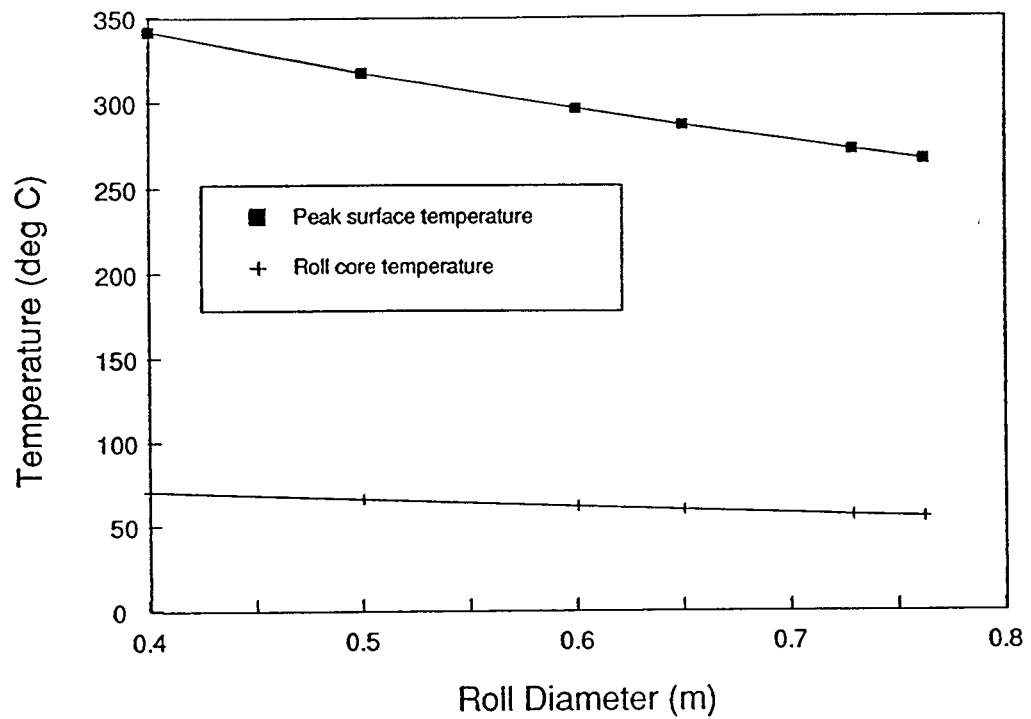


Fig.4.22 The effect of changing the roll diameter on the peak surface and core temperatures of the work roll.

4.8 ROLL SURFACE THERMAL LAYER THICKNESS δ

Devadas [9] has employed Tseng's definition [12] for determining the thickness of the thermal zone in the roll that undergoes thermal cycling during rotation ($\delta = C_t R P_e^{-1/2}$). He has selected the value of 7 for C_t from the curve shown in Fig.4.23 where the normalized temperature difference is 1%. It can be seen that the curve has been determined based on $Bi=10^2$, $Pe=10^5$, where Bi is the Biot number equal to hR/k . This indicates that a different curve can be obtained at a different Bi through the influence of the heat transfer coefficient. Devadas has taken account of normal work-roll cooling in a hot-strip mill which is different from the case considered by Tseng [12] where a uniform convection cooling over the roll circumference was assumed. For different cooling zones, the Biot number varies from 0 to 10^5 as shown in Table IV-V. Therefore the skin thickness needs to be re-evaluated in this case.

Because the cyclic temperature variations are limited within a very thin layer, the temperature along the interior boundary ($r=R-\delta$) should be uniform; otherwise, the skin thickness chosen is not adequate. Therefore a program has been written to obtain the normalized temperature difference $((T_{max} - T_{min})/T_{core})$ for a given surface layer depth. The normalized temperature decreases with increasing the depth until it is less than 1% for which δ is determined. For example, δ turns out to be 10.7mm for an operating condition from company B since at the depth the normalized temperature difference was less than 1%. The corresponding value of C_t is 10.3 which was calculated from the equation (2.6) for the Peclet number of 1.2×10^5 from company B operating parameters. Inside the interior boundary the temperature was about equal

4.8 ROLL SURFACE THERMAL LAYER THICKNESS δ

to 78.5°C. The calculated results have been given in Table IV-VI. A decrease in the normalized temperature was observed with increasing depth and the roll core temperature was determined as the temperature at the interior boundary.

In order to avoid the influence of numerical errors, the mesh spacing (Δr) has been fixed for all the calculations. Thus the number of nodes in the radial direction has been changed with the depth of the surface layer.

$$N_i = \frac{\delta_i}{\Delta r} + 1$$

where i is the indicator of changing variables.

Fig.4.24 has shown the temperature variation for different depths of the thermal zone. The temperature gradient decreases with increasing depth from the roll-surface indicating that a uniform temperature distribution is approached inside the roll. Fig.4.25 shows the roll surface temperature for three different values of thermal zone depths. The three curves overlap due to the very small temperature difference (within 1°C) between them. This indicates that the roll temperature distribution does not change for a small range of δ , and the restriction that the normalized temperature difference is less than 1% is not critical for determining the maximum surface temperature but has an influence on the roll core temperature.

4.8 ROLL SURFACE THERMAL LAYER THICKNESS δ

Table IV-V The Variation of h and Bi During Roll-Cooling

Cooling type	Surface Temp. (°C)	α (m ² /s)	C_p (J/kgK)	K (W/mK)	h (W/m ² K)	Bi (=hR/K)*
1	257	$5.4 \cdot 10^{-6}$	537	21.84	14.46	0.2438
2	119	$5.45 \cdot 10^{-6}$	511	20.97	8049.7	141.378
3	42	$5.38 \cdot 10^{-6}$	496	20.09	1059331	19420
2	53	$5.39 \cdot 10^{-6}$	497	20.17	4236	77
1	69	$5.39 \cdot 10^{-6}$	498	20.23	6	0.1
3	30	$5.34 \cdot 10^{-6}$	495	19.9	345458	6393
2	31	$5.34 \cdot 10^{-6}$	495	19.9	3872	71
3	27.8	$5.32 \cdot 10^{-6}$	494	19.8	680152	12657
2	37	$5.37 \cdot 10^{-6}$	495	20.02	3974	72.5
1	47.5	$5.38 \cdot 10^{-6}$	496	20	5.4	0.1

* The roll radius $R = 0.3683$ m.

The Peclet number is $1.2 \cdot 10^5$.

4.8 ROLL SURFACE THERMAL LAYER THICKNESS δ

Table IV-VI The normalized temperature at different depths

Test No.	Given depth (mm)	Δr (mm)	Total nodes	T_{\max} ($^{\circ}\text{C}$)	T_{\min} ($^{\circ}\text{C}$)	$(T_{\max} - T_{\min})/T_{\text{core}}$ (%)
1	8.11	0.368	23	80.07	76.95	3.94
2	9.96	0.368	28	79.05	77.89	1.45
3	10.7	0.368	30	78.74	78.07	0.91
4	11.43	0.368	32	78.57	78.08	0.63
5	12.17	0.368	34	78.43	78.13	0.37

4.8 ROLL SURFACE THERMAL LAYER THICKNESS δ

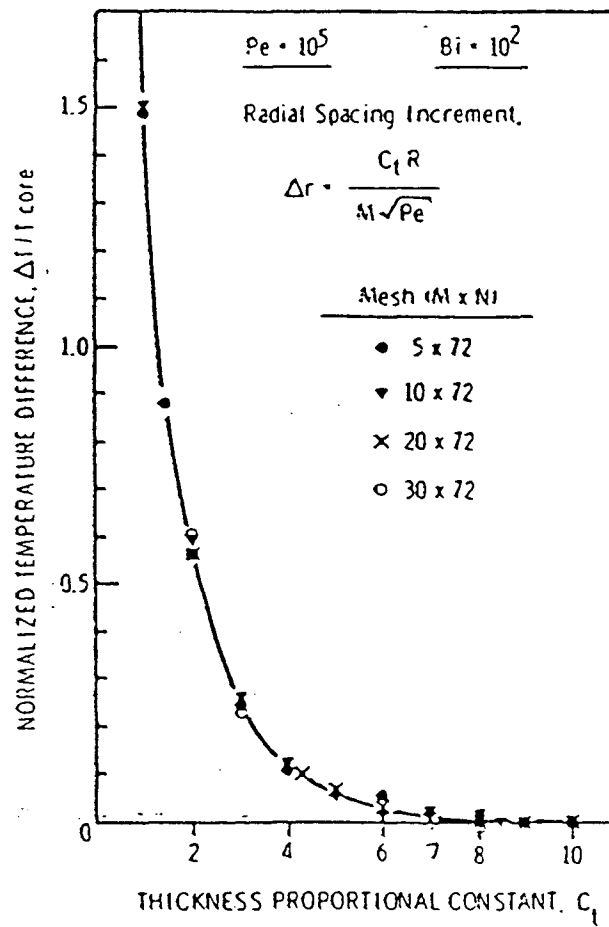


Fig.4.23 The normalized temperature difference vs. thickness proportional constant, C_t [12].

4.8 ROLL SURFACE THERMAL LAYER THICKNESS δ

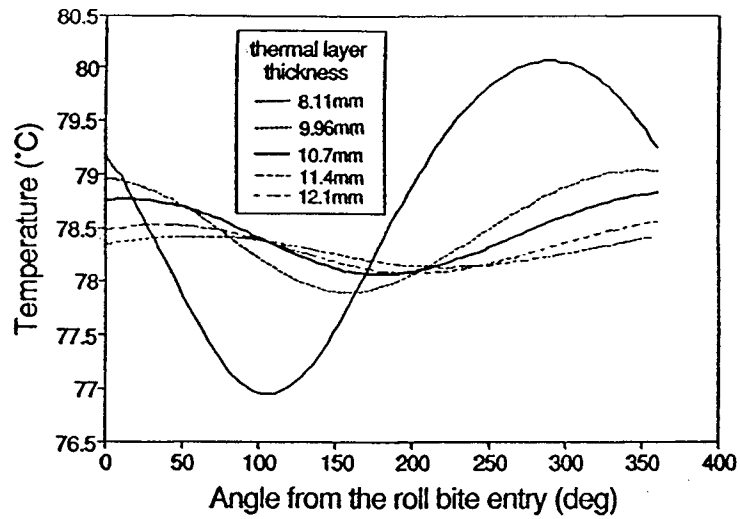


Fig.4.24 The temperature variation along the roll interior boundary at different surface layer depth.

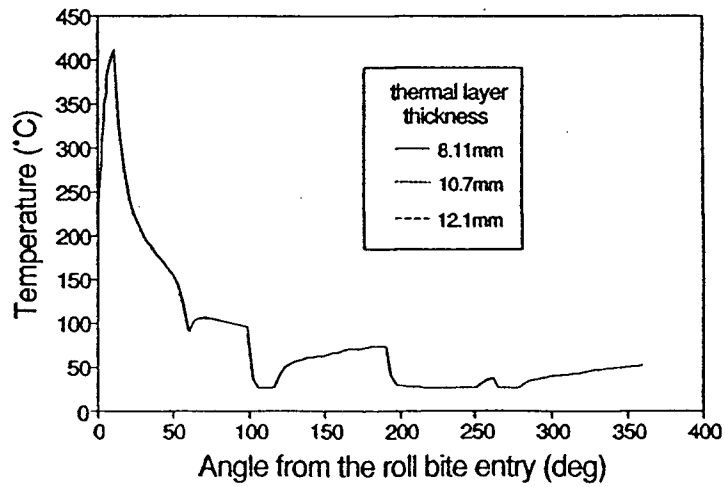


Fig.4.25 The roll surface temperature at different surface layer depth.

4.9 THE WORK ROLL TEMPERATURE FROM A SEVEN STAND FINISH MILL

The work roll temperature of a seven stand finish mill from company C has also been calculated in this investigation. The rolling parameters for all the seven stands are given in Table IV-VII. The cooling configurations for these stands are the same as shown earlier in Fig.4.18 c) except for stand F4 to F7 where there is no entry spray. The cooling conditions can be seen from Table IV-III. The roll gap heat transfer coefficients (HTC) shown in Fig.4.26 has been employed in the calculation. The curve of the solid line was utilized as the HTC for stand F1 and the curve of dashed line was employed as the HTC for stand F2 to F7. The calculated cyclic temperature results for the seven stand operation were shown in Fig.4.27. It can be observed that the peak surface temperature increased from 376°C at stand F1 to 455°C at stand F2. Pressure in the roll bite in stand F2 is greater than F1 because of the reduced thickness which is associated with a higher heat transfer coefficient [44]. The peak temperature decreased through the rest of stands from 347°C at stand F3 to 91°C at stand F7. Although rolling pressures for stand F3 to F7 are higher than for stand F1 (Table IV-VII) the contact time decreases which decreases the peak surface temperature. The decrease in the roll bite time is due to increasing roll speed and decreasing strip reduction towards finish mill exit as shown in Table IV-VII. It can be seen that the roll core temperature decreases from 60°C to 37°C through the seven stands except for stand F2 where there is slight increase in the roll core temperature compared to stand F1 due to the

4.9 THE WORK ROLL TEMPERATURE FROM A SEVEN STAND FINISH MILL

higher rate of heat transfer to work rolls. The decrease in the roll core temperature is the result of the increase in the relative cooling time in a total cycle due to increasing roll speed towards the finish mill exit, as given in Table IV-VII.

4.9 THE WORK ROLL TEMPERATURE FROM A SEVEN STAND
FINISH MILL

Table IV-VII Rolling Parameters for a Seven Stand Operation

Rolling parameters	Stand F1	Stand F2	Stand F3	Stand F4	Stand F5	Stand F6	Stand F7
Strip reduction(%)	45.4	38.8	28.7	28.7	26.3	19.9	12.4
Roll speed (rpm)	45.8	76.6	111.2	149.5	199.5	251	289
Roll bite time (sec.)	0.0408	0.0167	0.0077	0.0048	0.0029	0.0017	0.0010
Roll bite contact length (mm)	70.8	48	32.5	27.5	22.2	16.5	11.7
Roll forces (tones)	1580	1365	1389	1130	996	828	488
Rolling pressure (kg/mm ²)	17.77	22.64	34.04	32.72	35.72	39.95	33.21
Total time per cycle (sec.)	1.31	0.783	0.54	0.4	0.3	0.239	0.208
cooling time per cycle (sec.)	1.27	0.766	0.53	0.40	0.29	0.24	0.207
Cooling time over total time per cycle (%)	96.88	97.87	98.57	98.78	99.03	99.27	99.48
Peak surface temperature (°C)	376	455	347	272	209	147	91
Roll Core temperature (°C)	60	62	53	51	46	41	37

* Entry bar thickness at F1 is 30.48mm;
Strip width is 1.256m;
Exit bar thickness at F7 is 2.68mm;
Roll diameter is 0.7239m (28.5");
Strip temperature in coilbox is 1093°C

4.9 THE WORK ROLL TEMPERATURE FROM A SEVEN STAND FINISH MILL

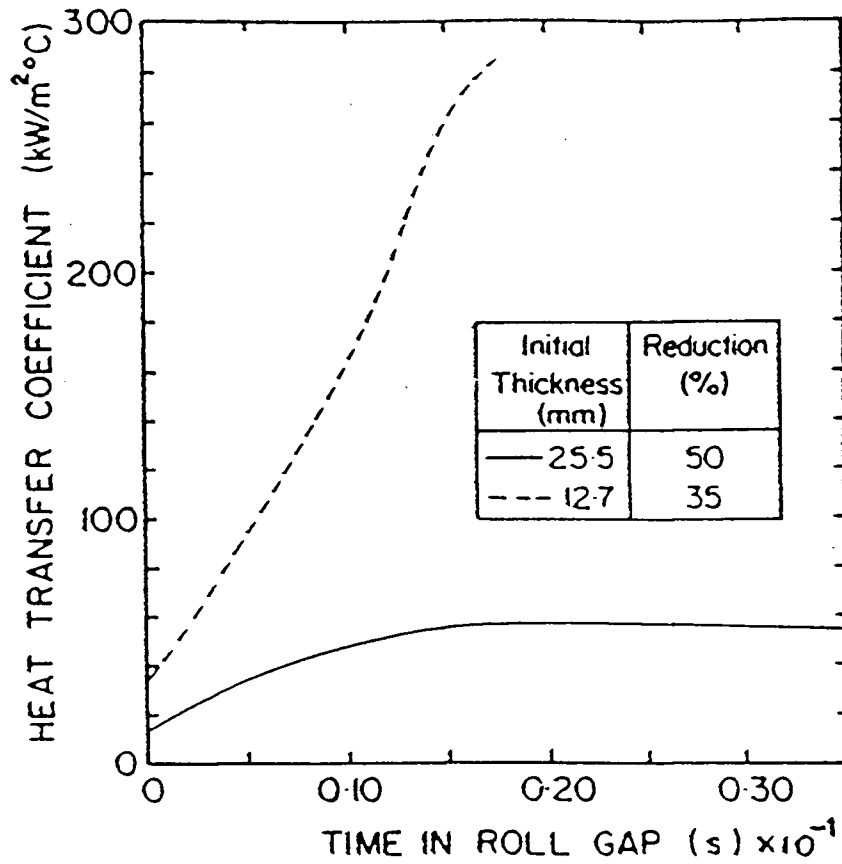


Fig.4.26 Computed variation of the roll-gap heat-transfer coefficient with time in the roll bite for two successive passes on a pilot mill.[44]

4.9 THE WORK ROLL TEMPERATURE FROM A SEVEN STAND FINISH MILL

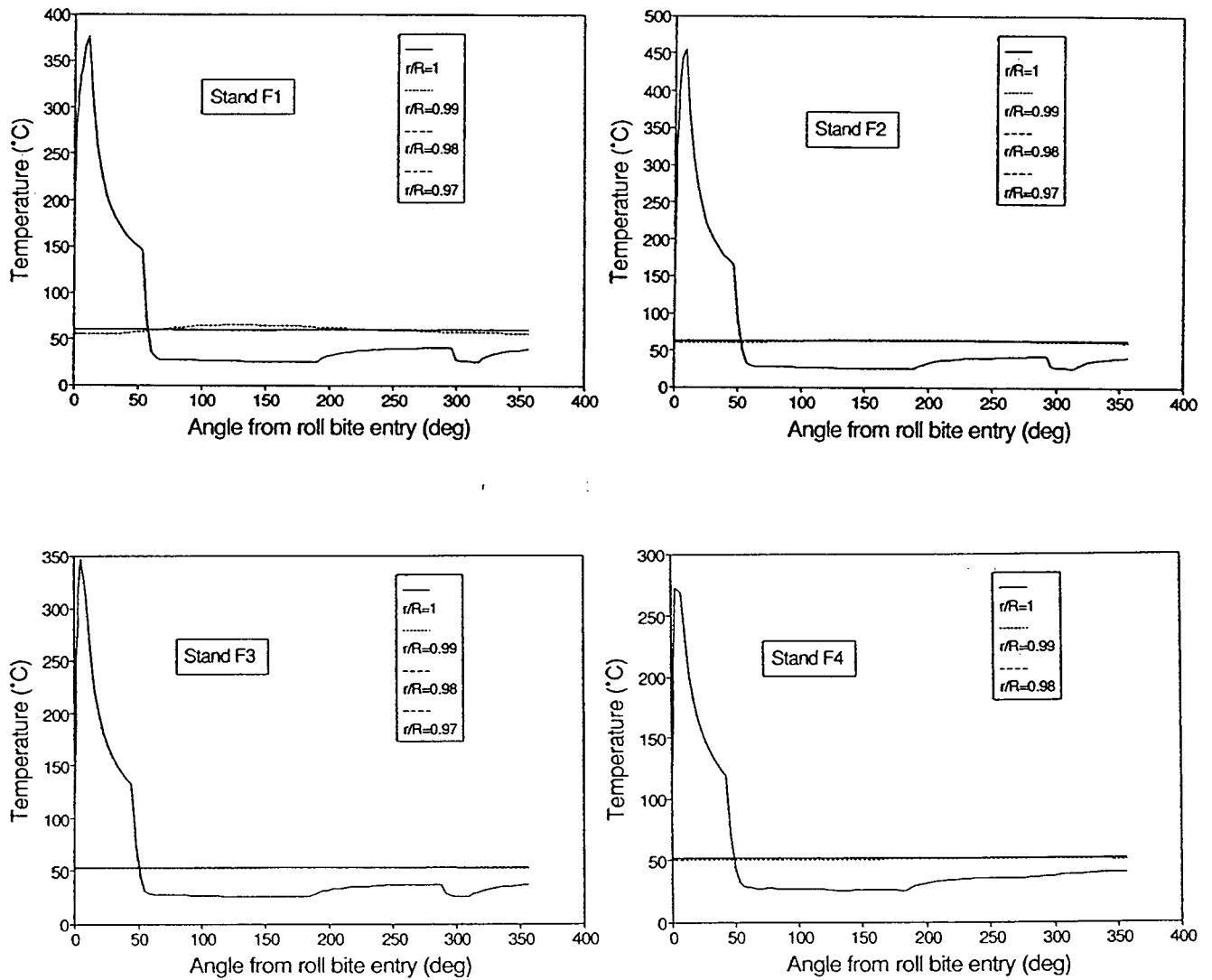


Fig.4.27 a). The work roll temperatures from a seven-stand finish mill.

4.9 THE WORK ROLL TEMPERATURE FROM A SEVEN STAND FINISH MILL

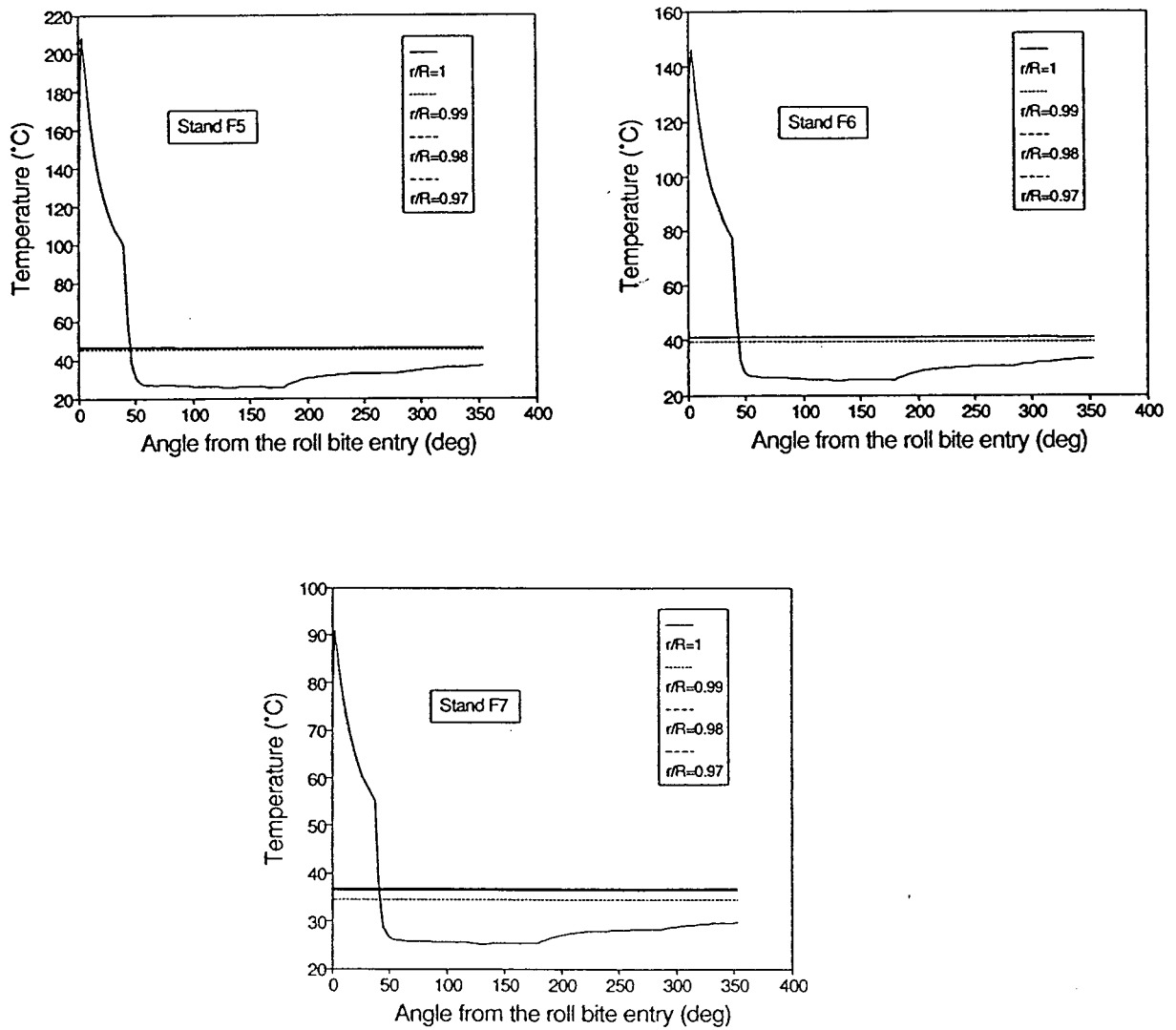


Fig.4.27 b). The work roll temperatures from a seven-stand finish mill.

5 THERMAL CROWN CALCULATION OF WORK ROLLS

The radial thermal expansion of a work roll gives rise to a thermal crown which could cause a change in roll gap geometry and dimensional precision problems for the strip. In order to control work roll surface profile to achieve the desired strip shape, an analysis of roll deformation is necessary. Thermal crown is developed due to non-uniform thermal expansion of the work roll along the roll axis induced by a thermal field inside the roll during rolling. Thus the thermal crown calculation was determined by two important steps. The first was to develop a work roll thermal model to calculate the thermal field inside the roll. The second was to calculate the thermal crown induced by the thermal field.

In this chapter, a two-dimensional thermal model of a work roll has been developed to predict the thermal field inside the roll, which was used to estimate thermal expansion of the work roll assuming axi-symmetric deformation of the roll. The model provides considerable engineering insight into the roll-heating phenomena, and is ideally suited for 'real-time' calculation or as a part of a hot-mill simulation. The fact that the model simulates operating conditions including the cooling configuration enhances its value in studying industrial rolling. It is an improvement over the calculations of Ueda referred to by Roberts [30] where heat-exchange theory was employed to approximate heating and cooling over a revolution by a single heat transfer coefficient. The latter approximation limits its application. Since obviously the equivalent heat transfer coefficient of roll cooling is dependent on the configuration of the roll-cooling system it is difficult to estimate accurately. An investigation of effects of roll-strip

5.1 MATHEMATICAL DESCRIPTION

heat transfer, roll spray-cooling arrangement and mill pacing on the roll thermal crown has also been conducted in this study, the results of which will be presented and discussed later in this chapter.

5.1 MATHEMATICAL DESCRIPTION

Fig.5.1 illustrates the different modes of heat transfer to and from the work rolls. The intensive heat from a hot strip is supplied to the center of the roll barrel in the deformation zone and the heat is lost through the roll surface beyond the roll gap and roll ends, in addition to heat loss to the backup roll. In the roll-axial direction there is a slow time-varying heat transfer induced by non-uniform spray distribution and roll-gap heat transfer.

The temperatures which develop in a work roll subject to cyclic boundary conditions are space- and time-dependent. To determine the temperature distribution within a work roll, a three-dimensional analysis including transient and roll rotation effects would be required. However, a simpler analysis can be adopted when only certain aspects of rolling are the subject of interest. Since the roll radial expansion and its variation along the roll axis are of interest, the heat transfer calculation along the axial and radial directions is essential. Under the following assumptions, a two-dimensional heat transfer equation can be formulated.

- 1). Since the roll speed is high, the heat transfer in the circumferential direction can be ignored relative to the heat transfer by bulk rotation.

5.1 MATHEMATICAL DESCRIPTION

- 2). The roll-gap heat transfer coefficient (HGP) is assumed to remain unchanged along the roll-strip contact, ignoring the strip-edge influence. Outside the roll-gap, the heat transfer coefficients along the roll surface due to spray cooling are considered to be uniform.
- 3). The heat loss to the backup roll is usually small and is ignored in this analysis.[28]
- 4). The temperature calculation has been conducted in a quarter plane shown in Fig.5.2 assuming that the thermal field is symmetric with respect to the axis r and z respectively.
- 5). The thermal field approaches a steady state.

The two-dimensional heat transfer equation governing the temperature distribution inside the roll can be obtained from the law of energy conservation. Mathematically it is expressed as follows:

$$\rho C_p \frac{\partial T}{\partial t} = \frac{1}{r} \frac{\partial}{\partial r} \left(kr \frac{\partial T}{\partial r} \right) + \left(k \frac{\partial^2 T}{\partial z^2} \right) \quad (5.1)$$

The thermal properties of the work roll, specific heat C_p and thermal conductivity k , are temperature and roll material dependent. The solution of the above differential equation, regardless of the mathematical method employed, requires that both the boundary and initial conditions be specified.

- (1). Over the center of the roll surface which comes into contact with the strip intermittently, represented by AB in Fig.5.1, the thermal boundary condition is expressed through a heat transfer coefficient.

5.1 MATHEMATICAL DESCRIPTION

$$0 \leq z \leq B/2, t \geq 0, \quad h_{sr}(T - T_s) = -k \frac{\partial T}{\partial r} \quad (5.2)$$

where B is the strip width; h_{sr} is the coefficient of heat transfer, representing the heat transfer along the boundary AB . It is assigned the value of roll gap heat transfer coefficient (HGP) within the roll bite, and beyond the roll gap it is determined by the modes of heat transfer depending on the roll cooling and roll surface temperature[9]; T_s is the temperature of the medium surrounding the roll along AB , which represents the strip temperature along the arc of contact within the roll bite. Outside the roll bite T_s is 25°C . The strip temperature for the calculation has been obtained from the simultaneous solution of the governing heat transfer equations for both the strip and work roll by Devadas and Samarasekera [1].

(2). Along the roll surface from the strip edge to the roll end, illustrated by BC in Fig.5.1,

$$B/2 \leq z \leq z_0, t \geq 0, \quad h_{rw}(T - T_w) = -k \frac{\partial T}{\partial r} \quad (5.3)$$

where z_0 is the half-roll length; h_{rw} is the coefficient of heat transfer, representing the heat loss by convection from the roll surface to the coolant or air. Depending on the surface temperature of the rolls it is determined by the modes of heat transfer indicated in chapter 4, equation (4.4) through (4.7) [9]. T_w is the coolant temperature equal to 25°C .

(3). At the roll end connecting the roll neck, $z = z_0$, illustrated by DE in Fig.5.1,

5.1 MATHEMATICAL DESCRIPTION

$$0 \leq r \leq D_n/2, t \geq 0, \quad h_n(T - T_n) = -k \frac{\partial T}{\partial z} \quad (5.4)$$

where D_n is the diameter of roll neck; h_n is the heat transfer coefficient, representing the heat loss by conduction to the roll neck, which has been estimated to be $10\text{W/m}^2\text{°C}$ through an equivalent heat transfer analysis along the boundary DE given in Appendix A; T_n is the roll neck temperature equal to the ambient temperature, 25°C .

(4). At the roll end exposed to the air, $z = z_0$, illustrated by CD in Fig.5.1,

$$D_n/2 \leq r \leq r_0, t \geq 0, \quad h_a(T - T_a) = -k \frac{\partial T}{\partial z} \quad (5.5)$$

where h_a is the heat transfer coefficient, representing the heat loss by convection to the air, which has been assumed to be $11\text{W/m}^2\text{°C}$ [39]. T_a is the air temperature equal to 25°C .

(5). Considering the thermal field symmetric to the roll axis z in Fig.5.2, at $r = 0$,

$$0 \leq z \leq z_0, t \geq 0, \quad \frac{\partial T}{\partial r} = 0 \quad (5.6)$$

(6). Considering the thermal field symmetric to the axis r in Fig.5.2,

at $z = 0$,

$$0 \leq r \leq r_0, t \geq 0, \quad \frac{\partial T}{\partial z} = 0 \quad (5.7)$$

5.1 MATHEMATICAL DESCRIPTION

The calculation of the roll thermal field is to begin with an initial temperature distribution inside the work roll, which has been assumed to be uniform in this study, *i.e.*

$$0 \leq r \leq r_0, 0 \leq z \leq z_0, \quad T(r, z, 0) = \text{constant} \quad (5.8)$$

The heat transfer equation (5.1) including these boundary conditions has been solved for the temperature field inside the work roll through the numerical finite difference method. The solution technique will be described in the following section.

Once the thermal field inside the work roll is known, the thermal expansion of the roll can be evaluated under the following assumptions.

(1). The roll is assumed to be homogeneous and isotropic.

(2). The strain and elastic deformation of the roll is assumed to be axi-symmetric, assuming an axi-symmetric temperature field of the roll. Again the cyclic variation of temperature within the thin boundary layer responsible for the roll surface fatigue is disregarded in the thermal crown calculation since the dominant factor is the bulk temperature of the roll which has little change along the circumferential direction. As a result, the radial and axial displacements U and W at any position inside the roll are both independent of θ , the circumferential direction, and the circumferential displacement V is assumed to be equal to zero.

(3). Any cross-sectional plane normal to the roll axis remains a plane after displacement, *i.e.* the shear displacement components can be disregarded.

5.1 MATHEMATICAL DESCRIPTION

Hence the equation of stress equilibrium in the radial direction derived from an expression of the law of Newtonian mechanics which requires that the resultant force acting on the body be equal to zero can be expressed mathematically [40]

$$\frac{\partial \sigma_r}{\partial r} + \frac{\sigma_r - \sigma_\theta}{r} = 0 \quad (5.9)$$

where σ_r and σ_θ represent the radial and axial stress components respectively.

The corresponding thermoelastic stress-strain relationship derived from the linear elastic theory under small-strain and small temperature change assumptions have been expressed for the axi-symmetric situation[40,41] as follows:

$$\begin{aligned} \sigma_r &= 2G \left(\epsilon_r + \frac{\mu}{1-2\mu} e \right) - mT \\ \sigma_\theta &= 2G \left(\epsilon_\theta + \frac{\mu}{1-2\mu} e \right) - mT \\ \sigma_z &= 2G \left(\epsilon_z + \frac{\mu}{1-2\mu} e \right) - mT \\ \sigma_{r\theta} &= \sigma_{\theta z} = \sigma_{rz} = 0 \end{aligned} \quad (5.10)$$

where $\sigma_{r\theta}$, $\sigma_{\theta z}$ and σ_{rz} represent the shear stress components; G is the shear modules, $G=E/2(1+\mu)$; μ is the Poisson ratio; m is the constant related to Lamé constant λ and the coefficient of linear thermal expansion α , $m = (3\lambda + 2G)\alpha$; e is the linear dilatation expressed as

5.1 MATHEMATICAL DESCRIPTION

$$e = \epsilon_r + \epsilon_\theta + \epsilon_z \quad (5.11)$$

where ϵ_r , ϵ_θ and ϵ_z are the strain components in the r, z and θ directions respectively. The corresponding strain-displacement relations derived from purely geometrical or kinematic concepts of deformation under the small strain assumption can be described mathematically [40] by

$$\begin{aligned} \epsilon_r &= \frac{dU}{dr} \\ \epsilon_\theta &= \frac{U}{r} \end{aligned} \quad (5.12)$$

$$\epsilon_z = \frac{dW}{dz}$$

$$\gamma_{r\theta} = \gamma_{\theta z} = \gamma_{rz} = 0$$

Substituting equations (5.10), (5.11) and (5.12) into (5.9), the equilibrium equation expressed by the displacement components is as follows:

$$\frac{d^2U}{dr^2} + \frac{1}{r} \frac{dU}{dr} - \frac{U}{r^2} = \alpha \left(\frac{1+\mu}{1-\mu} \right) \frac{\partial T}{\partial r} \quad (5.13)$$

The displacement boundary condition based on the axi-symmetric consideration can be expressed mathematically by

5.1 MATHEMATICAL DESCRIPTION

$$r = 0, \quad U(0, t) = 0, \quad (5.14a)$$

Considering only the thermally induced displacement of the roll during rolling, on the roll surface the stress boundary condition is expressed as follows

$$r = r_0, \quad \sigma_r = 0 \quad (5.14b)$$

Solving the equation (5.13), and observing the boundary condition, the thermally induced radial displacement at a radial position, r , is expressed by the following equation

$$U_r = \frac{\alpha(1+\mu)}{(1-\mu)r} \int_0^r T r dr + \frac{(1+\mu)(1-2\mu)\alpha r}{(1-\mu)r_0^2} \int_0^{r_0} T r dr \quad (5.15)$$

where r_0 is the radius of the roll. Therefore the roll surface displacement U_{r_0} at $r = r_0$ relative to an initial temperature T_0 can be given by the following equation

$$U_{r_0} = \frac{2\alpha(1+\mu)}{r_0} \int_0^{r_0} (T(r, z) - T_0) r dr \quad (5.16)$$

It can be seen from equations (5.15) and (5.16) that the roll radial displacement is related to the radial temperature distribution of the roll at an axial position. Thus the variation of the radial temperatures along the roll axis, *i.e.* the direction z , would induce a change in the roll radial expansion with changing axial position. Therefore it is the roll surface displacement variation along the roll axis that determines the roll thermal crown leading to a change in the roll surface profile.

5.1 MATHEMATICAL DESCRIPTION

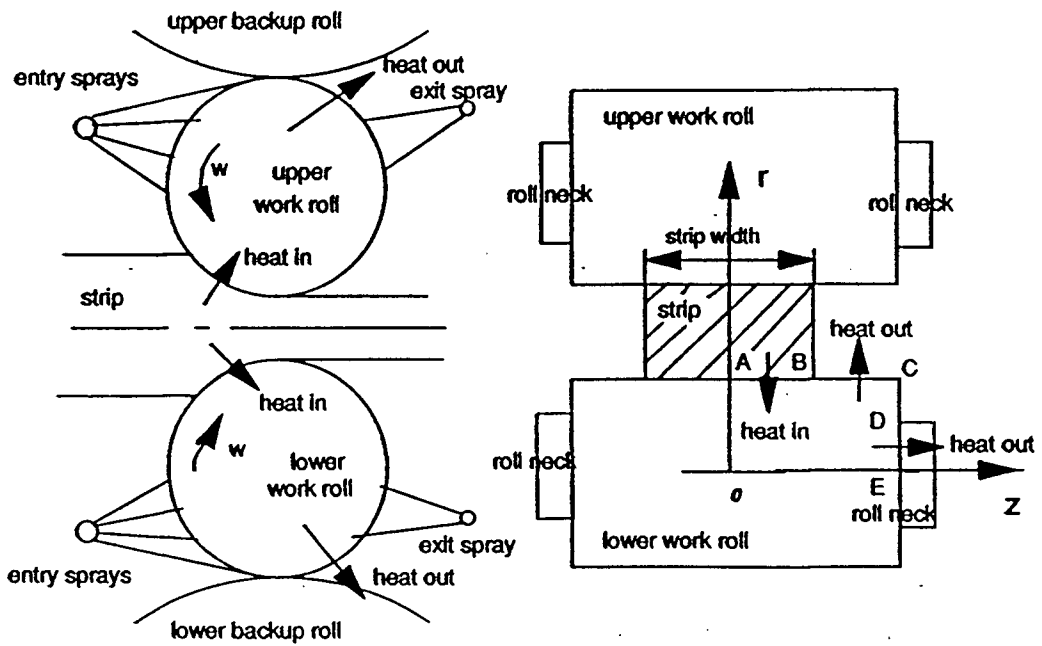


Fig.5.1 Schematic diagram showing different modes of heat transfer to work roll.

5.1 MATHEMATICAL DESCRIPTION

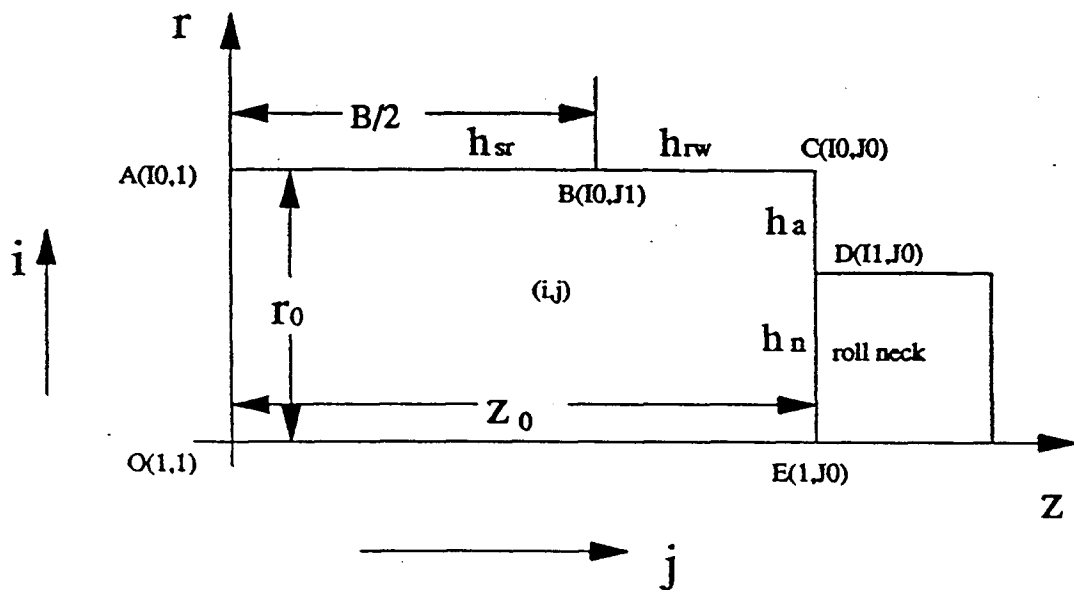


Fig.5.2 The computation domain and boundary conditions.

5.2 NUMERICAL SOLUTION

The two-dimensional heat transfer equation (5.1) has been solved by finite difference approximation. The set of finite difference equations are formed using the alternating direction implicit method (ADI) within the domain indicated below. In the ADI method, the incremental time (Δt) is executed in two steps. For the first half incremental time ($\Delta t/2$), the equation (5.1) is approximated implicitly in the radial direction and explicitly in the roll axial direction. For the second half incremental time ($\Delta t/2$) the approximation is reversed. The advantage of the ADI method is that a system of linear simultaneous equations having a tridiagonal coefficient matrix can be obtained and solved readily by the Gaussian elimination method. This method results in the minimum requirements of computer time and storage, and makes it possible to solve the problem on a PC. The ADI method is second-order accurate with a truncation error of $O((\Delta t)^2, (\Delta r)^2, (\Delta z)^2)$ and is unconditionally stable [42,43]. The finite difference node equations have been listed in Appendix B, and coded in Fortran. The program has been run on a PC, UBC Amdahl main frame as well as SGI (Silicon Graphics Inc. work station).

The domain in which calculations were performed is only one quarter of the central plane through the roll axis due to the assumption of symmetry, as shown in Fig.5.2. This domain is divided into a total of 2000 nodes (40 nodes in the radial direction r , 50 nodes in the axial direction z). Since temperature on the roll surface changes rapidly due to the rapid rotation of the roll as well as due to the large variation of the roll thermal boundary conditions, the computations must be conducted for short time increments and small mesh spacing. Mathematically since the large temperature gradient occurs on the roll surface in the radial direction especially in the roll bite,

5.2 NUMERICAL SOLUTION

a fine mesh spacing must be adopted near the roll surface to assure the accuracy of finite difference approximation there. Further inside the roll a larger mesh spacing can be utilized to reduce the total number of nodes and to save computational time. Therefore, a non-uniform mesh spacing has been considered in the radial direction and formed through a geometrically progressive factor (PF). The mesh spacing is described mathematically in the form of

$$i = 1, 2, \dots, i_0 - 2 \quad dR(i) = dR(i + 1) * PF \quad (5.17)$$

where $dR(i)$ is the mesh spacing between node i and $i+1$; PF is the progressive factor of the mesh determined by the roll radius, the number of nodes and a given spacing based on which subsequent spacings are developed. The given spacing for the calculation is the roll surface mesh spacing $dR(i_0-1)$ which has been chosen to be 0.36 mm in view of Devadas' calculation [9]. For a total of 40 nodes given in the radial direction, PF is calculated in program to be equal to 1.09933. i is the node number in the radial direction; i_0 is the node number of roll surface. The mesh spacing in the roll axial direction has been uniformly distributed since the temperature gradient is small in this direction. A further refinement of mesh size in the radial direction (80 nodes) yielded temperature changes within 1°C.

The model has employed 64 time steps to simulate one revolution of the work roll, 50 time steps uniformly around the roll periphery beyond the roll-gap and 14 time steps during the roll-gap depending on the strip reduction. In order to examine the effect of incremental time on temperature calculation, 100 time steps beyond the roll-gap was also used in the calculation instead of 50. The maximum temperature difference with this refinement was within 1.5°C. Therefore

5.2 NUMERICAL SOLUTION

depending on the complexity of roll boundary conditions the time step could be reduced even more to save computing time. Since an initial temperature is required, convergence is faster when the initial temperature was chosen close to the steady state temperature. In this study, 69°C was chosen for the roll initial temperature based on Devadas' calculation and 25°C was chosen for the corresponding roll surrounding temperature.

A previously developed one-dimensional numerical model [9] has been utilized to calculate strip surface temperature in the roll-gap, which has been obtained by the simultaneous solution of heat conduction equations for both strip and work-roll in the roll-gap. The surface friction and strip deformation were included in the calculation. The heat transfer coefficients around the roll periphery have been obtained depending on roll surface temperature and cooling type, *i.e.* natural, forced or boiling convection. The curve of heat transfer coefficient from pilot mill experiments given in Fig.4.12 with roll-lubrication has been employed as input to the 2-D thermal model. And an average HGP of 60kW/m²C for roll without lubrication is also employed to examine the effect on thermal crown of work roll. To examine the roll cooling effect on the roll thermal crown, roll cooling arrangement can be easily changed without any assumption in the calculation. This permits off-line assessment of the practical effect of roll-gap heat transfer (HGP) on the roll thermal crown and the effectiveness of cooling systems under mill-operating condition.

Numerically, the calculation of the roll surface thermal expansion based on the equation (5.16) can be expressed as follows

$$j = 1, 2, \dots, 50, \quad HC_j = (2/r_0)(1 + \mu)\alpha \sum_{i=1}^{10} (T(i, j, t) - T(i, j, 0))r_i \Delta r_i \quad (5.18)$$

5.2 NUMERICAL SOLUTION

where j represents the node number along the axial direction; α is the coefficient of thermal expansion of the work roll; $T(i,j,0)$ is the roll temperature relative to which the thermal expansion is developed. In view of Devadas' calculation, $T(i,j,0)$ has been assumed to be 69°C . In fact, the thermal crown can be established based on any given $T(i,j,0)$ since the crown is the relative difference in the expansion at the roll center *versus* the roll edges. The roll thermal field can be regarded as axi-symmetric ignoring the small influence of the roll cyclic temperature variation which occurs in a thin thermal zone near the roll surface; therefore any angular two-dimensional plane can be used for the thermal expansion calculation. In this study the temperature distribution at the two-dimensional plane just before the roll-gap entry has been utilized for the expansion calculation. The flow chart of the computer program is shown in Fig.5.3.

5.2 NUMERICAL SOLUTION

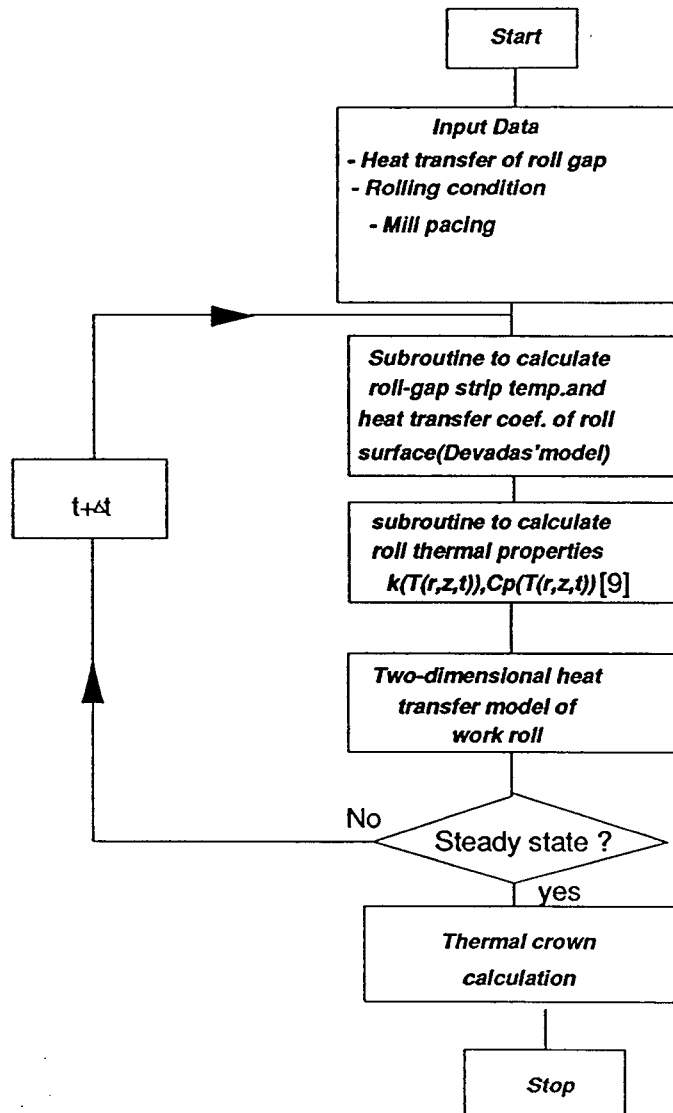


Fig.5.3 The flow chart of the roll thermal crown calculation.

5.3 VALIDATION OF THE MODEL

To assess the accuracy of the heat transfer model for the work roll, the 2-D model has been employed to reproduce the analytical solution for heating of a cylinder given by Kreith and Black [39]. The cylinder initially at a uniform temperature of 20°C was placed in an oven with an ambient temperature of 500°C and a convective heat transfer coefficient of 30W/m²K. One quarter of the cylinder is considered as the domain of computation. The domain is divided into 2000 nodes, 40 nodes non-uniformly distributed in the radial direction and 50 nodes uniformly in the axial direction. The incremental time has been chosen to be 10 seconds. After 30 minutes, the calculated maximum cylinder temperature located at the outer circumference at each end of the cylinder is 478°C compared to analytical result of 480°C, whilst the calculated minimum temperature located at the geometric center of the cylinder is 298.2°C compared to 297°C from analytical solution. The difference in temperature can be seen to be within 2°C. An increase in the number of nodes from 2000 to 3000 and changing the incremental time gave a calculated temperature difference within 1°C. This indicates that the model is stable and not sensitive to further refinement in mesh size. Therefore the formulation of the numerical model is correct and valid.

The temperature result predicted by the two dimensional thermal model for the company B rolling condition has been compared with the calculated temperature data by Devadas' one dimensional model. Fig.5.4 shows the comparison of the temperature results at the angular position before the roll bite. It can be seen that a temperature difference within 3°C for both the heat transfer coefficients has been obtained. The discussion of the figure will be given later in

5.3 VALIDATION OF THE MODEL

section 5.4.

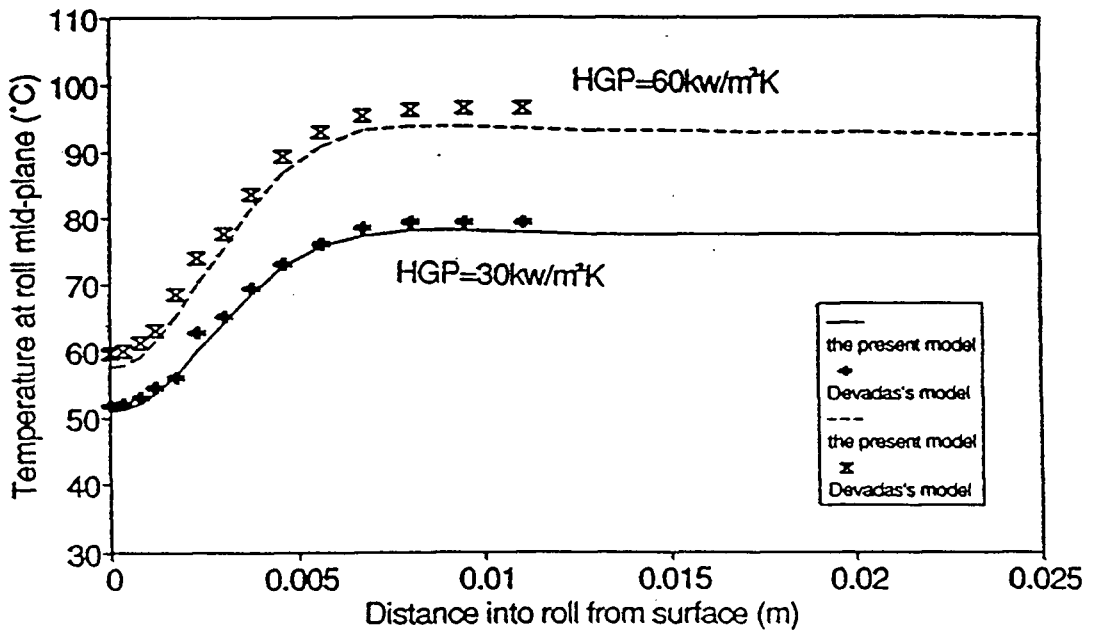


Fig.5.4 The temperature profiles at the angular position just before roll-gap entry (the predicted surface layer thickness is 10.7 mm.).

5.4 RESULTS AND DISCUSSION

The two dimensional temperature calculation has been conducted based on the company B rolling and cooling conditions mentioned earlier in section 4.5. The cooling configuration was shown in Fig.4.18 a) and the rolling condition was listed in Table IV-II. Fig.5.5--5.7 show respectively the calculated temperature results at the two-dimensional plane just before roll-gap entry for continuous rolling. Fig.5.5 shows the temperature contour at steady state for the roll gap heat transfer coefficient of $60\text{kW/m}^2\text{C}$. It can be seen that the maximum temperature inside the roll was about 95°C and high temperatures occurred in the region near the roll-strip contact, AB, due to the impulse of heat received during contact with the strip. Whilst low temperatures, of which the minimum temperature is about 25°C , occurred in the region near the cooling surface, BC, where the average rate of cooling around the whole roll thermal boundaries is largest due to the spray cooling action. Therefore the heat must flow into the roll through the roll-strip contact boundary AB and mostly out of the roll through the boundary BC, in addition to some heat loss through the boundary CE. With intense cooling outside the roll-gap, the roll surface temperature along the AB has been depressed to 57°C , even lower than inside the roll. Fig.5.6 and 5.7 show the temperature contours before the steady-state temperature field was reached. These isothermal lines also indicated that heat flowed into the roll through the boundary AB and out of the roll mostly through the boundary BC. Whilst the heat transfer was gradually penetrating into the roll center with rolling time. For instance, the isothermal line of 70°C was obtained at the roll radius about 0.18 m as shown in Fig.5.6 while it occurred almost at the roll center in Fig.5.7.

5.4 RESULTS AND DISCUSSION

It is evident from this calculation that it took a long time for the roll-center temperature to change. This could be clear from an analysis of thermal resistance of the work roll. Since thermal resistance of a solid is proportional to the distance of heat transfer, it increases with increasing the depth into the roll from the surface resulting in a decrease in the rate of heat transfer towards the roll center (Note: the roll thermal conductivity has a slight change inside the roll depending on temperature).

It is also evident that the steady-state temperature field is achieved after many cycles since the variation of temperature inside the roll is smaller in later cycles. It is necessary to emphasize that although beyond the roll-gap heat can be removed by the coolant as well as by the ambient air, the inner region still transfers heat even further because it is not directly affected by cooling impingement. As a result of roll cooling action the net rate of heat transfer into each node becomes smaller with time leading to an approach of steady-state. But a long time is required for the heat balance to be established because of the frequent and complex variation of roll boundary conditions. The steady-state temperature field could be reached earlier if a rolling condition is changed, such as mill pacing, as presented later in this section.

Fig.5.8 shows the temperature contour at steady state for the roll gap heat transfer coefficient (HGP) of $30\text{kW/m}^2\text{°C}$. The lower temperature of the roll has been obtained due to the lower roll gap heat transfer compared to that shown in Fig.5.5. The maximum temperature is 77°C and the temperature distribution is qualitatively similar to that shown in Fig.5.5. The temperature variation along the roll radius at the center of the roll was shown in Fig.5.4. for different HGP. It can be seen that the surface temperature has been depressed below the roll core temperature due to the intensive spray cooling in a cycle. The temperature changes greatly

5.4 RESULTS AND DISCUSSION

within a thermal layer near the surface and remains nearly unchanged over the remainder of roll radius. The thermal zone thickness is slightly affected by HGP since the thickness can be seen to be about 10mm for both the curves in Fig.5.4.

The predicted thermal crowns relative to the roll end based on the thermal fields from Fig.5.5--5.7 respectively have been shown in Fig.5.9. The thermally induced crown was of flattened belt shape along the axial direction. At steady state the maximum thermal crown was 287 microns. A reduction in roll-gap heat transfer and enhanced cooling would definitely contribute to improve roll surface shape. The crown buildup with rolling time can be seen from the three curves and the gradient decreased with the time indicating a steady state crown being approached.

From the industrial point of view, the work roll crown has an influence on strip flatness and thickness precision and has always been a major concern to both the mill designer and operator. In this calculation the difference in the expansion at the roll center *versus* the strip edge is 157 microns for the continuous rolling at steady state as shown in Fig.5.9.

The temperature distributions along the roll radius at various angular positions of the roll at steady state were shown in Fig.5.10. It can be seen that the maximum temperature on the roll surface was located at the roll-gap exit as a result of the impulse of heat injected during contact with the strip. As the roll rotated and was cooled outside the roll gap, the surface temperature decreased. With suitable cooling, the surface temperature can be depressed even lower than the internal temperatures as shown in the curve for the roll-gap entry. Also the cyclic temperature of the work roll only varied within a thin layer of roll surface over a penetration depth δ , and

5.4 RESULTS AND DISCUSSION

remained nearly unchanged over the remainder of the radius. The penetration depth was typically small (<1 mm) compared to the roll radius (368mm) and was a function of roll radius and rolling speed, as pointed out before in the literature review.

It was indicated from Fig.5.10 that the temperature field inside the roll was axi-symmetric except for the thin thermal zone near the roll surface where great temperature gradient was observed. Therefore the calculation for thermal crown based on the roll axi-symmetric deformation assumption was reasonable due to the axi-symmetric temperature field ignoring the small influence of the thin thermal zone, which greatly simplified the calculation.

5.4 RESULTS AND DISCUSSION

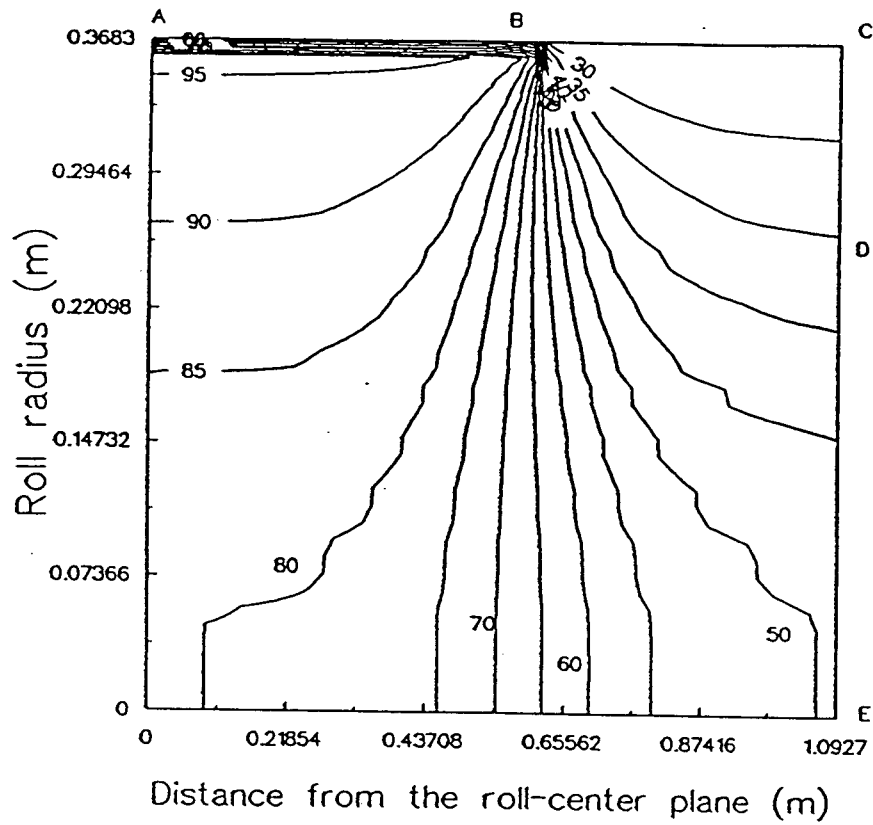


Fig.5.5 Temperature contour of the roll at steady state (HGP=60KW/m²°C, after 70 min. rolling).

5.4 RESULTS AND DISCUSSION

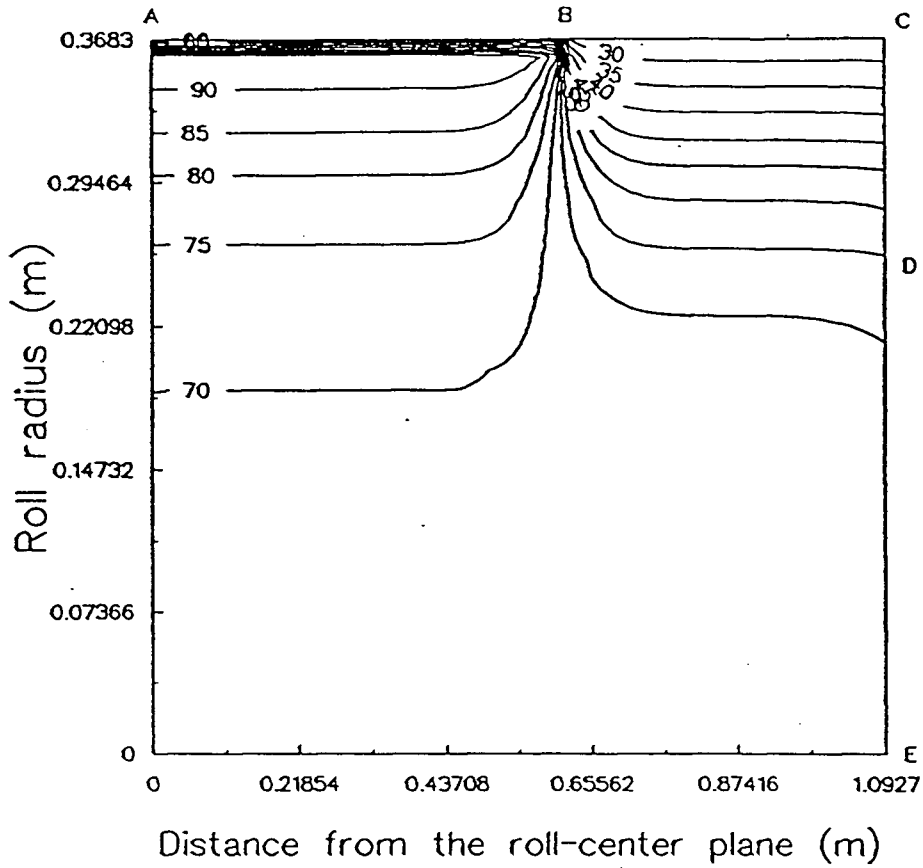


Fig.5.6 Temperature contour of the roll after 5 min. rolling
(HGP=60KW/m²°C).

5.4 RESULTS AND DISCUSSION

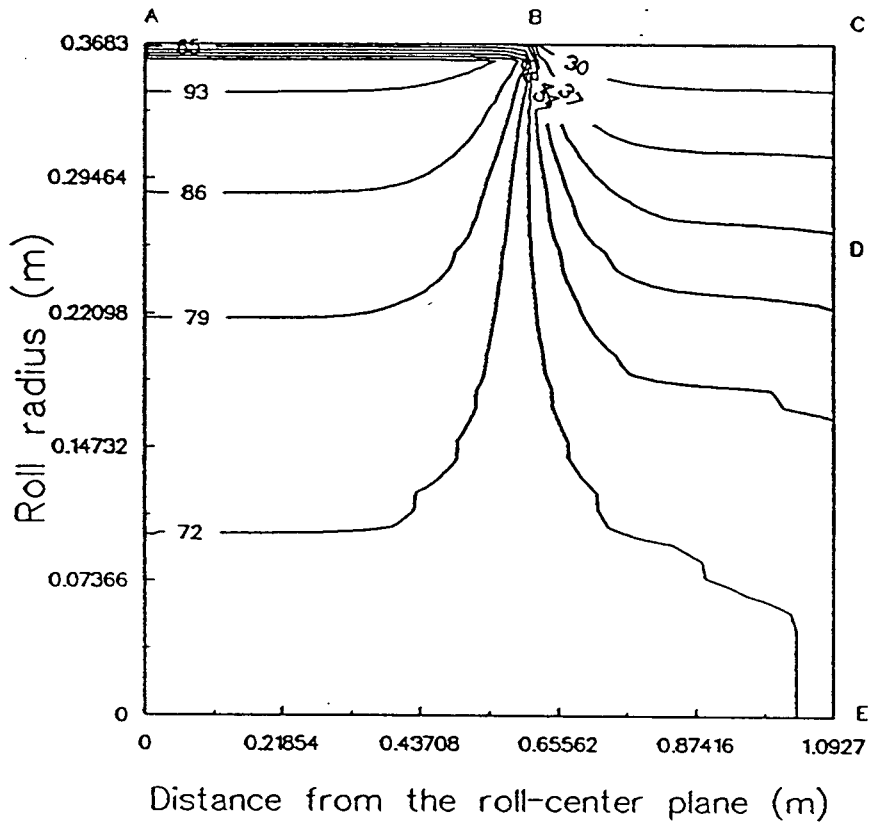


Fig.5.7 Temperature contour of the roll after 30 min. rolling (HGP=60KW/m²°C).

5.4 RESULTS AND DISCUSSION

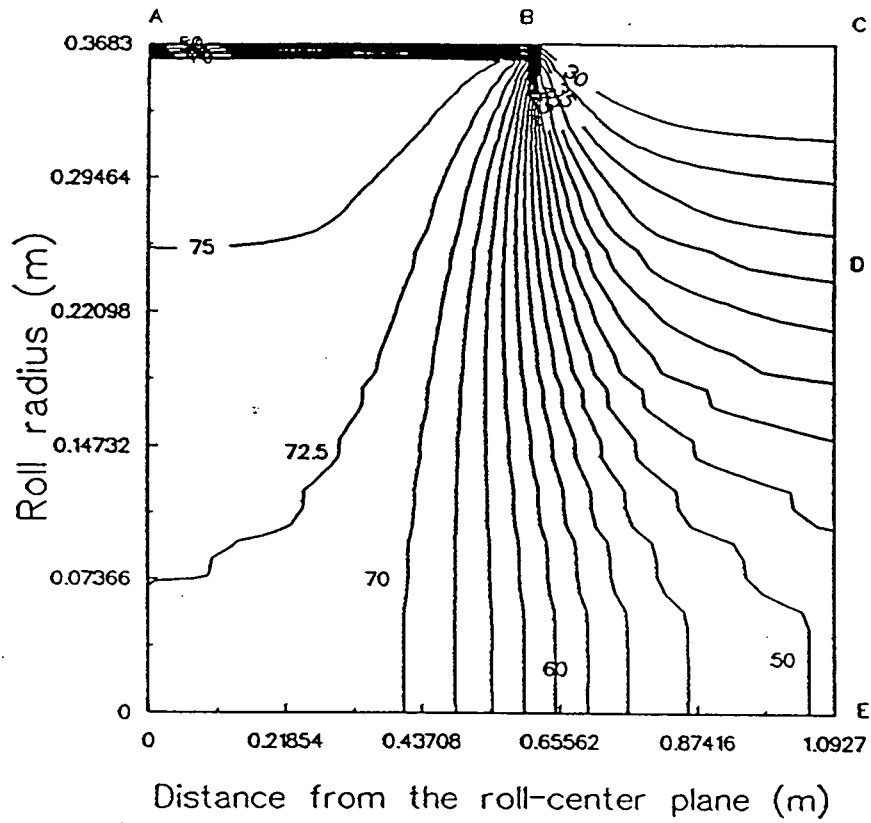


Fig.5.8 Temperature contour of the roll at steady state
(HGP=30kW/m²°C).

5.4 RESULTS AND DISCUSSION

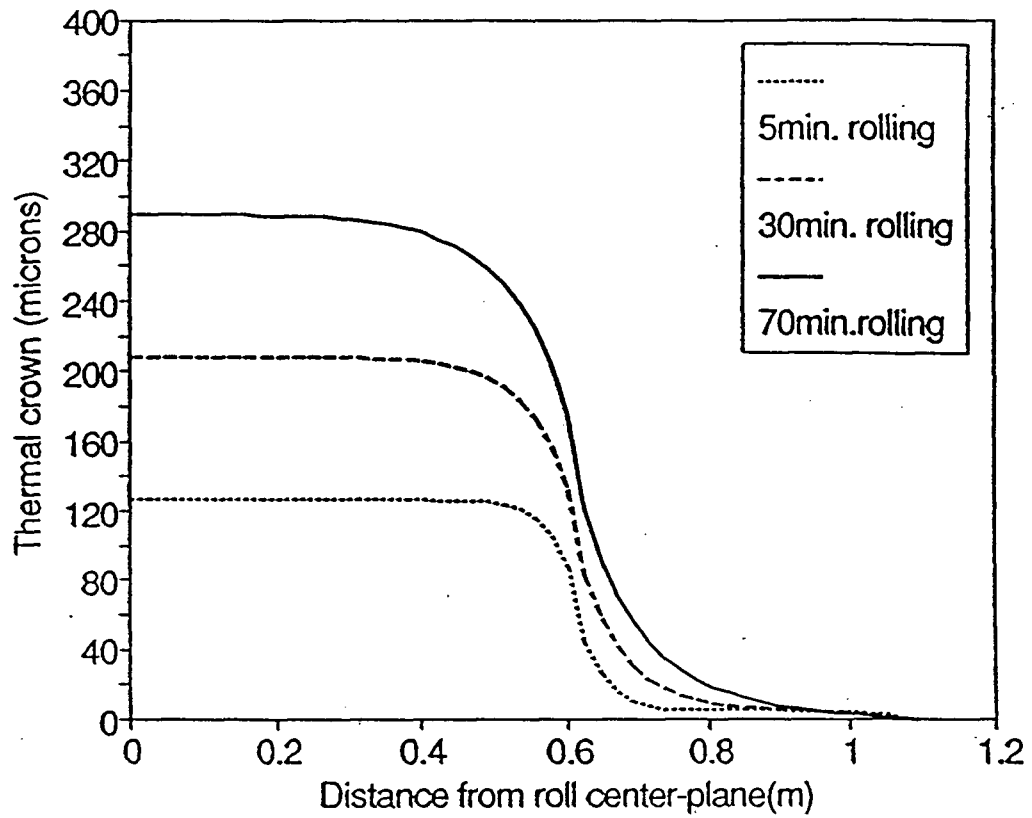


Fig.5.9 The thermal crowns from the temperature distributions shown in Fig.5.4 -- 5.6.

5.4 RESULTS AND DISCUSSION

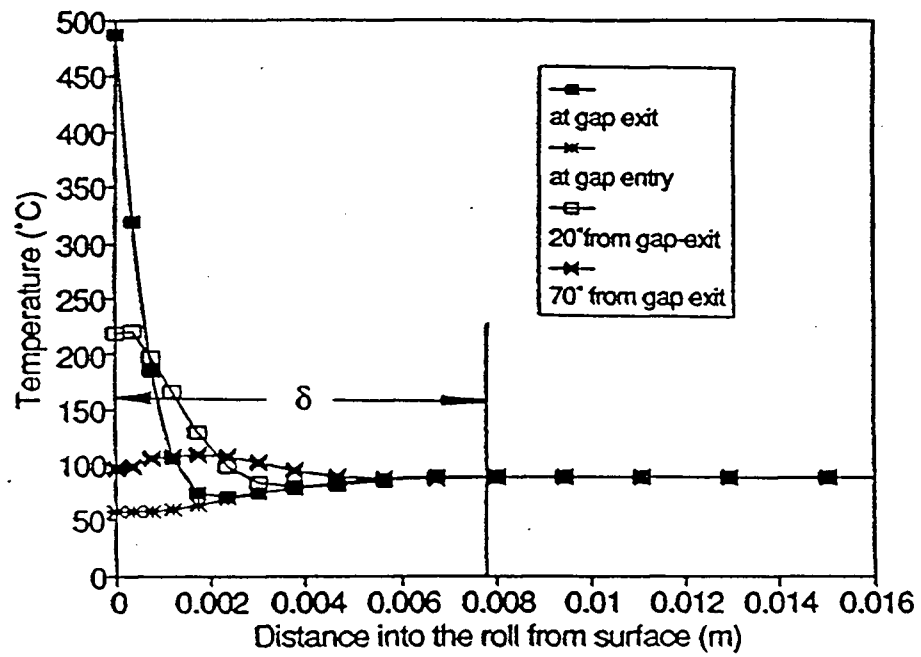


Fig.5.10 The temperature profiles for various angular positions of the roll at steady state ($HGP = 60\text{kW/m}^2\text{C}$).

5.4.1 Effect of Roll-Strip Heat Transfer on Roll Thermal Crown

Work roll lubrication has already been found to have a strong influence on the magnitude of the heat transfer coefficient in the roll gap (HGP) as recently discussed by Samarasekera [44] through the knowledge pertaining to friction in the boundary lubrication regime. In this study the roll-gap heat transfer coefficients from pilot mill experiments [9], the average value being $30\text{kW/m}^2\text{°C}$ with lubrication and $60\text{kW/m}^2\text{°C}$ in the absence of a lubrication, have been employed to examine the influence of lubrication on the roll thermal crown, and the results are shown in Fig.5.11.

It can be seen from this prediction shown in Fig.5.11 that the influence of HGP on thermal crown was large. The maximum value of thermal crown obtained for HGP of $30\text{kW/m}^2\text{°C}$ was 218 microns whilst the corresponding value for HGP of $60\text{kW/m}^2\text{°C}$ was 287 microns, an increase of 32 percent compared to the former one. With larger HGP, greater heat is supplied to the center of the roll in the deformation zone which results in higher temperatures and larger thermal crown. The influence decreased far from roll strip contact.

Fig.5.12 presents the development of roll thermal expansion at the center of roll surface before it reached steady state for both the roll-gap heat transfer coefficients respectively. Since the larger HGP caused a larger rate of heat transfer into the roll leading to a higher thermal field inside the roll compared to the lower HGP, a higher value of thermal expansion has been obtained for the larger HGP. The thermal expansion increased with time and the gradient of both the curves declined indicating that a steady-state was being approached.

5.4 RESULTS AND DISCUSSION

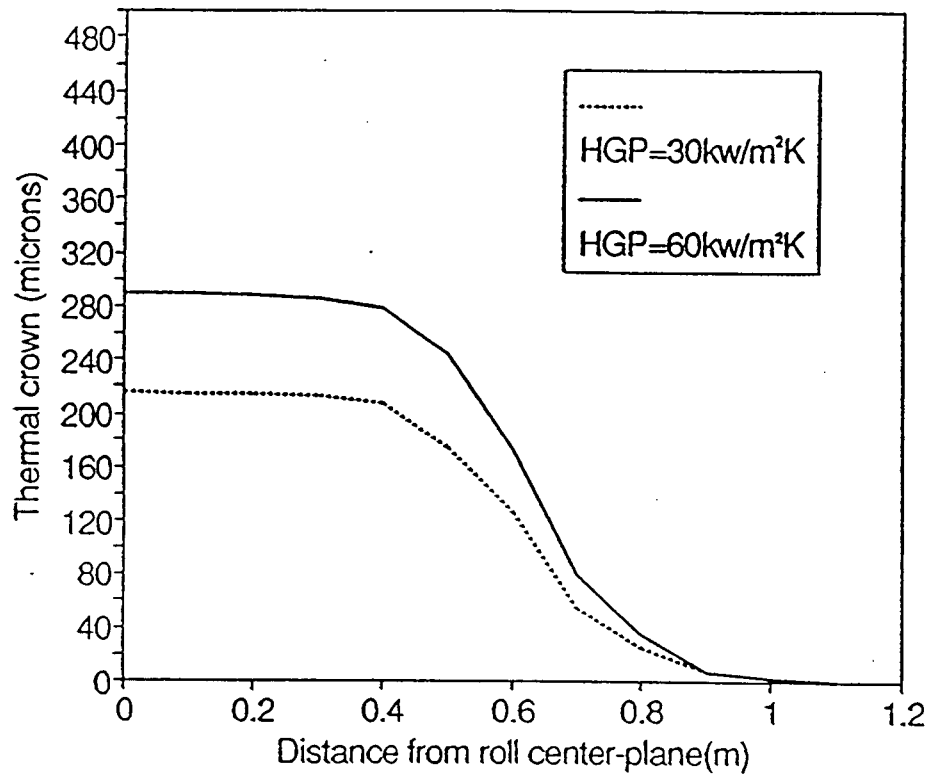


Fig.5.11 The effect of HGP on the thermal crown.

5.4 RESULTS AND DISCUSSION

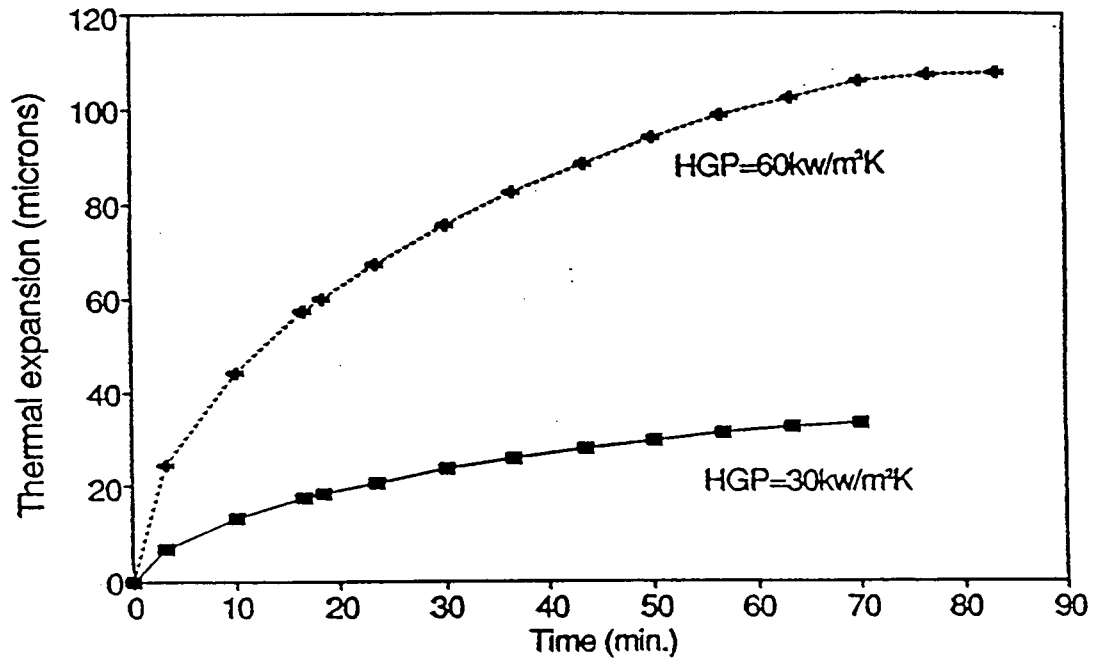


Fig.5.12 The development of the thermal expansion before steady state at HGP of 60 and 30 kW/m²°C.

5.4.2 Effect of Spray Cooling Arrangement on Roll Thermal Crown

To examine the influence of spray cooling configuration on thermal crown, three different spray-cooling arrangements of the work roll were under consideration. Their cooling configurations and conditions are given in Table.V-I. In case 1 the entry sprays were positioned closer to the roll gap compared to that of company B where the entry sprays were located near the work-backup roll contact. In case 2 the exit spray was located closer to the roll gap exit. In this investigation, the water flow rate for each spray has remained unchanged.

The crown results at steady state for the three cooling arrangements have been shown in Fig.5.13. It can be seen that the difference in thermal crown was obviously large due to the differences in the amount of heat removed by the three cooling arrangements. The arrangement in case 1 caused the maximum crown among the three cases, a 32 percent increase in the crown at the roll mid-plane compared to that for company B. It results from the fact that the distance (or time) between the entry sprays and exit spray is longer in case 1 compared to company B. This decreases heat removal and increases the amount of heat to transfer into the roll leading to a higher temperature.

It can also be seen from Fig.5.13 that the arrangement in case 2 gave rise to the minimum crown of the three arrangements. It could be deduced that since the maximum temperature of the roll surface occurred at roll-gap exit, an exit spray positioned immediately after the roll-gap exit would yield the highest cooling efficiency due to the rate of heat transfer being proportional

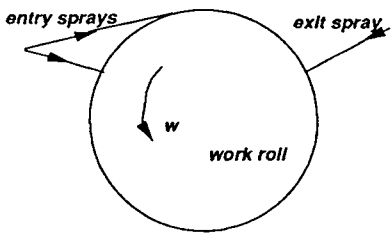
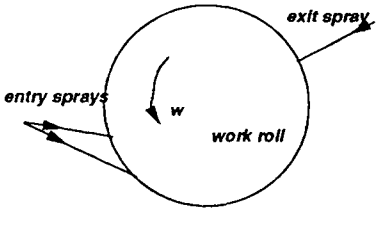
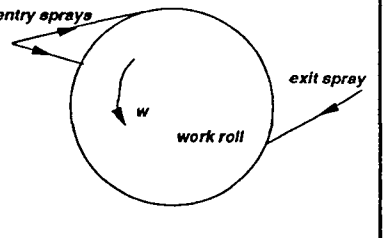
5.4 RESULTS AND DISCUSSION

to the temperature gradient. In other words, more heat flowed out of the roll before it transferred into the roll leading to a decrease in the roll temperature. This result was presented earlier in section 4.3 where the effect of exit spray arrangement was shown.

From Fig.5.13 it is evident that the different spray-cooling configurations had their greatest influence on thermal crown at the center of the roll ($z=0$) and the difference declined towards the ends of the roll. Furthermore the average temperatures along the radial direction at roll-end approached the same value for the three different cooling configurations at steady state.

The curves showing the development of thermal expansion at the center of the roll before it reached a steady state are presented in Fig.5.14 for the three different spray cooling configurations respectively. Among the three curves the greatest gradient at a time was obtained in case 1, which indicated that case 1 would have the greatest temperature variation and take the longest time to approach a steady state. While the case 2 where the smallest gradient was observed at a time would be the one to reach a steady state most quickly.

Table V-I Roll Spray-cooling Arrangement

Company B				Case 1 (entry sprays close to the roll-gap)				Case 2 (exit spray close to the roll-gap)			
											
Cool-ing zone Nu.	Degrees (°)	Type	Water Flow Rate l/min.	Cool-ing zone Nu.	Degrees (°)	Type	Water Flow Rate l/min.	Cool-ing zone Nu.	Degrees (°)	Type	Water Flow Rate l/min.
1	28	1	0	1	28	1	0	1	28	1	0
2	61	2	0	2	61	2	0	2	18	3	3884.8
3	18	3	3884.8	3	18	3	3884.8	3	61	2	0
4	13	2	0	4	13	2	0	4	13	1	0
5	20	2	0	5	20	2	0	5	20	1	0
6	20	1	0	6	20	1	0	6	20	1	0
7	20	1	0	7	79	1	0	7	20	1	0
8	59	3	1202.2	8	20	1	0	8	59	3	1202.2
9	10	2	0	9	20	3	1202.2	9	10	2	0
10	17	3	1202.2	10	20	2	0	10	17	3	1202.2
11	38	2	0	11	20	3	1202.2	11	38	2	0
12	45.3	1	0	12	30.4	1	0	12	45.3	1	0

* (1). Type 1: Radiation and Air Convection;

Type 2: Boiling and Water Convection;

Type 3: Spray Cooling.

(2). The twelve cooling zones have been illustrated in Fig.2.7, but certain changes have been done depending on different cooling configurations.

5.4 RESULTS AND DISCUSSION

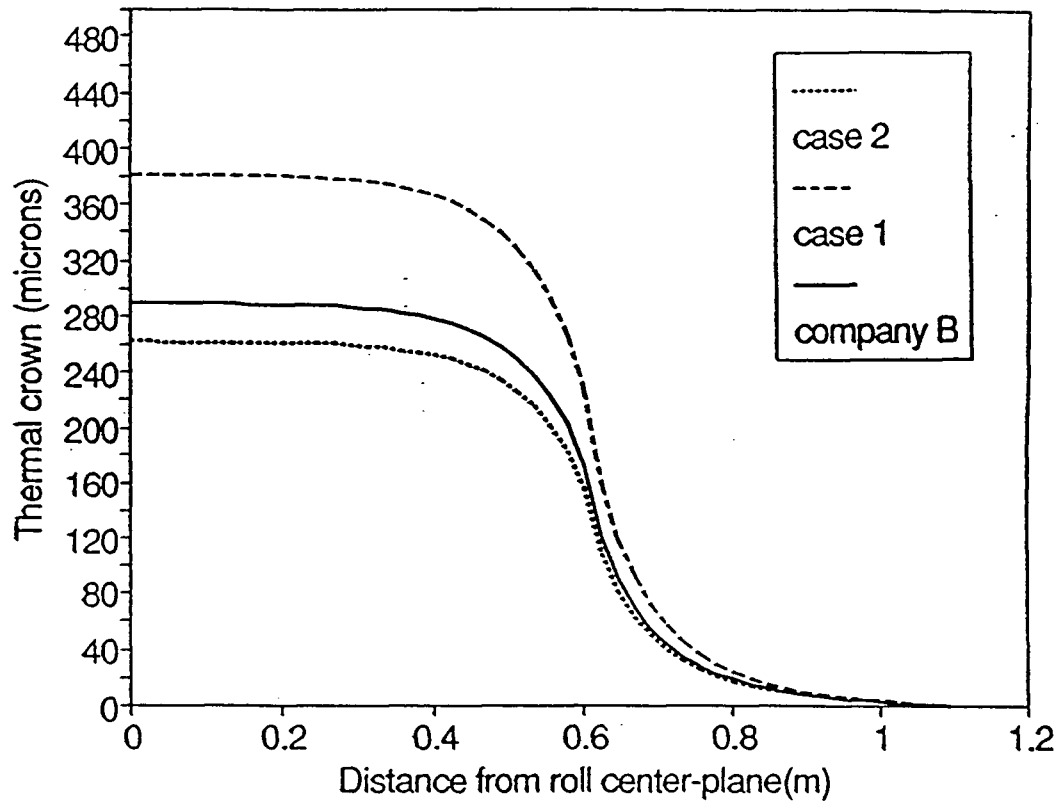


Fig.5.13 The effect of spray configurations on the thermal crown (HGP=60kW/m²°C).

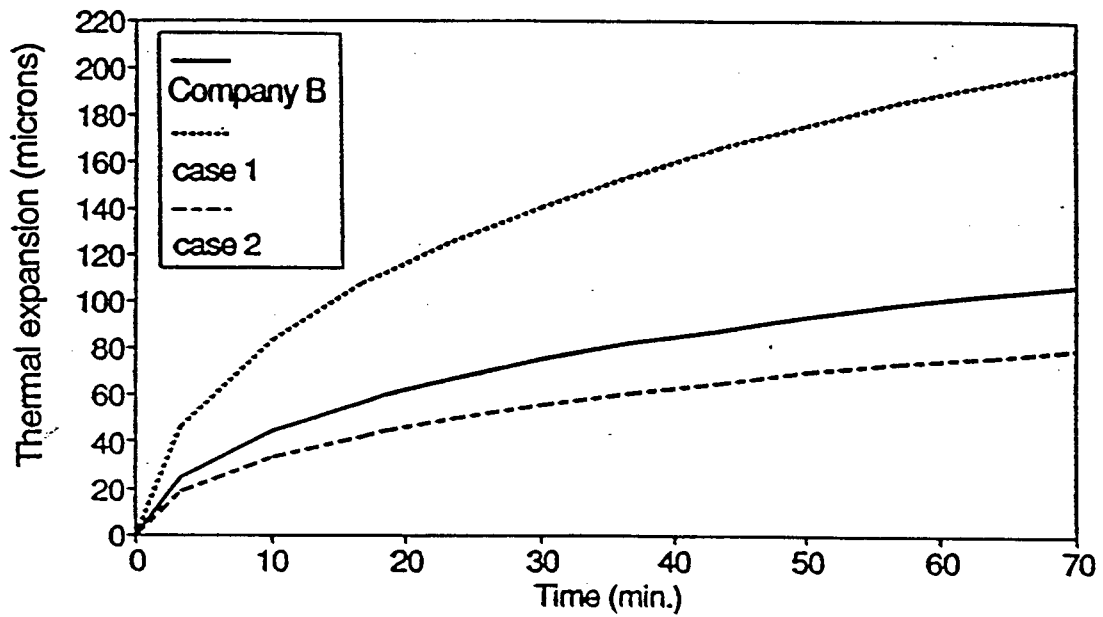


Fig.5.14 The development of thermal expansion before steady state at different spray configurations ($HGP=60\text{kW/m}^2\text{C}$).

5.4.3 Effect of Mill Pacing on Roll Thermal Crown

To examine the effect of mill pacing on roll thermal crown, two other values of mill pacing besides the continuous rolling have been chosen for the calculations. One was to consider the mill idle time equal to 1 min. and rolling time of 1 min., a condition employed by [30]. Another was to consider the rolling of a steel plate two meters long with an idle time of 1 min., which corresponded to the rolling time of 4 sec. The results have been shown in Fig.5.15. In comparison with the case of continuous rolling, the thermal crown with an idle time was smaller than that of continuous rolling. This was because during the idle time there is no heat input to the roll. When the idle time was much longer than the rolling time, the thermal crown could be restricted from developing, and the time that it needed to reach a steady state became shorter.

The results for all the rolling conditions involved in calculations mentioned above are also summarized in Table V-II. The rolling condition of a large roll-gap heat transfer and/or poor roll-cooling arrangement could induce the greatest thermal crown (ΔS), as indicated in case 3. Again it has been demonstrated that the employment of lubrication in the roll-gap and the improvement of roll-cooling condition would definitely lead to a small variation of roll temperature to cause a small thermal crown.

5.4 RESULTS AND DISCUSSION

Table V-II Summary of Results

Rolling conditions	No.1	No.2	No.3	No.4	No.5	No.6	No.7
HGP (kW/m ² C)	30	60	60	60	30	30	30
Spray cooling arrangements	Company B state	Company B state	Entry spray close to roll-gap	Exit spray close to roll-gap	Company B state	Company B state	Company B state
Idle time (sec.)	0	0	0	0	0	60	120
Rolling time (sec.)	Continue	Continue	Continue	Continue	Continue	60	4
Total rolling time (min.)	70	70	70	70	8.33	8.33	8.33
Initial roll-body temperature (°C)	69	69	69	69	25	25	25
Thermal expansion: S _{max} (microns)	33	107	200	78	83	40	3
S _{min} (microns)	-180	-180	-180	-180	0	0	0
Thermal crown ΔS (microns)	213	287	380	258	83	40	3
Temperature at plane before roll-gap: T _{max} (°C)	77	95	118	88	78	58	35
T _{min} (°C)	25	25	25	25	25	25	25
T _{average} (°C)	51	60	71	56	51	41	30

5.4 RESULTS AND DISCUSSION

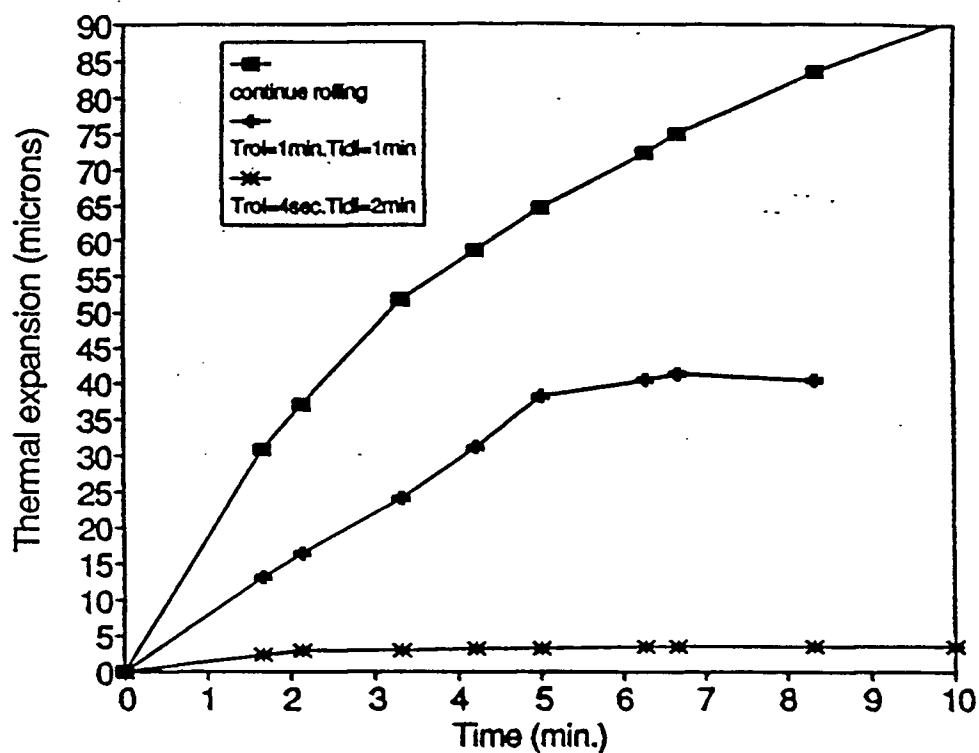


Fig.5.15 The development of thermal expansion at different mill pacing. ($HGP=30\text{kw/m}^2\text{°C}$, T_{rol} is the rolling time, and T_{idl} is the idle time.).

6 CONCLUDING REMARKS AND FURTHER WORK

The investigation of work roll cooling has provided an insight into the roll cooling arrangement for reducing the roll temperature. Work roll thermal behavior is indeed affected by the spray arrangement of work roll since it influences the rate of heat transfer out of the roll. It has been concluded from this investigation that (1) the roll-surface peak temperature can be decreased when either the entry or exit spray nozzles are positioned close to the roll-bite; (2) the upper nozzles and their positions influence both the roll-surface and the core temperatures whilst the influence on the core temperature is stronger; (3) the roll-core temperature can be reduced by increasing the spray contact area over the roll-surface; (4) the roll-core temperature is more sensitive to the exit-spray position than the entry one. Certainly work roll life benefits from a suitable spray arrangement. In this study the recommended spray configuration is the one with upper sprays close to work/backup roll contact and lower sprays close to the roll-bite since it produces the lowest temperature in the work roll. The thickness-proportional coefficient C_t has been found to be affected by Biot number. In this study the C_t for company B rolling condition is 10.7mm. The roll temperature decreases linearly with increasing the roll diameter due to the decrease in the roll bite time.

The thermal history of work roll in a hot rolling mill and the corresponding roll thermal crown has been computed. The magnitude of the calculated thermal crown that is consistent with some measured value demonstrates that the assumption of axi-symmetric deformation of the roll is reasonable. The effect of spray cooling arrangement on the resulting thermal crown in the roll has also been examined. Change of the roll-spray cooling arrangement has a significant

6 CONCLUDING REMARKS AND FURTHER WORK

impact on the resulting thermal expansion. The present study concludes that when the characteristic of water jets remains unchanged, the further the distance between entry-spray and exit-spray during roll-cooling, the less is the rate of heat transfer out of the roll resulting in larger thermal crown of work roll. As shown in Fig. 5.13 for case 1, the entry nozzles positioned close to the roll bite gives rise to a large distance between entry and exit sprays leading to large temperature buildup of the roll. Hence the design of entry spray immediately before the roll-bite is not desirable for reducing the crown. Again the present model that utilizes the real work roll state from a hot-rolling application in calculation provides the convenience for the prediction of work roll thermal crown.

For the purpose of the use of the roll cooling for shape and crown control, the following suggestions should be considered for future work:

1. Since the axial variation of roll-spray cooling may create various thermal crowns to compensate for the bending crown from deforming the strip [45], a non-uniform axial distribution of convective heat transfer coefficient should be considered in future calculation.
2. Since it is the combination of both mechanical and thermal actions that affects the roll gap shape, the bending crown from deforming the strip should be considered in future calculation.

7 REFERENCES

- 1 C.Devadas and I.Samaraskera: Iron & Steel Making, 1986, Vol. 13, No. 6, pp. 311-321.
- 2 P.G.Stevens, K.P.Ivens and P.Harper: J. Of the Iron and Steel Institute, Jan. 1971, pp.1-11.
- 3 Y. Sekimoto, M. Tanaka, R.Sawada and M.Koga: SEAIISI, Quarterly, April, 1977, pp.48-57.
- 4 P.Harper: Iron and Steel Making, Oct. 1988, pp.34-37.
- 5 H.J.Averink: Iron and Steel Making, May, 1989, pp.53-57.
- 6 W.J.Williams: Iron Steel, Aug., 1962, pp.372.
- 7 Y.Sekimoto: 'Effect of Rolling Conditions on the Surface Temperature of Work Rolls in Hot Strip Mill', British Industrial and Scientific International Translation Service, July, 1976, pp.1-12.
- 8 F.Kreith: "Principles of Heat Transfer", Third edition, 1973.
- 9 C.Devadas: "The Prediction of the Evolution of Microstructure During Hot Rolling of Steel Strip", Ph.D Thesis, UBC, 1989.
- 10 D.R.Hill and L.E.Gray: Iron & Steel Eng., June, 1981, pp.57-62.
- 11 A.A.Tseng: In Numerical Method in Industrial Forming Processes, Pineridge Press, Swansea, 1982, pp.767-776.
- 12 A.A.Tseng: Numerical Heat transfer, 1984, Vol.7, pp.113-125.
- 13 D.M.Parke and J.L.L.Baker: Iron and Steel Eng., 1972, Vol.49, pp.83-88.

- 14 E.J.Patula: J. Of Heat Transfer, Transactions of the ASME, Feb., 1981, Vol.103, pp.37-41.
- 15 W.Haubitzer: Arch. Eisenhuettenwes, 1974, Vol.46, pp.635-638.
- 16 C.Troeder, A.Spielvogel and Jin-wu Xu: Steel Research 56, 1985, No.7, pp.379-384.
- 17 S.Cerni, A.S.Weinstein and C.F.Zorowski: Iron Steel Eng. Year book, 1963, pp.717.
- 18 J.V.Poplawski and D.A.Secombe: Iron & Steel Eng., 1980, Vol.57, pp.47-58.
- 19 C.F.Peck Jr, J.M.Donetti and F.T.Maris: Iron and Steel Eng., Yearbook, Vol.31, 1954, pp.389-402.
- 20 M.Mitsutsuka: BISITS Vol.54, No.14, 1968, pp.675-680 (BISI 7767).
- 21 Y.Yamaguchi, M.Nakao, K.Takatsuka, S.Murakami and K.Hirata: Nippon Steel Tech., Rep., 1985, 33,(4).
- 22 W.L.Roberts: "Hot Rolling of Steel", pp.616-619, 1983, New York, Marcel Dekker.
- 23 R.R.Carpenter and P.J.Hannan:
Wean United, Inc., pp.69-71.
- 24 T.Masui, T.Nagai, T.Takigawa and Y.Takemoto: "Advances in cold Rolling Tech., The Institute of Metals, Book No.354, 1985, pp.143-151.
- 25 K.Klamma: Metallurgical Plant and Tech., 1985, Vol.8, No.3, pp.60-67.
- 26 K.Kizaki, N.Iwaanami, H.Kuwamoto and F.Fujita: "Advances in Cold Rolling Tech.", The Institute of Metals, Book No.354, 1985, pp.128-137.
- 27 K.Kajiwara, N.Fujino, H.Nish and M.Nihe: "Advances in Cold Rolling Tech., The Institute of Metals, Book No.354, 1985, pp.115-121.

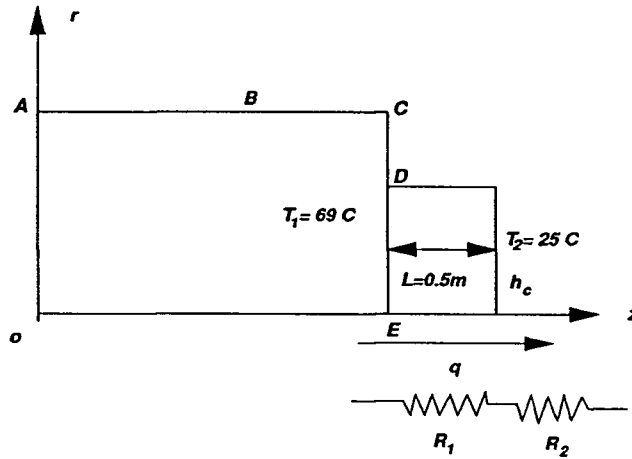
- 28 W.Y.D.Yuen, "On the Correction of Strip Shape By Localized cooling of The Work Rolls", Research and Technology Centre, BHP Steel International Group, Coated Products Division, Australia.
- 29 V.N.Khloponin, E.I.Latukhin, O.N.Soskovets, S.A.Burlakov: Steel in the USSR, Feb., 1988, Vol.18, pp.78-81.
- 30 W.L.Roberts: "Hot Rolling of Steel", Chap.23, pp.847-864, 1983, New York, Marcel Dekker.
- 31 S.Wilmotte and J.Mignon: "Thermal Variations of the Camber of the Working Rolls during Hot Rolling", CRM, No.34, March, 1973, pp.17-34.
- 32 N-G.Jonsson and P.Mantyla:
pp.129-136.
- 33 Y.Ohike, J.Sato, Y.Yamamoto, S.Honda and Y Tsutsumi: Stelco.
- 34 J.Burkhardt: 'Work roll preheating model', Project report, R & D 840006,Stelco.
- 35 J.G.Sibakin, J.S.Kide and W.Sherword: Proc. Met. Soc. Conf., Chicago, Jan., 1959.
- 36 W.M. Rohsenow: in " Developments in Heat Transfer ", pp.169-260, 1964, Cambridge, Mass, MIT press.
- 37 S. Nukiyama: J. Soc. Mech. Eng. Jpn. 1934, 37, P367-394.
- 38 F.Seredynski: J. Iron Steel Institute, 1973, 211, pp.197-203.
- 39 F.Kreith and W.Z.Black: "Basic Heat Transfer", 1980 pp.15.
- 40 A.P.Boresi: "Elasticity in Engineering Mechanics", 1965.
- 41 B.A.Boley and J.H.Weiner: "Theory of Thermal Stresses", 1960.

- 42 D.R.Croft and D.G.Lilley: "Heat Transfer Calculations using Finite Difference Equations", 1977.
- 43 R.W.Lewis, J.A.Johnson and W.R.Smith: "Numerical Methods in Thermal Problems", 1983.
- 44 I.V.Samarasekera: "Mathematical Modelling of Hot Rolling of Steel
Proceedings of the International Symposium, CIM/ICM, 1990, pp.148-167.
- 45 A.A.Tseng, F.H.Lin, A.S.Gunderia and D.S.Ni: Metallurgical Transactions A, 1989,
pp.2305-2320.

8 APPENDICES

APPENDIX A

The heat transfer coefficient h_n representing the heat loss by conduction to the roll neck has been approximately estimated through an equivalent heat transfer analysis along the boundary DE.



As illustrated above, the heat transfer can be treated within a thermal resistance network, and the rate of heat transfer is given by

$$q = \frac{T_1 - T_2}{R_1 + R_2} \quad (\text{A.1})$$

For conductive heat transfer, the thermal resistance

$$R_1 = \frac{L}{K} \quad (\text{A.2})$$

where $K = 54 \text{ w/m}^2\text{K}$ for carbon steel [39].

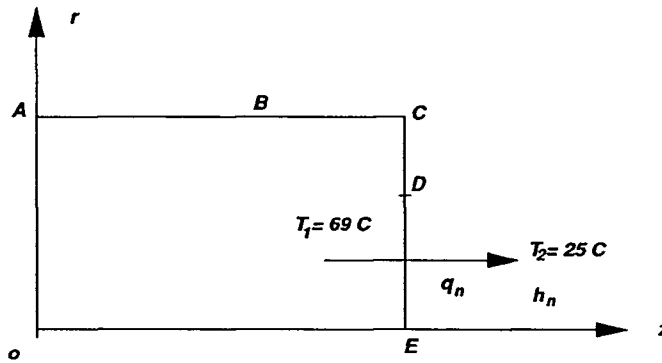
For convective heat transfer, the thermal resistance

$$R_2 = \frac{1}{h_c} \quad (\text{A.3})$$

where $h_c = 5 - 25 \text{ w/m}^2\text{K}$ for free convection, air [39].

$$q = \frac{T_1 - T_2}{\frac{L}{K} + \frac{1}{h_c}} = \frac{69 - 25}{\frac{0.5}{54} + \frac{1}{12}} = 475.2 \text{ w/m}^2 \quad (\text{A.4})$$

An equivalent heat transfer is considered along the boundary DE as illustrated below:



Then the rate of heat transfer is given by

$$q_n = h_n(T_1 - T_2) \quad (\text{A.5})$$

Let

$$q_n = q = 475.2 \text{ w/m}^2 \quad (\text{A.6})$$

Then

$$475.2 = h_n(69 - 25)$$

Therefore

$$h_n = 475.2 / (69 - 25) = 10.8 \text{ w/m}^2\text{C}$$

The estimated value of h_n has been used in calculation as the thermal boundary condition, representing the heat loss to the roll neck.

APPENDIX B

The set of finite difference equations of heat transfer of the work roll has been established based on the heat balance on each node by the energy analysis[39]. The finite difference approximation to the heat balance in the radial and axial direction has been employed in calculation. For the ADI method applied to solve the parabolic equations using the tridiagonal matrices, the incremental time step Δt has been divided into two steps.

For the first step ($t^{n+1/2} = t^n + \Delta t/2$), the implicit direction is in the radial direction (Fig.B.1).

The heat balance for an interial node (Fig.B.2)

$$\begin{aligned}
 & k_r \left(\frac{T_{i-1,j}^{n+1/2} - T_{i,j}^{n+1/2}}{\Delta r_{i-1,j}} \right) \left(r_{i,j} - \frac{\Delta r_{i-1,j}}{2} \right) \Delta \theta \Delta z \\
 & + k_r \left(\frac{T_{i+1,j}^{n+1/2} - T_{i,j}^{n+1/2}}{\Delta r_{i,j}} \right) \left(r_{i,j} + \frac{\Delta r_{i,j}}{2} \right) \Delta \theta \Delta z \\
 & + k_z \left(\frac{T_{i,j+1}^n - 2T_{i,j}^n + T_{i,j-1}^n}{\Delta z} \right) \left(\frac{\Delta r_{i-1,j} + \Delta r_{i,j}}{2} \right) r l_{i,j} \Delta \theta \\
 & = \rho c_p \left(\frac{T_{i,j}^{n+1/2} - T_{i,j}^n}{\Delta t/2} \right) \left(\frac{\Delta r_{i,j} + \Delta r_{i-1,j}}{2} \right) r l_{i,j} \Delta z \Delta \theta
 \end{aligned} \tag{B.1}$$

where $r_1(i,j)$ is the radial size of the element(i,j) center. Since the grid spacing in the radial direction has been considered to be non-uniformly distributed, $r_1(i,j)$ is derived geometrically (Fig.B.3)

$$r l_{i,j} = r_{i,j} - (\Delta r_{i,j} - \Delta r_{i-1,j})/4 \tag{B.2}$$

The heat balance for the roll surface nodes ($i=i_0; j=2, j_0-1$) (Fig.B.4)

$$\begin{aligned}
 & k_r \left(\frac{T_{i_0-1,j}^{n+1/2} - T_{i_0,j}^{n+1/2}}{\Delta r_{i_0-1,j}} \right) \left(r_{i_0,j} - \frac{\Delta r_{i_0-1,j}}{2} \right) \Delta \theta \Delta z \\
 & + h_{sr} (T_s - T_{i_0,j}^{n+1/2}) \frac{r_{i_0,j}^2}{r \Delta r_{i_0-1,j}} \\
 & + k_z \left(\frac{T_{i_0,j+1}^n - 2T_{i_0,j}^n + T_{i_0,j-1}^n}{\Delta z} \right) r_{i_0,j} \Delta \theta \frac{\Delta r_{i_0-1,j}}{2} \\
 & = c_p \rho \left(\frac{T_{i_0,j}^{n+1/2} - T_{i_0,j}^n}{\Delta t/2} \right) \Delta \theta r_{i_0,j} \Delta z \Delta r_{i_0-1,j} / 2
 \end{aligned} \tag{B.3}$$

The heat balance for the roll end nodes ($i=2, i_0-1; j=j_0$) (Fig.B.5)

$$\begin{aligned}
 & k_r \left(\frac{T_{i-1,j_0}^{n+1/2} - T_{i,j_0}^{n+1/2}}{\Delta r_{i-1,j_0}} \right) \left(r_{i,j_0} - \frac{\Delta r_{i-1,j_0}}{2} \right) \Delta \theta \Delta z / 2 \\
 & + k_r \left(\frac{T_{i+1,j_0}^{n+1/2} - T_{i,j_0}^{n+1/2}}{\Delta r_{i,j_0}} \right) \left(r_{i,j_0} + \frac{\Delta r_{i,j_0}}{2} \right) \Delta \theta \Delta z / 2 \\
 & + k_z \left(\frac{T_{i,j_0-1}^n - T_{i,j_0}^n}{\Delta z} \right) r l_{i,j_0} \frac{(\Delta r_{i-1,j_0} + \Delta r_{i,j_0})}{2} \Delta \theta \\
 & + h_n (T_n - T_{i,j_0}^n) r l_{i,j_0} \frac{(\Delta r_{i-1,j_0} + \Delta r_{i,j_0})}{2} \Delta \theta \\
 & = c_p \rho \left(\frac{T_{i,j_0}^{n+1/2} - T_{i,j_0}^n}{\Delta t/2} \right) r l_{i,j_0} \frac{(\Delta r_{i,j_0} + \Delta r_{i-1,j_0})}{2} \Delta \theta \Delta z / 2
 \end{aligned} \tag{B.4}$$

At the roll surface end ($i=i_0; j=j_0$), the heat balance equation (Fig.B.6)

$$\begin{aligned}
& k_r \left(\frac{T_{i0-1,j0}^{n+1/2} - T_{i0,j0}^{n+1/2}}{\Delta r_{i0-1,j0}} \right) \left(r_{i0,j0} - \frac{\Delta r_{i0-1,j0}}{2} \right) \Delta \theta \Delta z + h_{rw} (T_w - T_{i0,j0}^{n+1/2}) r_{i0,j0} \Delta z \Delta \theta / 2 \\
& + k_z \left(\frac{T_{i0-1,j0}^n - T_{i0,j0}^n}{\Delta z} \right) \frac{\Delta r_{i0-1,j0} r_{i0,j0} \Delta \theta}{2} + h_n (T_a - T_{i0,j0}^n) \frac{(\Delta r_{i0-1,j0} \Delta \theta r_{i0,j0})}{2} \\
& = c_p \rho \left(\frac{T_{i0,j0}^{n+1/2} - T_{i0,j0}^n}{\Delta t / 2} \right) r_{i0,j0} \Delta z \Delta \theta \Delta r_{i0-1,j0} / 4
\end{aligned} \tag{B.5}$$

For those nodes at the roll mid-plane ($i=1, i0-1$; $j=1$) and roll axis ($i=1$; $j=1, j0$), the heat balance equations can be obtained based on the temperature symmetrical conditions. The derivative of equations is the same as the above.

For the second step ($t^{n+1} = t^{n+1/2} + \Delta t / 2$), the implicit direction is in the roll axial direction (Fig.B.7). The heat balance for an interial node (Fig.B.2)

$$\begin{aligned}
& k_r \left(\frac{T_{i-1,j}^{n+1/2} - T_{i,j}^{n+1/2}}{\Delta r_{i-1,j}} \right) \left(r_{i,j} - \frac{\Delta r_{i-1,j}}{2} \right) \Delta \theta \Delta z \\
& + k_r \left(\frac{T_{i+1,j}^{n+1/2} - T_{i,j}^{n+1/2}}{\Delta r_{i,j}} \right) \left(r_{i,j} + \frac{\Delta r_{i,j}}{2} \right) \Delta \theta \Delta z \\
& + k_z \left(\frac{T_{i,j+1}^{n+1} - 2T_{i,j}^{n+1} + T_{i,j-1}^{n+1}}{\Delta z} \right) \left(\frac{\Delta r_{i-1,j} + \Delta r_{i,j}}{2} \right) r l_{i,j} \Delta \theta \\
& = \rho c_p \left(\frac{T_{i,j}^{n+1} - T_{i,j}^{n+1/2}}{\Delta t / 2} \right) \left(\frac{\Delta r_{i,j} + \Delta r_{i-1,j}}{2} \right) r l_{i,j} \Delta z \Delta \theta
\end{aligned} \tag{B.6}$$

The heat balance for the roll surface nodes ($i=i0$; $j=2, j0-1$) (Fig.B.4)

$$\begin{aligned}
& k_r \left(\frac{T_{i0-1,j}^{n+1/2} - T_{i0,j}^{n+1/2}}{\Delta r_{i0-1,j}} \right) \left(r_{i0,j} - \frac{\Delta r_{i0-1,j}}{2} \right) \Delta \theta \Delta z + h_{sr} (T_s - T_{i0,j}^{n+1/2}) \frac{r_{i0,j}^2}{r \Delta r_{i0-1,j}} \\
& + k_z \left(\frac{T_{i0,j+1}^{n+1} - 2T_{i0,j}^{n+1} + T_{i0,j-1}^{n+1}}{\Delta z} \right) r_{i0,j} \Delta \theta \frac{\Delta r_{i0-1,j}}{2} \\
& = c_p \rho \left(\frac{T_{i0,j}^{n+1} - T_{i0,j}^{n+1/2}}{\Delta t/2} \right) \Delta \theta r_{i0,j} \Delta z \Delta r_{i0-1,j} / 2
\end{aligned} \tag{B.7}$$

The heat balance for the roll end nodes ($i=2, i0-1; j=j0$) (Fig.B.5)

$$\begin{aligned}
& k_r \left(\frac{T_{i-1,j0}^{n+1/2} - T_{i,j0}^{n+1/2}}{\Delta r_{i-1,j0}} \right) \left(r_{i,j0} - \frac{\Delta r_{i-1,j0}}{2} \right) \Delta \theta \Delta z / 2 \\
& + k_r \left(\frac{T_{i+1,j0}^{n+1/2} - T_{i,j0}^{n+1/2}}{\Delta r_{i,j0}} \right) \left(r_{i,j0} + \frac{\Delta r_{i,j0}}{2} \right) \Delta \theta \Delta z / 2 \\
& + k_z \left(\frac{T_{i,j0-1}^{n+1} - T_{i,j0}^{n+1}}{\Delta z} \right) r_{i,j0} \frac{(\Delta r_{i-1,j0} + \Delta r_{i,j0})}{2} \Delta \theta \\
& + h_n (T_n - T_{i,j0}^{n+1}) r_{i,j0} \frac{(\Delta r_{i-1,j0} + \Delta r_{i,j0})}{2} \Delta \theta \\
& = c_p \rho \left(\frac{T_{i,j0}^{n+1} - T_{i,j0}^{n+1/2}}{\Delta t/2} \right) r_{i,j0} \frac{(\Delta r_{i,j0} + \Delta r_{i-1,j0})}{2} \Delta \theta \Delta z / 2
\end{aligned} \tag{B.8}$$

At the roll surface end ($i=i0; j=j0$), the heat balance equation (Fig.B.6)

$$\begin{aligned}
& k_r \left(\frac{T_{i0-1,j0}^{n+1/2} - T_{i0,j0}^{n+1/2}}{\Delta r_{i0-1,j0}} \right) \frac{\left(r_{i0,j0} - \frac{\Delta r_{i0-1,j0}}{2} \right)}{2} \Delta \theta \Delta z + h_{rw} (T_w - T_{i0,j0}^{n+1/2}) r_{i0,j0} \Delta z \Delta \theta / 2 \\
& + k_z \left(\frac{T_{i0-1,j0}^{n+1} - T_{i0,j0}^{n+1}}{\Delta z} \right) \frac{\Delta r_{i0-1,j0} r_{i0,j0} \Delta \theta}{2} + h_n (T_a - T_{i0,j0}^{n+1}) \frac{(\Delta r_{i0-1,j0} \Delta \theta r_{i0,j0})}{2} \\
& = c_p \rho \left(\frac{T_{i0,j0}^{n+1} - T_{i0,j0}^{n+1/2}}{\Delta t / 2} \right) r_{i0,j0} \Delta z \Delta \theta \Delta r_{i0-1,j0} / 4
\end{aligned} \tag{B.9}$$

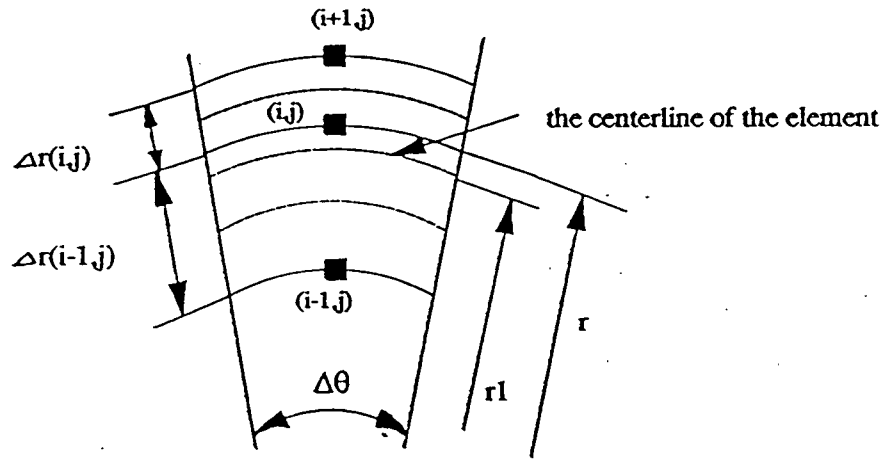


Fig.B.3 Schematic illustrates the position of r_1 .

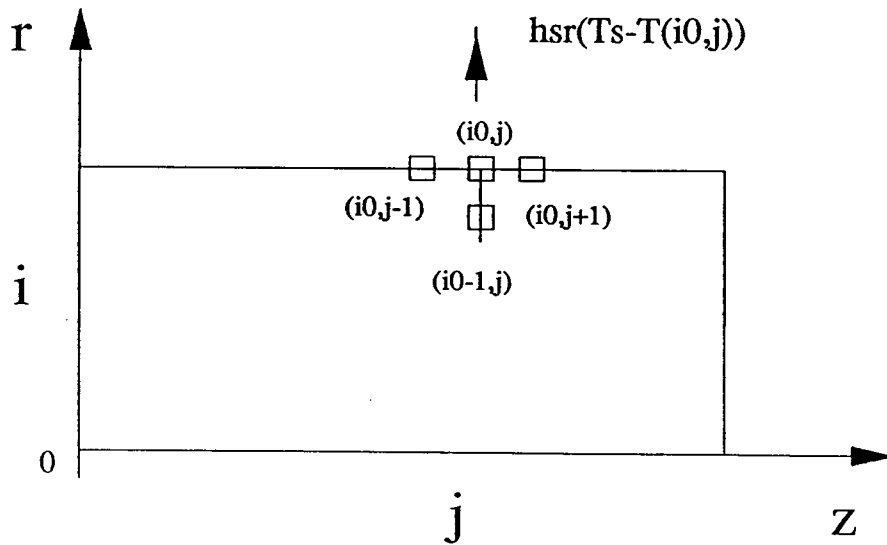


Fig.B.4 Schematic illustrates the surface nodes.

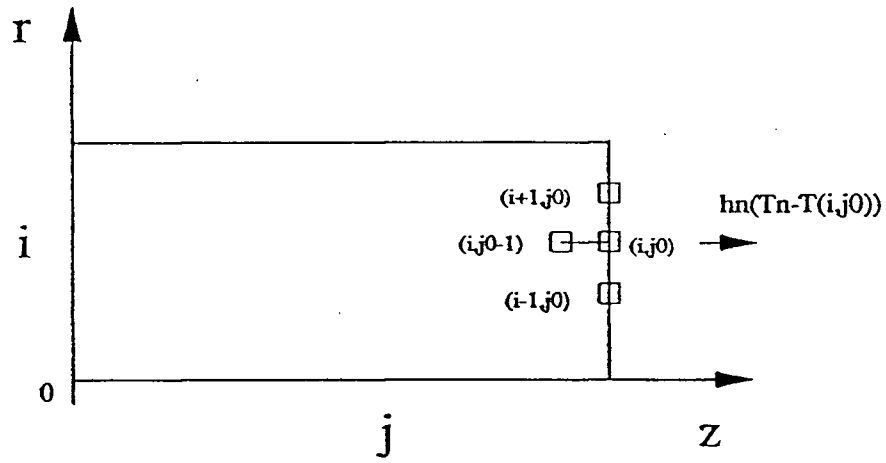


Fig.B.5 Schematic illustrates the roll-end nodes.

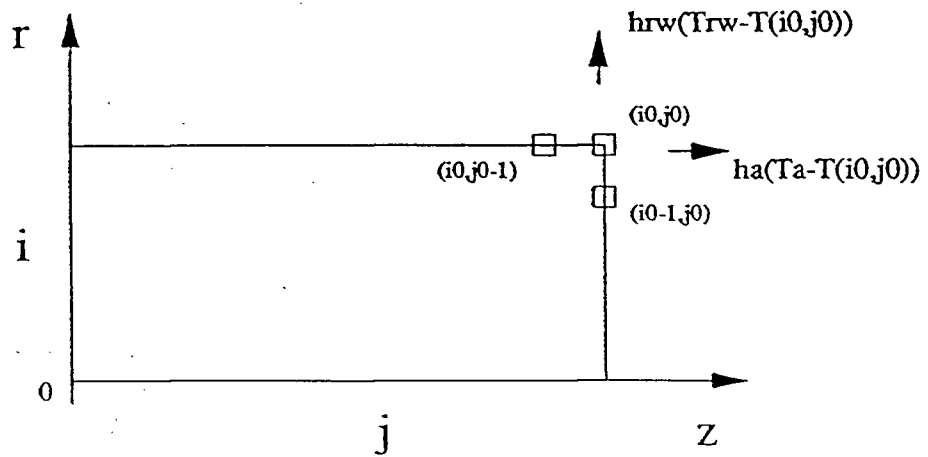


Fig.B.6 Schematic illustrates the roll-end corner nodes.

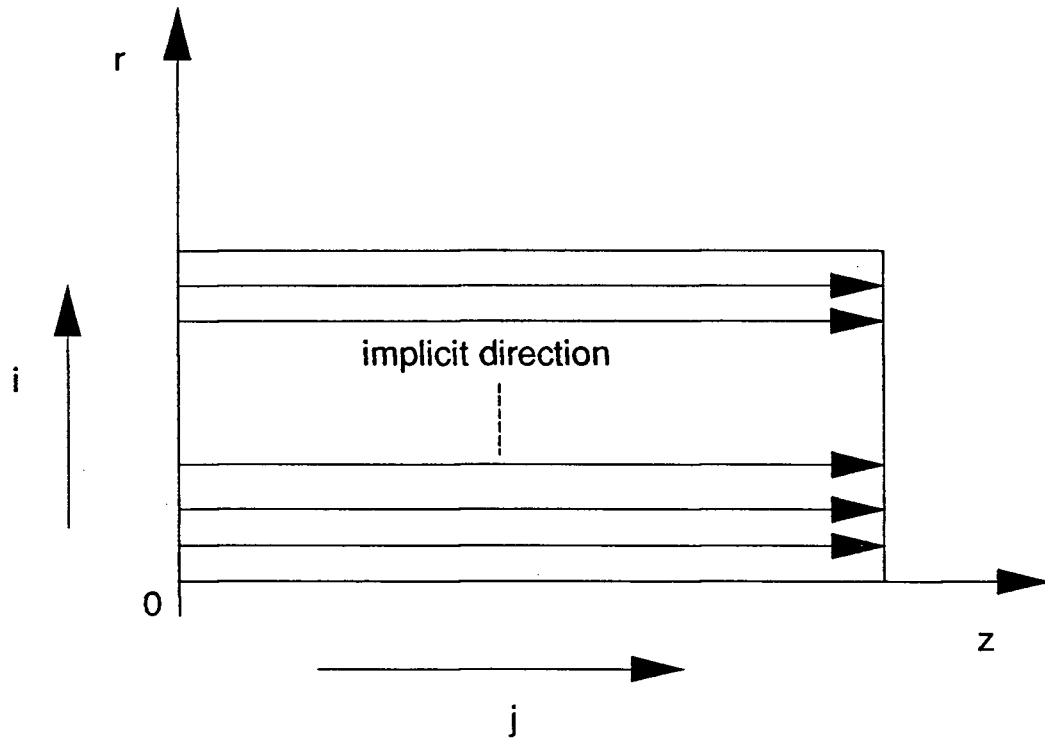


Fig.B.7 Schematic illustrates the implicit direction for the second step in ADI.